p5

Department of AERONAUTICS and ASTRONAUTICS
STANFORD UNIVERSITY

ADMINISTRATIVE & SUMMARY TECHNICAL REPORTS

NASA Ames Research Center
Grant No. NGT 2-52212

1996 NASA-ASEE-STANFORD SUMMER FACULTY FELLOWSHIP PROGRAM

Ames Research Center
Dryden Flight Research Center
Stanford University

October 1996

SUMMARY TECHNICAL REPORT

1996 NASA-ASEE-STANFORD SUMMER FACULTY FELLOWSHIP PROGRAM

Ames Research Center
Dryden Flight Research Center
Stanford University

October 1996

PREFACE

As is customary, the final technical report for the NASA-ASEE Summer Faculty Fellowship Program at the Ames Reseach Center, Dryden Flight Research Center and Stanford University essentially consists of a compilation of the summary technical reports of all the fellows. More extended versions done either as NASA publications, archival papers, or other laboratory reports are not included here. The reader will note that the areas receiving emphasis were the life sciences, astronomy, remote sensing, aeronautics, fluid dynamics/aerophysics, and computer science. Of course, the areas of emphasis vary somewhat from year to year depending on the interests of the most qualified applicants. Once again, the work is of especially high quality.

The reports of the first and second year fellows are grouped separately and are arranged alphabetically within each group.

Michael Tauber and Sylvia Stanley
Co-Directors
Summer Faculty Fellowship Program at
Ames Research Center, Dryden Flight
Research Center and Stanford University

OMIT TO P.1

1996 NASA-ASEE-Stanford Summer Faculty Fellowship Program

Topics Researched and Reported By First Year Fellows

Faculty Fellow & (NASA Colleague/Divison)	University Affiliation	Title of Research Project
Asst. Prof. Jorge Ballester (Alexander Thielens/SST)	Dept. of Physics Emporia State University	Recombination Rates of Electrons with Interstellar PAH Molecules
Professor Daniel Biezad (Lee Duke/XR)	Dept. of Aeronautical Engineering California Polytechnic State University, San Luis Obispo	WEBPRESS: An Internet Outreach from NASA Dryden
Asst. Prof. Wanda L. Boda (Alan Hargins/SLR)	Dept. of Kinesiology California State University, Sonoma	A Comparison of the Physiology and Mechanics of Exercise in LBNP and Upright Gait
Asst. Prof. Debora A. Compton (David Driver/ADT)	Dept. of Aerospace and Mechancial Engineering Boston University	Flow Field Measurements in a 3-D Separating Flow
Asst. Prof. John C. Crepeau (Murray Tobak/ADF)	Dept. of Mechanical Engineering University of Idaho	The Center Manifold in Fluid Transition
Asst. Prof. James M. Donohue (Douglas Fletcher/STA)	Dept. of Mechanical Engineering Santa Clara University	Emission Spectral Measurements in the Plenum of an Arc Jet Wind Tunnel
Professor Barry D. Ganapol (David Peterson/SGE)	Depts. of Hydrology & Water Resources and Aerospace & Mechanical Engineering University of Arizona, Tucson	A Within-Leaf Radiative Transfer Model with AnisotropicScattering
Professor Catherine G.R. Jackson (John Greenleaf/SLR)	School of Kinesiology and Physical Education University of Northern Colorado	Effect of +Gz Acceleration on the Oxygen Uptake-Exercise Load Relationship During Lower Extremity Ergometer Exercise
Assoc Prof. Barbara Johnson-Wint (Emily Holton/SL)	Dept. of Biological Sciences Northern Illinois University	Collagen Gel Contraction by Fibroblasts: The Role of Myosin II and Gravity Effects
Professor Fazal B. Kauser (Bill Burcham/XRP)	Dept. of Aerospace Engineering California State Polytechnic University, Pomona	Performance of Soviet NK-321, Mixed Stream, Triple Spool, Augmented Turbofan Engine

Asst. Prof. Mark S. Marley (Christopher McKay/SST)	Dept. of Astronomy New Mexico State University	Atmosphere Models for the Brown Dwarf Gliese 229B and the Extrasolar Giant Planets
Assoc. Prof. Richard H. Miller (Bruce Smith/SST)	Dept. of Astronomy and Astrophysics University of Chicago	Dynamics of Nuclear Regions of Galaxies
Assoc. Prof. Ronald E. Nelson (Martin Brenner/XRDV)	Dept. of Engineering Arkansas Tech University	Use of the Matching Pursuit Algorithms for Flight Flutter Test Data Analysis
Asst. Prof. Stephen M. Ruffin (Grant Palmer/STA)	School of Aerospace Engineering Georgia Institute of Technology	Supersonic Channel Concept for Enhancement of Lift/Drag Ratio
Professor Ravi P. Sinha (James Brass/SGE)	Dept. of Geosciences Elizabeth City State University	1) Curriculum Development in Remote Sensing at California State University, Monterey 2) Deforestation and Biogenic Trace Gas Emissions from Brazilian Cerrado
Professor Paul P. Szydlik (Theodore Bunch/SSX)	Dept. of Physics State University of New York at Plattsburgh	Interplanetary & Interstellar Dust Particles: Reentry Heating and Capture in Aerogel
Professor Richard H. Tipping (Charles Chackerian/SGP)	Dept. of Physics University of Alabama	Line Coupling in Atmospheric Spectra
Professor Hsien-Yang Yeh (Lance Richards/XRS)	Dept. of Mechanical Engineering California State University, Long Beach	The Yeh-Stratton Criterion for Stress Concentration on Fiber-Reinforced Composite Materials

1996 NASA-ASEE-Stanford
Summer Faculty Fellowship Program

Topics Researched and Reported
By Second Year Fellows

Faculty Fellow & (NASA Colleague/Divison)	University Affiliation	Title of Research Project
Asst. Prof. Michael Babich (Emily Holton/SL)	Dept. of Biomedical Sciences Univ. of Illinois College of Medicine	Mechanisms of Bone Mineralization and Effects of Mechanical Loading
Assoc. Prof. Ronald J. Bieniek (S. Sharma & T. Edwards/STA)	Dept. of Physics University of Missouri-Rolla	Semiquantal Modeling of Molecular Energy Transfer in Shocked Environments
Asst. Prof. Gregory A. Blaisdell (Karim Shariff/ADT)	School of Aeronautics and Astronautics Purdue University	Simulation and Modeling of the Elliptic Streamline Flow
Dr. Stephen C. Brawley (Daniel Bencze/AAH)	Dept. of Aeronautics and Astronautics Naval Postgraduate School	Aerodynamic Optimization of the High Speed Civil Transport
Professor Delano P. Chong (Charles Bauschlicher/ST)	Dept. of Chemistry University of British Columbia	Use of Density Functional Method to Study Molecular Vibrations
Assoc. Prof. Daniel L. Ewert (James Connolly/SLE)	Dept. of Electrical Engineeirng North Dakota State University	Development of Minimally-Aortic Pressure and Flow Instrumentation
Assoc. Prof. Amitabha Ghosh (Patti Schumacher/AOW)	Dept. of Mechanical Engineering Rochester Institute of Technology	Development of a Driver Code for the WICS Project
Assoc. Prof. M. Susan Hallbeck (Bruce Webbon/STE)	Dept. of Industrial & Management Systems Engineering University of Nebraska, Lincoln	Effects of Gloves, Temperature and their Interaction on Finger, Hand, and arm Blood Flow & Skin Temperature: A Pilot Study
Professor David Manor (Robert Curry/XRA)	Dept. of Aerospace Engineering Parks College of St. Louis University	Further Study of 'Pop-Up' Vortex Generators
Assoc. Prof. Robert A. Morris (Keith Swanson/IC)	Dept. of Computer Science Florida Institute of Technology	A System for Automatically Generating Scheduling Heuristics
Assoc. Prof. Thomas Nygren (Judith Orasanu/AFO)	Dept. of Psychology Ohio State University	The Role of Risk in Pilots' Perceptions of Problem Situations

Assoc. Prof. Bradley M. Stone (Louis Allamandola/SSA)	Dept. of Chemistry California State University, San Jose	Absorption Spectroscopy of Polycyclic Aeromatic Hydrocarbons Under Interstellar Conditions
Professor H. William Wilson (Max Lowenstein/SGG)	Dept. of Chemistry and Scientific Services Western Washington University	Tunable Diode Laser Spectrometers and the Stratospheric Ozone-Nitrous Oxide Connection
Professor Ira Wolinsky (Sara Arnaud/SLR)	Dept. of Human Development University of Houston	Calcium Balance in Mature Rats Exposed to a Space Flight Model

omit this page

1996 NASA-ASEE-Stanford Summer Faculty Fellowship Program

Topics Researched and Reported By Graduate Student Fellows

Graduate Student Fellow & (NASA Colleague/Divison)	University Affiliation	Title of Research Project
Joshua McBee (Max Lowenstein/SGG)	Dept. of Chemistry Western Washington University	The Effects of Sulfur Compounds (Specifically Carbonyl Sulfide OCS) on the Stratosphere
Eric B. Villeda (Judith Orasanu/AFO)	Dept. of Psychology Ohio State University	Loss of Situation Awareness in Pilots: Analysis of Incident Reports

1996 NASA-ASEE Summer Faculty Fellowship Final Report

MECHANISMS OF BONE MINERALIZATION AND EFFECTS OF MECHANICAL LOADING

Michael Babich, Ph.D.
Assistant Professor of Pharmacology
University of Illinois College of Medicine
Rockford, Illinois

INTRODUCTION

The study of osteoblast function under different gravitational forces is important to understand and prevent loss of bone mass associated with spaceflight-induced weightlessness. Osteoblasts are bone-forming cells responsible for the production of a mineralized collagenous matrix. They appear in clusters of cuboidal cells on the bone surface, similar to the side by side orientation of simple epithelium, and are considered the primary target cells for bone regulating agents. Osteoblasts also regulate bone resorption indirectly. In accordance with a current hypothesis on bone remodeling, factors that cause osteoblasts to contract and separate from one another enable the osteoclast, the cells responsible for resorption, to gain access to the mineralized matrix. Subsequent stimulation of osteoblasts by hormones or cytokines following disruption of cadherin-mediated cell-cell adhesion may then activate specific signals that either generate osteoclast activating factors or promote the growth of bone.

Parathyroid hormone is a classic regulatory hormone for bone that stimulates adenylate cyclase and phospholipase C. However, the reported effects of PTH on 1,4,5-IP_3 accumulation and intracellular free calcium, as an index of PLC stimulation, are variable (0- to ~3-fold increases). Furthermore, the control of these cellular pathways and their role in mediating the physiologic effects of PTH are poorly understood. It is also perplexing how, in certain circumstances, PTH elicits both catabolic and anabolic effects on bone. In this regard, the relationship between cell shape and function has long been noted, but the regulation of this relationship and whether shape dictates function (or vice versa) is not understood. Protein kinase C (PKC) presumably is one cellular factor that affects cell morphology and regulates hormonal signaling. Data with various osteoblastic cell models demonstrate that PKC activators enhance intercellular osteoblast contact. Subsequently PTH-stimulated adenylate cyclase and cellular contraction is potentiated, whereas no change in cellular 1,4,5-IP_3/Ca_i^{2+} is detected. In contrast, PKC inhibitors induce cellular contraction with distinct stellate configurations. In addition, an ability for PTH to elicit 1,4,5-IP_3/Ca_i^{2+} increases and cellular respreading is unmasked.

The available data suggest that factors which affect osteoblast cell shape (e.g., via PKC effects on CSPs) may alter cellular responses to agonists. The idea that gravity itself is a cell modulating factor is supported by observations during spaceflight whereby cultured osteoblasts become contracted (Genry et al., *J Bone Min Res* 8(1):S367, 1993; Hughes-Fulford and Lewis, *Expt Cell Res* 224:103-109, 1996) and the effectiveness of PKC on proto-oncogene expression is decreased (de Groot et al., *Exp Cell Res* 197:87-90, 1991). Thus, microgravity conceivably induces an osteoblastic state that favors bone

resorption. Experiments related to osteoblast CSPs and signal transduction with a centrifuge cell culture system (Malouvier et al., *Am Soc Grav Space Biol Bull.* 8(1):180, 1994) will therefore contribute to our knowledge of bone and mineral metabolism regulation by gravitational force. Furthermore, a greater understanding of the normal mechanisms of bone mineralization is important to determine how the process is changed upon spaceflight or certain Earth-borne bone diseases.

METHODS and RESULTS

Prenatal rat calvarial bone was isolated in enzymatically digested to yield primary cultures of osteoblasts. Cells were cultured onto 8-well plastic chamber slides or 35 mm culture dishes. Three days after the initial cell isolation, ascorbic acid and beta-glycerol phosphate was added to the normal growth medium to initiate differentiation to a more mature osteoblastic phenotype. On day ten, evidence of mineralization of the cell cultures (i.e., nodules) became evident and continued to enlarge up through day 17. At day 10, various treatments were added to the cells to ascertain the mechanism of nodule formation and the mechanism of PTH action on bone mineralization.
The following analyses were performed:
1) immunocytochemical fluorescence microscopy techniques to localize key cytoskeletal proteins involved in cell signaling and shape (cadherins, profilin, actin)
2) analytical biochemistry (glucose consumption/lactate production)
3) centrifugation, treatment with bovine parathyroid hormone (1-84) (PTH) and/or signaling modulators (i.e., specific enzyme activators or inhibitors)
4) microphotographs of nodule formation within each cell culture well.

EFFECTS OF PTH AND PKC INHIBITOR ON BONE CELL MINERALIZATION.

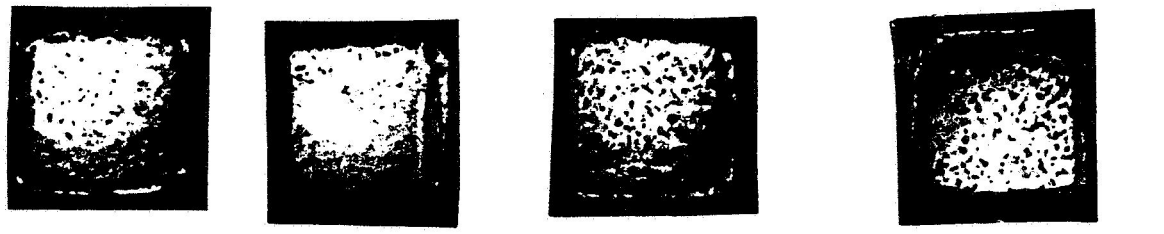

VEHICLE PTH CALPHOSTIN C CALPHOSTIN C + PTH

Rat osteoblasts grown in 8-well chamber slides were treated with either vehicle, bPTH(1-84) (100 nM), the protein kinase C inhibitor calphostin C (30 nM), or a combination thereof. Phase-contrast microscopy was used to photograph and visualize the nodules (dark spots; day 13 of cell culture shown).

Little is known regarding the cellular second messengers that affect bone mineralization. Recent work indicates that cyclic AMP is an intracellular mediator of decreased nodule formation. Furthermore, PTH stimulates cAMP production in osteoblasts and inhibits mineralization. Because the PTH receptor is a target of PKC-

mediated phosphorylation and presumably regulation, we therefore examined the effects of PTH on bone mineralization in the presence and absence of a protein kinase C inhibitor (i.e., staurosporine or calphostin C, as shown). Nodule formation was evident and progressive from days 10 through 17 (Figure above; day 13 shown). PTH had an inhibitory effect on nodule formation. In stark contrast, inhibition of PKC led to an increase in nodule formation, and reversed the inhibitory effects of PTH. The results are consistent with the idea that PTH produces cAMP-dependent inhibition of nodule formation. The data also suggest that PKC exerts an endogenous inhibitory tone on nodule formation.

The energy requirements and sources were initially investigated by measurements of glucose consumption and lactate production (Table below). There was a progressive utilization of glucose by control and PTH treated cells (i.e., no significant glucose remaining in the medium) that was associated with an expected increase in lactate production. In contrast, PKC-inhibitor treated cells (calphostin C shown) do not utilize glucose and little lactate is produced. The data indicate that alternative energy sources are utilized by osteoblasts in the process of mineralization.

GLUCOSE CONSUMPTION AND LACTATE PRODUCTION OF OSTEOBLASTS

	CONTROL	PTH	Cal C	PTH + Cal C
GLUCOSE	0	0	5.9	5.8
LACTATE	8.8	9.0	2.7	2.6

Samples of the growth medium (containing ~5.8 mmol glucose/L) were taken at various time points following treatment (24 treatment shown) and analyzed for glucose consumption and lactate production. The data represent the mean (mmol/L) of 4 samples each (standard error was within 5% of each mean).

CONCLUSIONS and FUTURE DIRECTIONS

The data suggest that PTH and PKC inhibit nodule formation, and that alternative energy sources are utilized by osteoblasts in the process of mineralization. The conditions and techniques to grow, fix, photograph, and measure bone mineralization in vitro were defined. The results are presently in preliminary form and require further assessment as follows;

- quantitate the surface area of nodules ± treatments via computer-aided image analysis
- use PTH ± inhibitors of signaling pathways to determine the mechanism of nodule formation
- determine how protein kinase C is involved as a promotor of nodule formation
- cell proliferation vs. cell death affected by modulation of signal transduction (i.e., PTH, enzyme inhibitors and activators)
- identify mRNA induced or decreased in response to PTH and signaling modulators that encode proteins that regulate cell morphology, proliferation, and nodule formation.

Therefore, several follow-up studies between the laboratories at NASA-Ames Research Center and my laboratory at the University of Illinois have been initiated.

1996 NASA-ASEE-Stanford Summer Fellowship
Final Report

Analytic Methods for Predicting Significant Multi-Quanta Effects in Collisional Molecular Energy Transfer

Ronald J. Bieniek
Associate Professor, Physics Department
University of Missouri-Rolla

1. Introduction

Collision-induced transitions can significantly affect molecular vibrational-rotational populations and energy transfer in atmospheres and gaseous systems. This, in turn, can strongly influence convective heat transfer through dissociation and recombination of diatomics, and radiative heat transfer due to strong vibrational coupling. It is necessary to know state-to-state rates to predict engine performance and aerothermodynamic behavior of hypersonic flows, to analyze diagnostic radiative data obtained from experimental test facilities, and to design heat shields and other thermal-protective systems. Furthermore, transfer rates between vibrational and translational modes can strongly influence energy flow in various "disturbed" environments, particularly where the vibrational and translational temperatures are not equilibrated.

However, it is generally very difficult to measure these experimentally, due to high temperatures and coupled decay paths. Generally, only the lowest vibrational transitions are known, and usually only over a limited temperature range [1]. Thus it is vital to have a means of accurately predicting desired, but unknown transition rates from only a few known rates. The Reacting Flows Environment Branch (STA) of NASA's Ames Research Center has been at the forefront of incorporating such information is aerospace design and analysis.

Generally, only transitions between adjacent vibrational levels are included in modeling calculations. This situation arises because of major difficulties in measuring multi-quanta rates experimentally and complexities in theoretical computations beyond first-order. However, a method of accounting for multi-quantum effects, based on a perturbation expansion of analytic first-order elements, was investigated as this summer's project. As before, $N_2(n) + N_2(v)$ collisions were studied because of their importance in aerospace studies [2]. The approach proved to a relatively easy and accurate method of predicting multi-quantum transitions and their effects on single-quantum rates.

2. Multi-Quanta Methods

Vibrational excitation and relaxation can be adequately described by the breathing-sphere approximation [3]. The perturbation between colliding molecules *1* and *2* can be modeled by an exponential repulsive interaction $V(r,R) = A \exp[-\alpha(R - s_1 r_1 - s_2 r_2)]$, where R is the collisional distance, r is the molecular stretch coordinate, s the relative strength of vibrational coupling, and α is the exponential slope of the collisional interaction, the only adjustable parameter in the model. Morse oscillators were used to evaluate vibrational coupling elements $Vq_{i-f} = \langle n_{q,i} | \exp(s_q \alpha r) | n_{q,f} \rangle$ analytically.

While working last year in branch STA with NASA colleague Dr. S. Sharma, I produced a very simple first-order expression for collisional transition rates, based on the analytic evaluation of

the coupling between the continuum scattering states of an exponential potential [4] and employment of the method of steepest descent to do the thermal average over collisional energies:

$$R_{sd}(T)_{i\text{-}f} \approx C\frac{|\Delta\varepsilon_{i\text{-}f}|^4}{(k_BT)^{3/2}}\, V1^2_{i\text{-}f}\, V2^2_{i\text{-}f}\, |F_{21}(Y_{i\text{-}f})|^2\, e^{g_{i\text{-}f}(Y_{i\text{-}f})}\sqrt{\frac{2\pi}{\left|g''_{i\text{-}f}(Y_{i\text{-}f})\right|}}$$

where $g_{i\text{-}f}(y) = \beta_{i\text{-}f}\left[\sqrt{ay} - \sqrt{1+ay}\right] - \dfrac{|\Delta\varepsilon_{i\text{-}f}|}{k_BT}y + \ln(y)$, with $Y(T)_{i\text{-}f}$ the root of:

$$2Y\cdot g'_{i\text{-}f}(Y) = \sqrt{aY} - \frac{aY}{\sqrt{1+aY}} - \left[\frac{2|\Delta\varepsilon_{i\text{-}f}|}{\beta_{i\text{-}f}k_BT}\right]Y + \frac{2}{\beta_{i\text{-}f}} = 0 \ , \quad \text{and } \beta_{i\text{-}f} = 2\pi\frac{\sqrt{2\mu|\Delta\varepsilon_{i\text{-}f}|}}{\hbar\alpha}$$

$\Delta\varepsilon_{i\text{-}f}$ is the change in vibrational energy, μ is the collisional reduced mass, $a = 0.85$, and C is a constant that depends upon the particular collision system under study. $F_{21}(y)$ is a particular evaluation of the hypergeometric function ${}_2F_1$. The most effective incident kinetic energy causing the transition (i→f) is $K_e(T)_{i\text{-}f} = \Delta\varepsilon_{i\text{-}f}\cdot Y(T)_{i\text{-}f}$, which is several times $^3/_2\, k_BT$.

The analytic first-order coupling elements between continuum scattering states can used to obtain an Nth-order perturbation expansion of the full transition matrix . Five quantum numbers are needed to specify these elements <n,v,L,E|V|n',v',L,E> within the breathing-sphere approximation: collisional angular momentum L, initial vibrational state (n,v), and final state (n',v'). The first-order matrix **t** is constructed as $t(L,E)_{n\cdot nt2+v,n'\cdot nt2+v'}$ = <n,v,L,E|V|n',v',L,E> (where *nt2* is the size of the vibrational basis set for molecule 2), but can be designated as $t^{vv'}_{nn'}$. Using spectral decomposition techniques, one can accurately compute the Nth-order transition matrix $\mathbf{T}^N$ and corresponding quantal partial-wave rates $R^N_Q(K_i,L)_{i\text{-}f}$ for incident collisional energy K_i (associated with total energy $E_i = K_i + \varepsilon_i$) to determine state-to-state rates $R^N_Q(K_i)_{i\text{-}f} = \sum R^N_Q(K_i,L)_{i\text{-}f}$ summed over all L:

$$R^N_Q(K_i,L)_{i\text{-}f} = \left[\frac{2K_i}{\mu}\right]^{1/2}\frac{2\pi^3\hbar^2}{\mu K_i}(2L+1)|T^N(E,L)_{i\text{-}f}|^2 \quad \text{with} \quad \mathbf{T}^N(E,L) \approx \frac{i}{\pi}\sum_{k=1}^{N}[-i\pi\mathbf{t}(E,L)]^k$$

Much interpretive insight into multi-quanta effects comes from the analytic nature of the underlying first-order **t**(E,L). The elements $t^{vv'}_{nn'}$ have two important functional behaviors: 1) they get larger as the total change in vibrational energy gets smaller because of better overlap of the continuum collisional wavefunctions, and 2) they get smaller with increasing change in vibrational quantum numbers because of the rapid decrease in the strength in the vibrational coupling $Vq_{i\text{-}f}$.

3. Summary of Results

Convergence of cross sections to two-significant figures was obtained using a vibrational basis set for a given molecule that was one higher than $\max(n_{qi},n_{qf})$ and one lower than $\min(n_{qi},n_{qf})$, and that $N = nt1\cdot nt2$. The perturbation expansion then produces a sum of products of first-order elements that represent all transitional paths from $(n_i,v_i) \rightarrow (n_f,v_f)$. For example, for the (8,0)→(6,0) transition, $T^{00}_{86} = t^{00}_{86} + (-i\pi)[\, t^{00}_{87}\, t^{00}_{76} + t^{01}_{87}\, t^{10}_{76} + \cdots] + (-i\pi)^2\, [t^{00}_{89}\, t^{01}_{97}\, t^{10}_{76} + \cdots]$. It was discovered that

the dominate contributions to a given rate come from single-quanta transitional paths, e.g., the virtual-path term $(-i\pi)[\, t_{87}^{00}\, t_{76}^{00} + t_{87}^{01}\, t_{76}^{10}\,]$ for the (8,0)→(6,0) transition.

Numerical predictions of rates by the expression $Rsd(T)_{i-f}$ are in excellent agreement with the temperature-dependent experimental results [1] for the lowest (1,0)→(0,0) transition in $N_2 + N_2$ collisions. They also agree well with detailed trajectory computations [5] for higher initial activation ($n_i \leq 20$) at temperatures $T \leq 2000$ K, using an exponential slope α fitted to the full theoretical potential. However, the predicted relative rate for (20,0)→(19,0) is a factor of 3 too large at 6000 K. Attempts have been made to find semi-empirical correction factors to such first-order theories [6]. But these are totally heuristic and require prior knowledge from large-scale computations of the very collision being modeled, and cannot be transferred from system to system. It was discovered that theoretical rates and semi-empirical correction factors can be extremely sensitive to the system parameters employed, and care must be taken in comparing results from different computations.

Multi-quanta effects may produce the high temperature discrepancy at high initial vibrational excitation. Since the thermally averaged first-order expression $R_{sd}(T)_{ni-ni-1}^{00}$ accurately predicts the temperature dependence for the (1,0)→(0,0) transition, it can be used as a base to predict multi-quanta phenomena. Such effects can be incorporated analytically by appropriate scaling factors $c_{Lmax}(T)_{i-f}$ formed from the ratio of multi-order to first-order quantal rates evaluated at the most effective collisional energies out of the thermal ensemble: $R(T)_{i-f} = c_{Lmax}(T)_{i-f}\, R_{sd}(T)_{ni-ni-1}^{00}$. Two somewhat different correction factors were tested, $c_0(T)_{i-f}$ obtained from s-wave scattering ($L_{max}=0$) and $c_\infty(T)_{i-f}$ obtained from quantal rates incorporating all collisional angular momenta ($L_{max} = \infty$):

$$c_0(T)_{i-f} = \frac{R_Q^N(K_e(T)_{n_i-n_f}^{v_i-v_f}, L=0)_{n_i-n_f}^{v_i-v_f}}{R_Q^1(K_e(T)_{n_i-n_i-1}^{0-0}, L=0)_{n_i-n_i-1}^{0-0}} \quad \text{and} \quad c_\infty(T)_{i-f} = \frac{R_Q^N(K_e(T)_{n_i-n_f}^{v_i-v_f})_{n_i-n_f}^{v_i-v_f}}{R_Q^1(K_e(T)_{n_i-n_i-1}^{0-0})_{n_i-n_i-1}^{0-0}}$$

As hoped, $c(T)_{i-f}$ was near unity for $T \leq 2000$ K, retaining the excellent agreement with trajectory computations. For T = 6000 K, $c_0(T)_{1-0}^{00} \approx c_\infty(T)_{1-0}^{00} \approx 1$, while $c_0(T)_{20-19}^{00} \approx ½$ and $c_\infty(T)_{20-19}^{00} \approx ⅓$. The latter brought the predicted rates into excellent agreement with the trajectory computations at high initial activation for elevated temperatures. Furthermore $c_\infty(T)_{i-f}$ predicts double-quanta rates, e.g. (n,1)→(n+1,0), to within an order of magnitude. It was determined that double-quanta rates and multi-quanta effects would significantly impact diagnostics based on vibrational populations, and noticeably affect bulk energy-transfer rates in certain aerothermodynamic circumstances.

References

[1] R. Millikan and D. White, *J. Chem. Phys.* **39**, 3209 (1963).

[2] S.P. Sharma, W.M. Huo, and C. Park, *J. Thermophys. Heat Trans.* **6**, 9 (1992); S.P. Sharma, S.M. Ruffin, W.D. Gillespie, and S.A. Meyer, *J. Thermophys. Heat Trans.* **7**, 693 (1993).

[3] R.J. Bieniek, *J. Chem. Phys.* **73**, 851 (1980); and references therein.

[4] T.F. Ewing and R.W. Conn, *Chem. Phys.* **26**, 201 (1977).

[5] G.D. Billing and E.R. Fisher, *Chem. Phys.* **43**, 395 (1979).

[6] S.M. Ruffin, *Vibrational Energy Transfer of Diatomic Gases in Hypersonic Expanding Flows*, Ph.D. dissertation, Stanford University, 1993.

1996 NASA-ASEE-Stanford Summer Faculty Fellowship Program

Final Report

Simulation and Modeling of the Elliptic Streamline Flow

Gregory A. Blaisdell

Assistant Professor, School of Aeronautics and Astronautics

Purdue University, West Lafayette, IN

1 Introduction

This summer was the second year of my NASA-ASEE Summer Faculty Fellowship. I worked in the Turbulence Physics and Modeling Branch in collaboration with Karim Shariff. We used direct numerical simulation (DNS) to study homogeneous turbulence with a mean flow having elliptic streamlines. This flow combines the effects of rotation and strain on the turbulence. There are many important reasons for studying the elliptic streamline flow. This flow contains the effects of both rotation and strain and is therefore similar to the mean flow in a vortex strained in the plane perpendicular to its axis. Such flows provide insight into the fundamental vortical interactions within turbulence. A strained vortex also occurs in airplane wakes, in which each wingtip vortex induces a strain field on the other. The strain field can affect the stability of these vortices and thereby their turbulent structure downstream. The ability to understand and predict the turbulent structure of the vortices is important to the wake hazard problem which is of major concern for the safety of commercial aircraft.

The elliptic streamline flow is also a good test case for turbulence models for rotating flows. Current engineering turbulence models generally do not perform well in rotating flows. The DNS of the elliptic streamline flow will provide detailed information that can be used to test and improve turbulence models. The elliptic streamline flow has an added complication beyond that of pure rotation, which has been studied previously.

The elliptic streamline flow is depicted in figure 1. The mean velocity is linear in space and combines solid body rotation, with rotation rate γ, and uniform strain at 45°, with strain rate e. Two parameters for the elliptic streamline flow which can be derived from γ and e are E the aspect ratio of the elliptic streamlines and Ω the rotation rate of a fluid element traversing the elliptic streamline.

This work is the continuation of a project first started during the 1994 Center for Turbulence Research summer program. In the summer of 1994 a computer code developed by Bob Rogallo (NASA Ames Associate) was modified to do the elliptic streamline case. The subroutines for calculating statistics and spectra were expanded and some preliminary simulations were performed. Last summer a series of simulations were performed in order to gain insight into the behavior of the turbulence in the elliptic streamline flow.

The objectives of the work this summer were to perform larger simulations in order to better understand the flow physics and to create data for comparison with turbulence

models. Simulations were performed over a range of the parameter space which includes the aspect ratio of the elliptic streamlines, E, the ratio of the turbulence time scale to the rotation time scale, $\gamma k/\varepsilon$, where k is the turbulent kinetic energy and ε is the dissipation rate, and the Reynolds number.

2 Simulations and Results

The numerical simulations were performed on the IBM SP2 parallel computers at NASA Ames and Purdue. Preliminary simulations were done using grids with $128 \times 220 \times 128$ grid points and longer simulations were done using grids with $256 \times 440 \times 256$ grid points.

Special care was taken to ensure the simulations captured the instability predicted by linear stability analysis. The elliptic streamline flow is unstable for nonzero values of the strain rate (E not equal to 1), as shown by the stability analyses of Bayly (1986) and Landman and Saffman (1987). However, for aspect ratios E close to one it is difficult for the numerical simulations to capture the instability. Cases with low strain rates are especially of interest for the airplane wake hazard problem because there the strain rates are low. The problem is that only a small band of Fourier modes are unstable. If the computational domain does not support any of these modes then the instability can be lost. However, by choosing the computational domain in such a way that the some of the unstable modes are supported, the instability can be captured. Much of the work of last summer involved testing the variability of the simulation results to numerical parameters such as grid aspect ratio. This summer simulations were performed using grid arrangements that captured the instability.

Simulations were performed for aspect ratios $E = 1.1, 1.25, 1.5, 2.0$, and 3.0. Although the simulations at $E = 1.1$ capture the instability, the band of unstable wavenumbers is so thin that the sampling of unstable modes is low and so the results are unreliable.

The simulations show that linear effects are dominant during the early times and that nonlinear effects become significant at later times. During the early portion of the simulations, the turbulence follows the trends from linear stability analysis and the simulations with higher γ (lower E for fixed e) have higher growth rates. However, at later times the turbulence seems to approach a lower growth rate that is independent of E.

The simulation results were compared to two full Reynolds stress models — the Lander, Reece and Rodi (LRR) model and the Sarkar, Speziale and Gatski (SSG) model. Figure 2 shows the turbulent kinetic energy for the case $E = 1.25$, which is a strongly rotating flow. The turbulence models both predict that the strong rotation stabilizes the flow; however, the DNS shows exponential growth. For aspect ratios $E = 2.0$ and 3.0 the models give growth, but at too low a rate. The models are seen to give the wrong behavior in this flow making prediction of such flows difficult.

3 Future Work

The DNS performed this summer are useful in both understanding the physics of the elliptic streamline flow and in making comparisons with turbulence models. However, the simulations were started in a way that makes the Reynolds number very low — lower than what is necessary. It was found that the rate of growth of the turbulence statistics is dependent on Reynolds numbers for the low Reynolds numbers used in the simulations.

Therefore, in order to use quantitative results from the simulations in developing high Reynolds number turbulence models, simulations at higher Reynolds numbers are needed. By altering the method for generating initial conditions higher Reynolds numbers can be achieved. Future work will focus on performing these simulations. In addition other homogeneous flows with combinations of strain, fluid rotation (vorticity) and system rotation will be considered.

References

Bayly, B. J. 1986 Three dimensional instability of elliptic flow. *Phys. Rev. Lett.* **57**, 2160–2171.

Landman, M. J. & Saffman, P. G. 1987 The 3-D instability of strained vortices in a viscous fluid. *Phys. Fluids* **30**, 2339–2342.

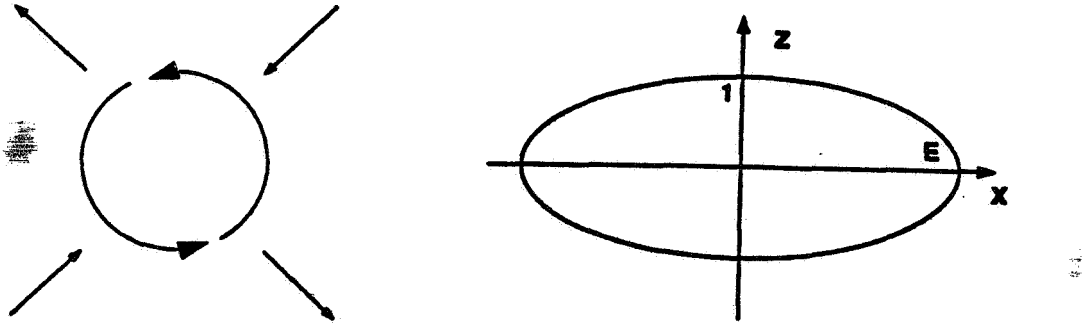

Figure 1. (a) Schematic view of the combination of rotation and strain. (b) Elliptic streamline.

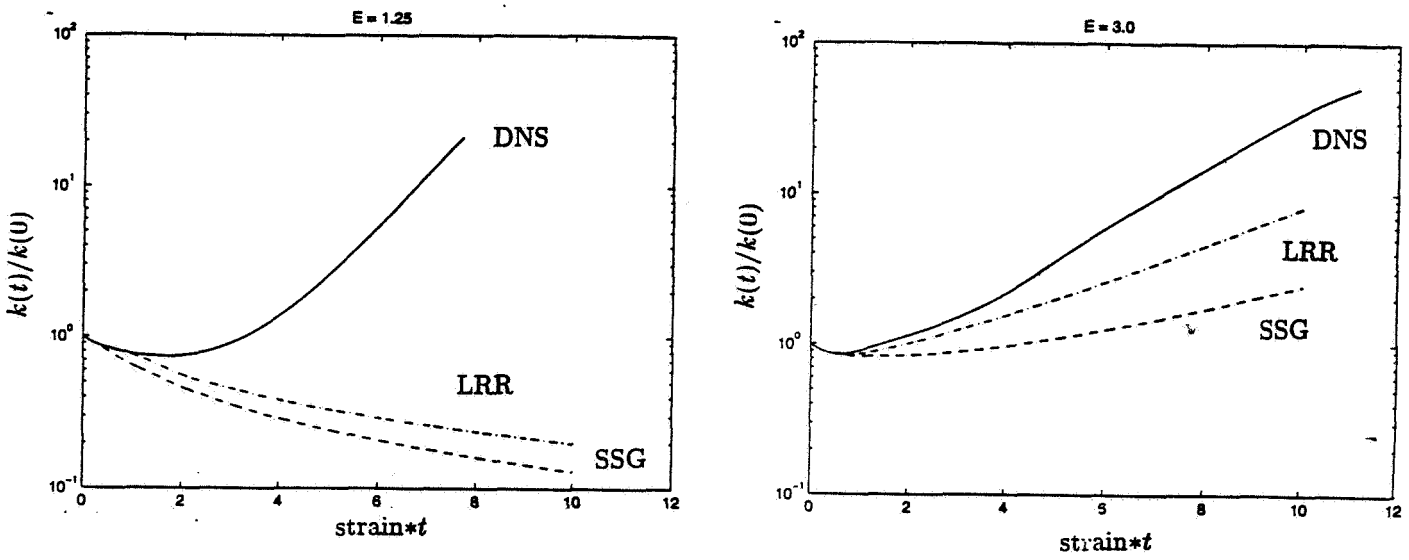

Figure 2. Evolution of the turbulent kinetic energy, k, for (a) $E = 1.25$ and (b) $E = 3.0$.

AERODYNAMIC OPTIMIZATION OF THE HIGH SPEED CIVIL TRANSPORT

54-05
60 7860
25776|
P5

Stephen C. Brawley
1996 NASA-ASEE-Stanford Summer Faculty Fellow

Abstract

The aerodynamic optimization program used for wing and fuselage optimization of the High Speed Civil Transport was modified for utilization of multiple processors on parallel processor computers. The modified version uses multiple processors to simultaneously conduct three-dimensional flow solutions of different wing and fuselage geometries for calculations of the gradient functions and for directional searches to minimize an objective function. Demonstrations have shown the parallel program to be useful for coarse grid optimization, however memory problems for processors on the IBM SP2 were encountered when finer grid sizes were used.

Introduction

The High Speed Civil Transport (HSCT) is a future supersonic commercial transport for up to 300 passengers and with a maximum range of 5000 nautical miles. Preliminary development of the NASA High Speed Civil Transport has been conducted by NASA Langley and NASA Ames Research Centers, Boeing Corporation, and McDonnell Douglas Corporation . The cruise speed for the transport is Mach 2.4. Primary aerodynamic research has focused upon drag reduction of the wing-body configuration with nacelles. Optimization techniques have been used on supersonic wing-body configurations with gradient-based searches to minimize an objective function based upon drag.

One optimization program, QNMDIF, utilizes a quasi-newton method to search for a minimum[1]. In QNMDIF, a multivariable objective function, f, is defined by a vector of n design variables:

$$f(\mathbf{X}) = f(x1, x2, x3 \ldots xn) \quad (1).$$

The gradient, **G**, is the vector of first order partial derivatives of the objective function with respect to the design variables:

$$\mathbf{G} = \delta\mathbf{X}/\,\delta f = (\,\delta x1/\,\delta f, \delta x2/\,\delta f, \delta x3/\,\delta f, \ldots, \delta xn/\,\delta f\,) \quad (2).$$

The partial derivatives can be calculated by using central differences as follows:

$$\delta x1/\,\delta f = (\,f(x1+\Delta x, x2, \ldots, xn) - f(x1-\Delta x, x2, \ldots, xn)\,) \,/\, (\,2\,\Delta x\,) \quad (3).$$

For n design variables, 2n function evaluation would be required for each gradient calculation using central-differencing. Of note, Reuther has developed an alternative method using adjoint solutions in aerodynamic optimization to obtain the components of the gradient[2].

After the gradient is calculated, the quasi-Newton optimization program uses an estimate of the Hessian matrix of second-order partial derivatives, **H**, to calculate a vector to search for a local minimum of the objective function, **P**:

$$\mathbf{H} = \delta^2\mathbf{X} \,/\, \delta f^2 \quad (4),$$

$$\mathbf{H}\,\mathbf{P} = -\,\mathbf{G} \quad (5).$$

The new set of design variables is described by the equation:

$$\mathbf{X}^{k+1} = \mathbf{X}^k + \alpha\,\mathbf{P} \quad (6),$$

where α is a positive scalar defining the distance along **P** being searched for a minimum.

A directional search is conducted in the direction **P** with varying α to locate a new set of design variables which correspond to a minimum objective function. After the line search is completed, the optimization cycles continues with more gradient calculations and directional searches based upon the new set of design variables.

Utilization of Parallel Processors

Brawley has successfully used parallel computers for two-dimensional aerodynamic optimization of airfoils and turbine blades[3,4]. Utilization of multiple processors can greatly reduce the amount of processing time required for optimization applications involving expensive objective functions, such as with aerodynamic optimization. Multiple objective function calculations are required for estimations of the gradient vectors using finite differences and for directional searches to locate a minimum.

The IBM SP2 parallel computer of the Numerical Aerodynamic Simulation laboratory (NAS) at NASA Ames Research Center consists of 160 RISC System processors. Each processor functions at a speed of 66.7 megahertz and has 256 megabytes of memory. Also, communication between processors can be accomplished using MPI message passing routines. In comparison, the Cray C-90 has 16 processors, each with faster speeds and more memory, but currently does not support MPI message passing routines.

For gradient calculations, each partial derivative requires two function evaluations for central-differencing estimates as shown by equation (3). For 50 design variables, 100 function evaluations would be required. Utilizing 100 processors of the IBM SP2, all 100 function evaluations can be conducted simultaneously with each processor evaluating a different set of design variables.

Similarly, directional searches can be conducted in parallel. After the direction of search is calculated, each processor is assigned a unique value of α to evaluate a new set of design variables as shown in equation (6). The resulting objective functions are compared, and the design variables corresponding to the minimum objective function becomes the new baseline set.

Application to High Speed Research

For aerodynamic optimization of the High Speed Civil Transport, each objective function calculation requires a complete computational fluid dynamics (CFD) flowfield solution. Typically the objective function to be minimized is the drag or drag-to-lift ratio. A Runge-Kutta scheme Euler flow solver is used, and grid sizes vary with finer and courser versions. The design variables define airfoil thickness and camber at different points of the wing and factors such as its taper ratio.

The parallel version of QNMDIF was used with the 3-D flow solver and grid generator for optimization of the HSCT at cruise Mach number of 2.4. Figures 1 and 2 show pressure distributions of the surface of an optimized design with higher pressures corresponding to the red side of the visible spectrum and lower pressure at the violet side. In Figure 1, no strong shocks are seen on the upper surface of the design. Figure 2 shows that the primary regions of design changes involve the 4 nacelles which have strong shocks associated with them.

Initial utilization of the parallel optimization routine on the IBM SP2 for HSCT research revealed memory limitations compared with similar applications run on the Cray C-90. This problem was handled by reducing the number of grid points and using a lower numerical precision. Although, the code was tested and shown to work correctly, the results were not reliable due to the reduced precision and coarser grid sizes.

Future Work

Future HSCT optimization applications should use the parallel QNMDIF optimization scheme when practical. The replacement for the IBM SP2 will have sufficient memory for HSCT research, and it should be at NAS by September, 1997. Additionally, HSCT parallel optimization applications can be run on the Cray C-90 beginning in October, 1996 after MPI message routines are supported for its use. Furthermore, two dimensional

aerodynamic optimization problems with fewer grid points than used for HSCT research applications can use the parallel optimization program.

References

[1] R. Kennelly. Improved method for transonic airfoil design-by-optimization. *AIAA paper 83-1864*, AIAA Applied Aerodynamics Conference, Danvers, Massachusetts, July 1983.

[2] J. Reuther. Aerodynamic shape Optimization of complex aircraft configurations via an adjoint formulation. *AIAA paper 96-0094*, AIAA 34th Aerospace Sciences Meeting and Exhibit, Reno, Nevada, January 1996.

[3] S. Brawley. Airfoil Design Utilizing Parallel Processors. *AIAA paper 95-125*, AIAA 33th Aerospace Sciences Meeting and Exhibit, Reno, Nevada, January 1995.

[4] S. Brawley. Advanced Turbine Blade Optimization Utilizing Parallel Processors. *AIAA paper* , AIAA 34th Aerospace Sciences Meeting and Exhibit, Reno, Nevada, January 1996.

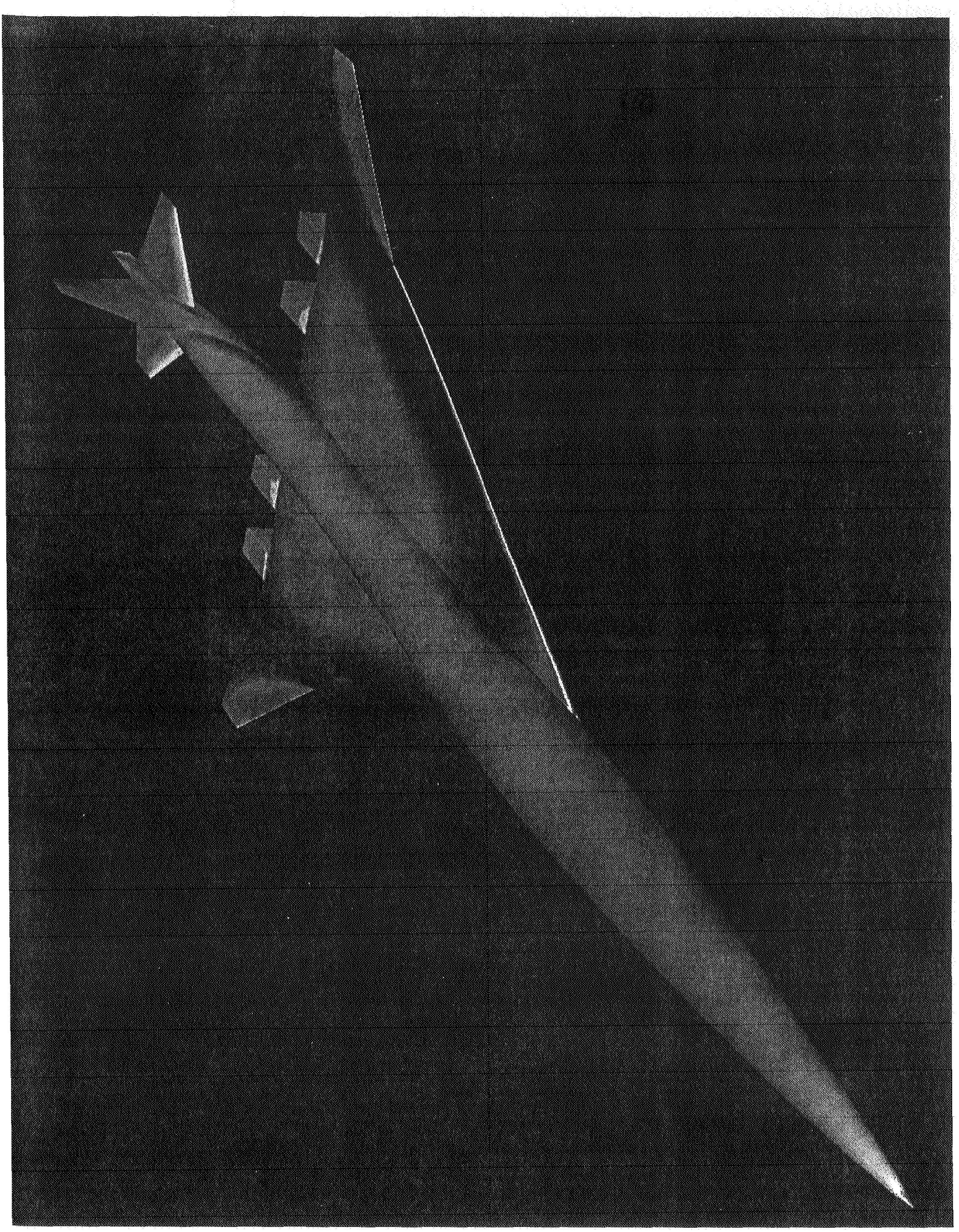

Figure 1

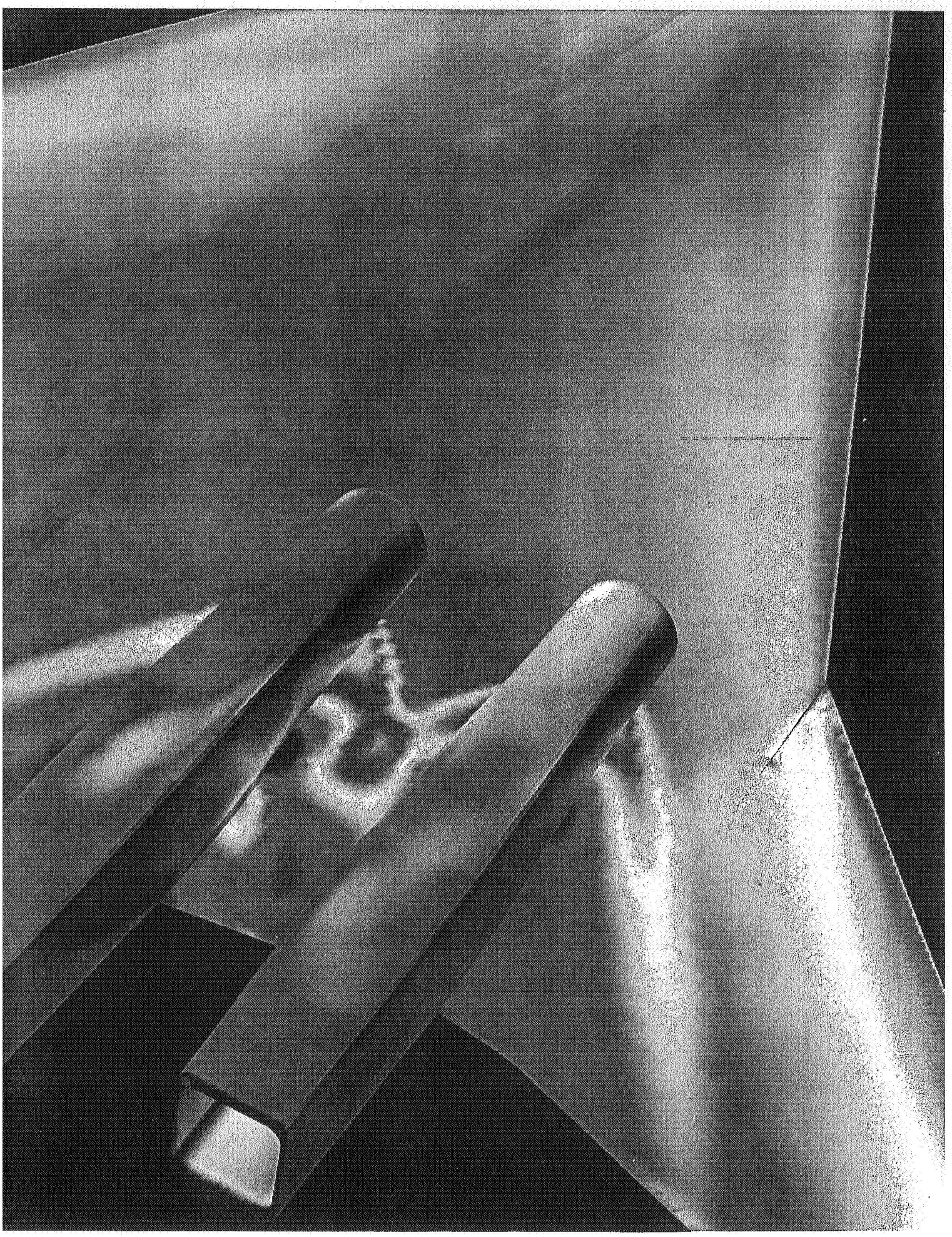

Figure 2

1996 NASA-ASEE Stanford Summer Faculty Fellowship Final Report

Use of Density Functional Method to Study Molecular Vibrations

Delano P. Chong, Professor of Chemistry, University of British Columbia
Vancouver, B.C., Canada V6T 1Y6

Introduction. The work I carried out during the summer of 1995, in collaboration with my NASA Ames colleague Dr. C.W. Bauschlicher, Jr., involves the use of density functional theory (DFT), rather than traditional *ab initio* quantum chemistry, to model the thermochemistry of reactions of water with the nonablating reusable heat shields, hereon called the heat tiles (or tiles for short), which are composed of porous composite of silica, alumina, and aluminoborosilicate fibers. In order to eliminate the labor-intensive waterproofing of the tiles after each reentry, we tried to find a way to modify the tile material chemically to make the surface hydrophobic, such as replacing the surface -OH groups with -X (X = F, Cl, or other groups), while maintaining thermal stability. Before my arrival at NASA, Bauschlicher had already compared DFT with high-level *ab initio* computations for some simple models of silica-water reactions, and concluded that DFT with the exchange-correlation functional known as B3 for exchange and LYP for correlation gives semiquantitative results. He had also studied the problem of waterproofing silica by chemical modification, with 1 to 4 silicon atoms in the model cluster using the B3LYP functional. My project then was to investigate the alumina-water reactions in a parallel study.

My computations in the summer of 1995 were concerned with reactions of surface -OH bonds with water. My model clusters consisted of two aluminum atoms with bridging OH groups as well as terminating O or OH groups. I found that replacing the bridging OH by F or Cl did not make the halogenated model molecules hydrophobic as indicated by exothermic wetting reactions. We conclude that it is highly unlikely that one could alter the chemical surface of the heat tiles to make them hydrophobic. Consequently, the project this summer changes to trying to understand surface infrared (IR) measurements of the heat tiles. To model the tiles, we use molecules containing H, Si, and O, up to $H_8Si_4O_{12}$.

Computational Details. For each molecule, we first optimize the geometry of the structure using the B3LYP functional and a polarized valence double-zeta basis set called 6-31G** with the computer program Gaussian 94, installed on a cluster of ten IBM RS/6000 workstations at the Computational Chemistry Branch. Then, the harmonic vibrational frequencies (f) are computed. The B3LYP functional has been shown by other workers to give the most reliable potential energy surface for molecular vibrations. The choice of 6-31G** basis is a compromise between accuracy and computational efficiency.

We first validate our method, abbreviated as B3LYP/6-31G**, by comparing the vibrational frequencies of nine molecules, whose experimental harmonic frequencies ω are known. This set of molecules includes OH, HF, H_2O, CO_2, N_2O, H_2CO, HCN, HNC, and O_3. The wavenumbers ν of the vibrations range from 490 cm^{-1} to 3958 cm^{-1}. The results of our initial calculations are summarized in Table 1.

Table 1. Validation of scaled B3LYP/6-31G** method for molecular vibrations

(1) ω(obs)	ν(obs)	average absolute difference = 72 cm^{-1}
(2) 0.96 $\times$ ω(obs)	ν(obs)	average absolute difference = 25 cm^{-1}
(3) f(DFT)	ω(obs)	average absolute difference = 43 cm^{-1}
(4) f(DFT)	ν(obs)	average absolute difference = 95 cm^{-1}
(5) 0.96 $\times$ f(DFT)	ν(obs)	average absolute difference = 28 cm^{-1}

Based on our limited data set, we can draw some tentative conclusions: From comparison (1), we see that approximating vibrations by harmonic frequencies leads to errors of the order of 72 cm^{-1}. Fortunately, anharmonicities are large for the high-frequency stretching vibrations and tend to be small or negligible for low-frequency bending and other vibrations. Consequently, scaling ω by a factor of 0.96 in comparison (2) reduces the average absolute difference to 25 cm^{-1}. (3) compares

DFT harmonic frequencies against experimental harmonic frequencies and the result indicates that the chosen procedure of B3LYP/6-31G** can be quite efficient in modelling reality. (4) shows that f(DFT) is not much worse than ω(obs) in predicting ν(obs). It is the last comparison which is important for the present study. The scaled f(DFT) performs almost as well as the scaled ω(obs), with an average absolute deviation of only 28 cm^{-1} from experiment.

Molecules Detected by Withnall and Andrews. In 1985, Withnall and Andrews condensed SiH_4 and O_3 in argon at 17 K and recorded the IR spectra of the products of photolysis. By using isotopic SiD_4 and $^{18}O_3$, they were able to identify the silicon analogs of many common molecules like CH_3OH, CH_3OCH_3, H_2CO. HCOOH, and H_2CO_3. In Table 2, we compare our scaled B3LYP/6-31G** frequencies u(DFT) with the observed IR absorption in argon matrix.

Table 2. Comparison of scaled B3LYP/6-31G** frequencies[a], in cm^{-1}, with IR absorption in argon matrix

	^{16}u(DFT)	$^{16}\nu$(obs)	dev	^{18}u(DFT)	$^{18}\nu$(obs)	dev
trans HSiOH	3684	3661	23	3671	3649	22
	1932	1846	86	1935	1842	93
	940	938	2	935	933	2
	815	847	32	788	820	32
	780	723	57	779	720	59
	674	596	78	671	594	77
trans DSiOD	2681	2667	14	2665	2651	14
	1394	1352	42	1394	1359	35
	813	837	24	785	809	24
	702	716	14			
	564	523	41			
	492	448	44	489	445	44
cis DSiOD	816	843	27	791	817	26
SiH_3OH	876	859	17	869	851	18
SiD_3OD	844	874	30	822	850	28
H_2SiO	1170	1202	32	1133	1162	29
	683	697	14	679	694	15
D_2SiO	1155	1189	34	1115	1147	32
	530	533	3	526	530	4
SiH_3OSiH_3	1091	1101	10	1044	1060	16
	938	961	23	936	960	24
	722	746	24	717	740	23
SiD_3OSiD_3	1080	1087	7	1031	1039	8
	691	703	12	691	703	12
HSiOOH	1217	1249	32	1180	1211	31
DSiOOD	1211	1245	34	1172	1210	38
	850	891	41	817	866	49
H_2SiO_3	3713	3677	36	3700	3667	33
	1241	1270	29	1205	1232	27
	987	1023	36			
	438	453	15	436	451	15
	310	359	49	297	353	56
D_2SiO_3	2705	2710	5	2686	2694	8
	1241	1267	26	1204	1229	25
	954	994	40	929	969	40

788	919[b]	131	746	896[b]	150
356	376	20	348	368	20
293	349	56			

[a] $u(\mathrm{DFT}) = 0.96 \times f(\mathrm{DFT})$

[b] It is obvious that these two vibrations have been misassigned to D_2SiO_3.

Discarding the two misassigned absorptions, the average absolute difference between seventy scaled f(DFT) values and the experimental ν(obs) is only 30 cm^{-1}, in spite of the fact that the IR spectra were measured in solid argon. The results in Table 2 confirms almost all of the assignments of Withnall and Andrews as well as the reliable performance of our scaled B3LYP/6-31G** method.

Raman Spectra of Vitreous SiO_2 by Galeener and Mikkelsen. In 1981, Galeener and Mikkelsen reported the Raman spectra of a film of vitreous silica. By combined use of the ^{18}O-substituted spectrum and a central-force model, they assigned some vibrations to network, some to -OH, and some to defects. In subsequent papers, Galeener assigned the defect absorptions to planar rings of $(SiO)_n$, with $n = 3$ and 4. In order to understand the observe Raman spectra, I tested four cyclic silicon oxy-hydroxides with scaled B3LYP/6-31G** for frequencies and parallel *ab initio* RHF calculations for Raman intensities. $H_2Si_2O_5$ and $H_4Si_2O_6$ model face-sharing and edge-sharing tetrahedra, respectively, while $H_6Si_3O_9$ and $H_8Si_4O_{12}$ are 3-fold and 4-fold rings, respectively. The results are presented below.

Table 3. Comparison of $^{16}\nu$(obs) - $\Delta\nu$[a] with ^{16}u(DFT) - Δu[b] from various model molecules, all values in cm^{-1}

	Raman	$H_2Si_2O_5$	$H_4Si_2O_6$	$H_6Si_3O_9$	$H_8Si_4O_{12}$
Network	450 - 30				
Network	800 - 12		806 - 14	808 - 15	808 - 10
			817 - 12	825 - 16	
Network	1065 - 40				
Network	1200 - 45				
Defect D_1	495 - 30				459 - 19[c]
Defect D_2	606 - 31			579 - 32	
Si-(OH)	970 - 20		957 - 21	954 - 19	981 - 23
			960 - 19	976 - 19	
O-H	3695 - 15	3722 - 12	3727 - 12	3732 - 13	3740 - 12
		3724 - 13	3728 - 12	3732 - 12	3740 - 11
			3736 - 11	3735 - 11	
			3737 - 12	3736 - 12	

[a] $\Delta\nu = {}^{16}\nu(\mathrm{obs}) - {}^{18}\nu(\mathrm{obs})$ [b] $\Delta u = {}^{16}u(\mathrm{DFT}) - {}^{18}u(\mathrm{DFT})$ [c] Δu very different from $\Delta\nu$

It is not surprising that some of the network vibrations are difficult to model with two to four tetrahdra, whereas the Si-(OH) and O-H vibrations are present in all of our model molecules. Galeener's assignment of defect D_1 to $H_8Si_4O_{12}$ is not confirmed by our calculations, but his association of defect D_2 with $H_6Si_3O_9$ is very likely to be correct.

Conclusion Use of a scale factor reduces the errors in computed vibrational frequencies (errors due to anharmonicities, basis set deficiencies, and approximate treatment of electron correlation). Additional errors come from modelling solids with small molecules. Nevertheless, we hope that the present calculations add to the understanding of surface IR measurements of the heat tiles.

References

[1] R. Withnall and L Andrews, J. Phys. Chem. **89** (1985) 3261.
[2] F.L. Galeener and J.C. Mikkelsen, Jr., Phys. Rev. **B 23** (1981) 5527.

NASA-ASEE-Stanford Summer Fellowship 1996 - Final Report

Development of Minimally-Invasive Aortic Pressure and Flow Instrumentation

Dan Ewert
Associate Professor, Electrical Engineering
North Dakota State University, Fargo 58105

1. INTRODUCTION

To better understand the mechanisms underlying the effects of microgravity on the cardiovascular system, cardiovascular models have been developed [1]. These computational models estimate changes in cardiovascular parameters such as total peripheral resistance and systemic arterial compliance, and require high quality aortic pressure and flow measurements as their input. Many of these measurements are obtained in experimental animals and therefore the invasiveness of the instrumentation must be as kept to a minimum. These considerations are the primary motivation behind this work.

Minimally-invasive aortic pressure and flow instrumentation requires that the measurements are taken outside the aorta, information is telemetered out of the animal (no wires), and if possible, the transducers are positioned using thoracoscopic surgery techniques.

During the 1995 Summer Fellowship, a 5 MHz extravascular aortic pressure and flow device, suitable for use with Rhesus monkeys, was conceptualized, analyzed and designed. A proof-of-concept device was built and tested during the subsequent academic year through a NASA-Ames University Consortium grant. The objectives for the 1996 Summer fellowship were to: 1) demonstrate proof-of-concept, 2) redesign a 20 MHz proof-of-concept device for the smaller rat aorta, 3) reduce power consumption, 4) reduce component count, 5) add flow direction capability, and 5) use a PC 104 form factor.

2. MINIMALLY-INVASIVE PRESSURE AND FLOW MEASUREMENT

The pressure and flow measurement approach taken here is an extension of the extravascular pressure and flow cuff which has already flown aboard two Cosmos missions (1514 and 1667) and which measured pressure and flow in the carotid artery of a Rhesus monkey [2]. The main difference between this device and the Cosmos device is that the newer design uses pulsed-wave (PW) Doppler rather than continuous-wave (CW) Doppler. PW Doppler was chosen because a long-term goal of this work is to measure aortic pressure and flow from the body surface of humans and PW Doppler is the best choice for non-invasive (body surface) measurements. By using PW Doppler for this project, the technology deveoped here can be applied to the longer term goal. Pressure measurement is accomplished by an extravascular Konigsberg pressure transducer positioned between the cuff and the outer wall of the partially flattened aorta. (Flattening is required for accurate pressure measurement and is called aplanation pressure measurement). A graphical depiction of the device can be seen in Figure 1.

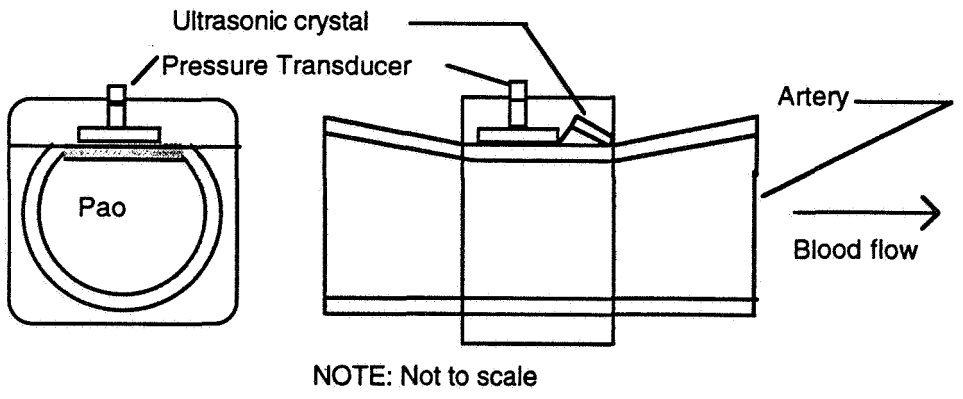

FIGURE 1 Pressure and Flow Cuff

3. ACCOMPLISHMENTS

5 MHz Functionality Test

The 5 MHz proof-of-concept circuitry was bench-tested. The test system consisted of a variable speed pump, tubing, and fluid. The fluid was a 2% by volume corn starch suspension in water. The starch scatters and reflects the ultrasound. It can be seen in Figure 2 that the circuit produces an increasing Doppler shift for increasing flow rates, as was expected.

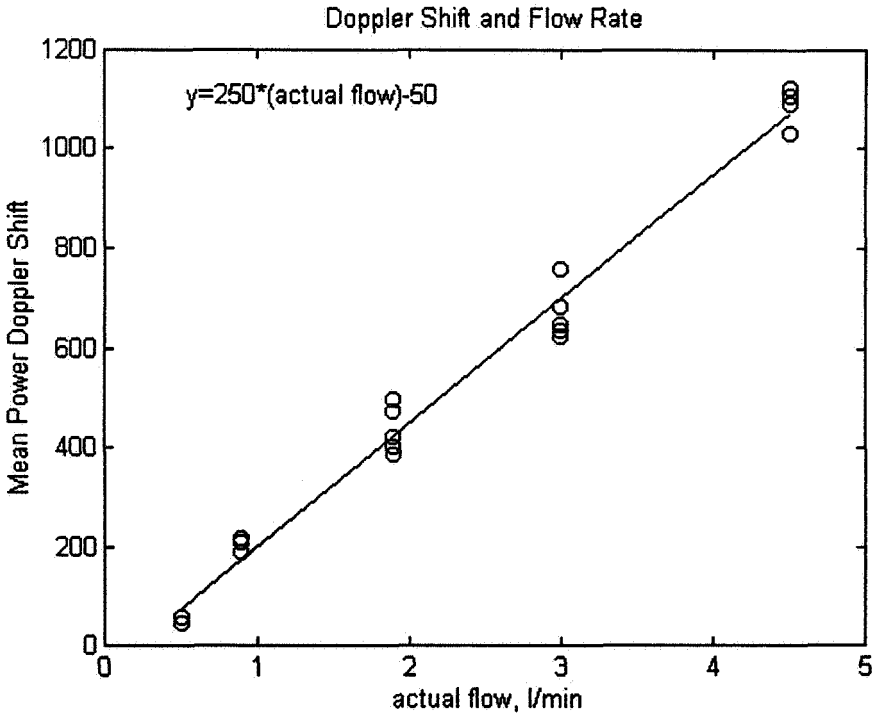

FIGURE 2: 5 MHz Functionality Test

20 MHz Rat Aorta Design

Shown below in Figure 3 is a highly simplified block diagram of the re-designed 20 MHz system to measure the aortic pressure and flow in the rat.

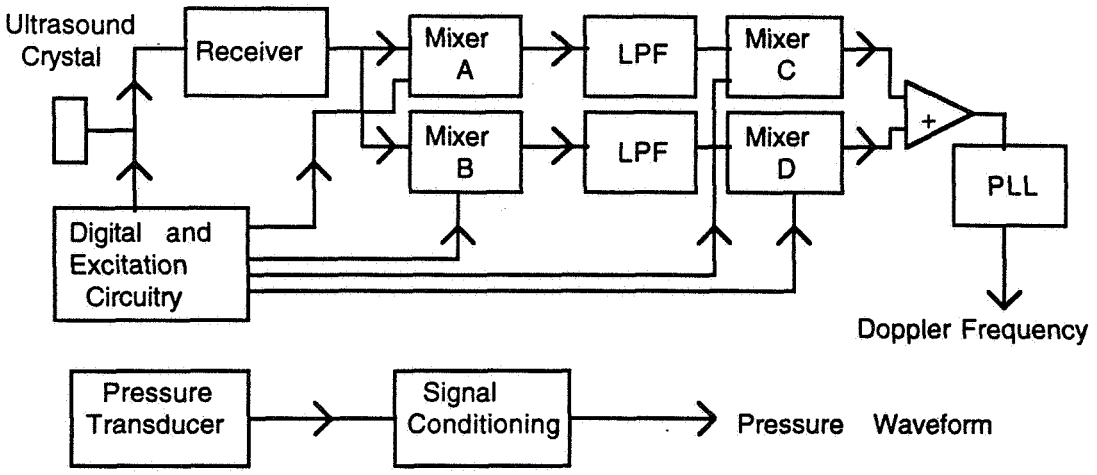

FIGURE 3 Simplified Block Diagram

Directional Doppler Capability

Direction of flow is determined by the addition of mixers B, C, D, summing amplifier and the phase-locked-loop. This technique is referred to as heterodyning.

Power Reduction and Component Count Reduction

The power consumption in the redesign will be reduced mainly due to use of CMOS logic and lower power amplifiers. Overall the component count remained about the same, but the new circuit can detect the direction of blood flow.

4. FUTURE ACTIVITIES

Future work will involve constructing and bench-testing the 20 MHz prototype. each sub-system will be constructed and electrically tested. Next, the subsystems will be joined and the overall circuit will be electrically tested. Lastly, the performance of the circuitry will be tested on a steady-flow bench.

5. REFERENCES

1. Self, D.A., Ewert, D. L., Swope, R. D., Crisman, R. P., and R. D. Latham, "Beat-to-Beat Determination of Peripheral Resistance and Arterial Compliance During +Gz Centrifugation", Aviation, Space and Environmental Medicine, (1994), 65: pp396-403

2. Sandler, H., Skidmore, M., Hines, J., Osaki, R., Agasid, E., MacKenzie, R. Krotov, V. P., Bazunova, E. G., Belgorodsky, A. O., Estratov, Y. A. and A. N. Nazin, Final Report of the U. S. Experiment Flown on the Soviet Biosatellite Cosmos 1667, NASA TM 108803, May 1994 (Edited by J. Hines and M. Skidmore)

1996 NASA-ASEE-Stanford Summer Fellowship - Final Report

DEVELOPMENT OF A DRIVER CODE FOR THE WICS PROJECT

Amitabha Ghosh*

Department of Mechanical Engineering
Rochester Institute of Technology

Introduction

Wall Interference Correction System (WICS) is a computational technique to evaluate the wind tunnel wall interference corrections for blockage, Mach number, dynamic pressure and angle of attack. The objective is to predict the effects of the bounding walls on wind tunnel measurements [1]. The procedure attempts to compute these corrections in real time so that the test engineer can implement these by adjusting wind tunnel controls for angle of attack and dynamic pressure while the test is in progress in the 12 ft. pressure wind tunnel at the Ames Research Center [2]. The technique utilizes an ideal flow solver PMARC (Panel Method developed at the Ames Research Center) to compute influence coefficients in an internal flow mode by representing a paneled model of the tunnel for (a) fullspan and (b) semispan tests.

For fullspan models, the lifting models of the wing and tail are calculated by replacing them by line doublets, the volume blockage is represented by a source and sink of equal and opposite strengths and the wake model is represented by two sources placed about the wing. The treatment of the semispan models is similar. Semispan model testing is advantageous because it allows much larger scaling of the prototype. Although there are typically 18 to 20 singularities in case of fullspan models, the lifting model is completely determined by making a least squares fit to the elliptic distribution about the wing and the tail and solving the maximum circulation of the wing and the tail from a set of lift and pitching moment measurements during the experiment.

A set of static pressure measurements are used to obtain the experimental results at 240 ports along the 8 rows of pressure taps (Fig. 1). These measurements are also used to obtain the solution of the unknown sources representing the blockage and the wake by a similar least squares fit as before. The correction in the velocity potential function thus computed may be superimposed with the velocity potential due to the fitted pressure signatures to produce the velocity potential for the free air flow. However the focus of this technique is not to produce a detailed flow field but the far field effects of the volume and the wake blockage. Real time influence coefficient calculations are facilitated by pre-computing an influence coefficient database using PMARC with unit singularities at a given set of reference points such that the solution can be quickly computed by interpolating in this database.

Progress Report

Although WICS project has progressed for over three years the concept of WICS has so far been tested only by performing PMARC calculations of known body shapes in free-air flows. Last summer, I examined the proof of concepts using a simplified tunnel model with 76 ports. There was some concern regarding the convergence of solutions in PMARC, which has been addressed by introducing double precision arithmetic in PMARC calculations. We have also begun investigating the structure and quality of the PMARC matrices in a co-operative research agreement [3] between NASA and Rochester Institute of Technology.

True success of WICS may be assessed by comparing corrected force and moment coefficients with the flight test data. However to facilitate this, WICS must be fully integrated with the experimental data acquisition system at the 12 ft. pressure tunnel. This summer, the project has entered an experimental phase with several major tests planned for the next year. Models of real aircraft flight conditions will be simulated utilizing full and semispan modes in WICS. Thus a driver code would be necessary to test the compatibility of the experimental data with WICS and return corrections to the test engineer in real time.

Goals

The layout of the WICS program is shown in a block diagram below (Fig. 2). A large facility such as the 12 ft pressure wind tunnel has several groups of engineers performing different experimental and analytical tasks. A main driver program of WICS (nicknamed the ALPHA code) was developed to process the experimental data emerging from the Standard Data System (SDS) and make it available to WICS in real

* Associate Professor .

time. After invoking WICS, it must report the corrections back to the SDS. This process involves several steps stated below.

WICS needs four input files in specific data formats which are not available directly from the SDS. Therefore compatibility between the two computers is an important issue. Next, the wind tunnel measurement files and the calibration files are obtained at different times using a set of control variables that are not identical. Thus support calibration files corresponding to the matching experimental files must be supplied to WICS. Furthermore, the experimental results for lift and pitching moments are obtained in a non-inertial coordinate system, whereas all results in WICS are with respect to a tunnel-fixed inertial system. Also, the data acquisition system sometimes develops unwanted errors, which must be corrected before supplying data to WICS.

The coding in ALPHA itself must satisfy some desirable features as follows. It must be system independent such that it accommodates several operating computer systems. The data must be processed speedily such that WICS succeeds in real-time data processing. There must be some built-in internal checks and reporting of progress as processing continues. The data acquisition must not be aborted due to the failure of these internal checks. The program must be user-friendly and interactive with the least amount of vulnerability.

Description of ALPHA

To best satisfy the independence from different operating systems, ALPHA was developed as a UNIX shell script program which invokes execution of several FORTRAN programs and also the shell script code in WICS. The tunnel operating envelope (Fig. 3) was input to ALPHA as a means to check viability of operating conditions. The execution of test runs involves variations of the tunnel total pressure, Mach number, dynamic pressure (or, the Reynolds number), temperature, density, as well as the model orientation (measured to reflect changes in the pitching, yawing and rolling angles). The variability of tunnel operating conditions was reduced to two variables required by WICS for processing, which are the total pressure and the Mach number. Thus the tunnel operating envelope was furnished to WICS in terms of these two variables. The other variables are reported back to the SDS for validating WICS results later. Once a set of specific test conditions is realized, ALPHA supplies to WICS the non-dimensional velocity at the 240 pressure ports corresponding to the test Mach number and total pressure.

In improving computational efficiency, a code should limit the number of logical tests and arithmetic operations. To speed up the processing time, it was decided that a nearest neighbor approach will be employed rather than a linear interpolation at the 240 ports.

The limitations imposed by the tunnel operating envelope were converted into marking a full cell, a boundary cell and an empty cell in total pressure versus the Mach number plot (Fig. 4). If the operating conditions for a specific test are inside or on the edge of the operating envelope, the user is informed of the accuracy of processing accordingly. This feature is necessary to provide a health check for WICS as well as being the basis of future refinements.

Often experimental test results include inaccuracies. For example, although a test set is supposed to provide constant pressure and Mach number for the whole set, leaving angles as variables only, the actual data reports variability in the pressure and Mach number values. Thus, ALPHA first screens the data to provide WICS a set of consistent results. The rounding operation that it uses to achieve this is considered desirable rather than an error.

Next ALPHA provides the coordinate transformation for the singularity and reference locations to supply WICS the values in tunnel-fixed coordinates. Then it starts the WICS calculations to process a large set of experimental data automatically and reports three different files containing relevant information. These are convenient to summarize, elaborate or detail what the previous WICS runs produced. In the execution of ALPHA, a user is allowed to make some choices interactively and correct them if mistakes are made. This process will require further refinements as time progresses since all the needs of the user in managing the code are not apparent at this time. Details of operations in ALPHA as well as the shell script coding and FORTRAN programs are available in the operations guide [4].

Several test runs were made on the Silicon Graphics' Challenge workstation running ALPHA and WICS together with some experimental files acquired earlier. Both fullspan and semispan executions of WICS were successful with compatible input/output formats. Typically an interactive run of ALPHA in conjunction with WICS took 22 seconds per test data point, where ALPHA's processing took about half a second and WICS used the remaining time. ALPHA was able to process 236 test runs of WICS in about 1 hour and 40 minutes in a time sharing mode adding a considerable step toward productivity (compared with earlier efforts of running WICS one test run at a time). There

seemed no problems for these runs on the Challenge machine whatsoever.

Future Directions

Though the testing of WICS and ALPHA running together has been checked thoroughly, some of the questions could not be answered at this stage due to the lack of proper experimental data. When testing proceeds on a production basis, some issues that are related to the correlation between experimental data and theoretical modeling in WICS will arise. These issues will perhaps necessitate changing part of the WICS coding and thus the ALPHA code. Morever, presentation of the WICS results effectively will necessitate developing several interactive graphics programs. I hope to maintain contact with the test engineers to be able to participate in such issues.

References

[1] Hackett, J. E., Wilsden, D. J. and Lilley, D. E., "Estimation of Tunnel Blockage from Wall Pressure Signatures: a Review and Data Correlation," NASA CR–152241, Lockheed–Georgia Company, Marietta, Georgia, March 1979 .

[2] Ulbrich, N. and Steinle, F. W., "Real–Time Wall Interference Calculation in Three–Dimensional Subsonic Wind Tunnel Testing, " AIAA 94–0771, presented at the 32nd Aerospace Sciences Meeting, Reno, Nevada, January 10–13, 1994 .

[3] Ghosh, A.,"An Investigation of the Convergence Characteristics of PMARC Internal Flow Calculations applied to the WICS Project at the 12 ft Pressure Tunnel," NASA Ames/University Consortium Grant, NCC2-937, December 1, 1995 - May 31, 1997 .

[4] Ghosh, A., "Operations Guide for the WICS Driver - ALPHA", Final Report presented to NASA Ames Research Center, Mofett Field, California, August 1996.

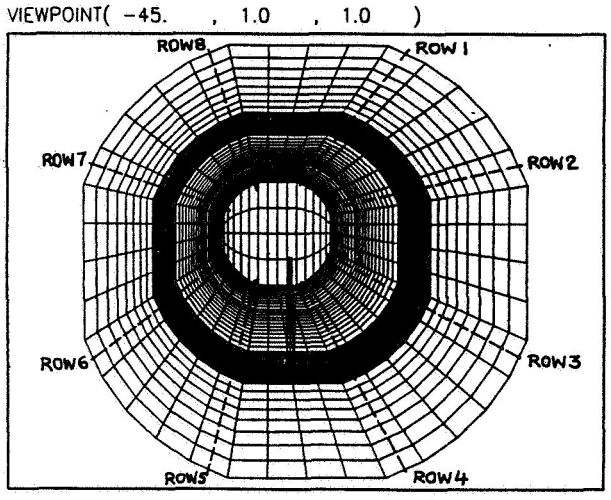

Figure 1. Placement of Pressure Ports

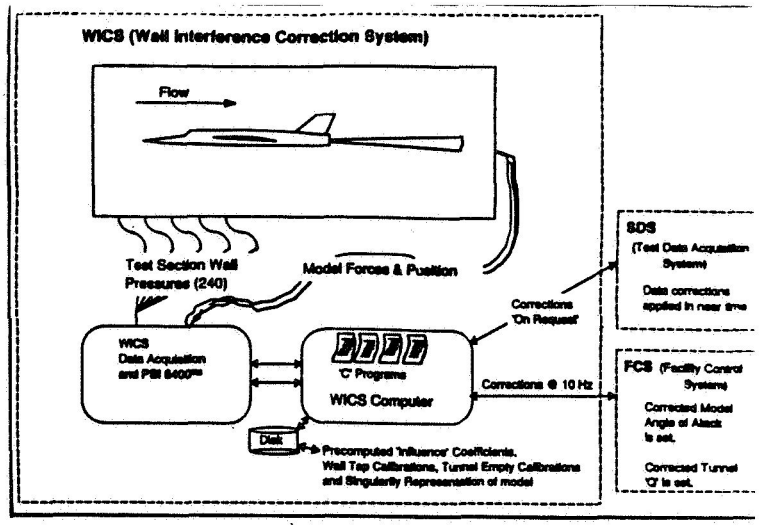

Figure 2. Layout of WICS

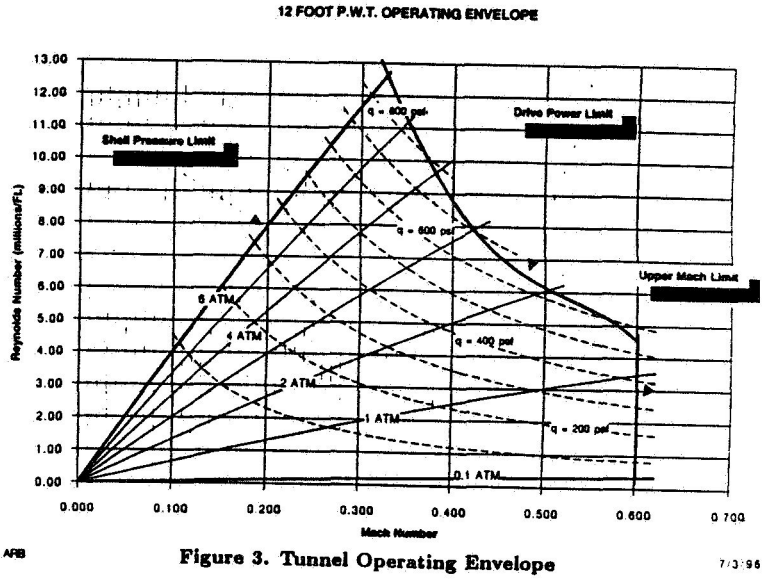

Figure 3. Tunnel Operating Envelope

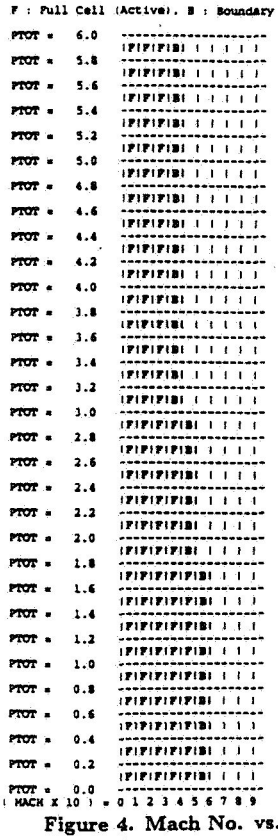

Figure 4. Mach No. vs. P-tot in ALPHA

1996 NASA-ASEE-Stanford Summer Fellowship Final Report

Effects of gloves, temperature and their interaction on finger, hand, and arm blood flow and skin temperature: A pilot study.

M. Susan Hallbeck, Ph.D.
Associate Professor of Industrial and Management Systems Engineering

OBJECTIVE

The objective of this study is to investigate the effects of cold only, commercially available gloves only, and the combination of gloves and cold on the blood flow and surface (skin) temperature of the medial and proximal phalanxes of digit 3, the metacarpal region of the hand, and the forearm.

STATEMENT OF THE PROBLEM, IMPORTANCE, AND IMPACT OF PROPOSED RESEARCH:

Glove liners are worn under the EVA glove during extravehicular activity (EVA). Several different types of glove liners have been employed; however, most crew members like a formfitting surgical glove liner made of knitted polyethylene. This glove liner is tight on the hand, constricting the small vessels, especially in the fingertips. The effect of this surface pressure on blood flow through the hand and fingers is not known.

Astronauts are also exposed to a wide range of hand temperatures (STS-63 recorded 20°F to 110°F for hand temperatures) (Grahne, Grasiosi, and Pauly, 1995). To prevent temporary or permanent hand damage, the temperature of the hand should be maintained between 7°C (45°F) and 45°C (113°F) (Grahne et al., 1995). When the hand is exposed to temperatures below a "normal ambient" temperature of about 70-75°F, the hands experience vasoconstriction, which further lowers hand temperature (reducing heat loss from the deep body core). The lower the ambient temperature, the more the vasoconstriction to reduce heat loss. Any reduction in blood flow due to the glove tightness may increase the likelihood of cold hands during an EVA mission.

The interaction of surface pressure and hand cooling has not been found in the literature, thus a study is proposed to examine each effect on blood flow and skin surface temperature of the hand and fingers, as well as their interaction.

If the surface pressure is found to constrict the blood flow either in "normal" (about 70°F) or cooled (45°F) temperature environments, it would be an indication that the current use of the tight glove liner is contraindicated for EVA.

METHOD:

Subjects:

One male with no self-reported upper limb disorders of the blood flow (including diabetes and high blood pressure) or musculoskeletal disorders (such as carpal tunnel syndrome or vibrational white finger) will volunteer for the blood flow study. If this study is continued, 11 more male subjects will be measured. Only males will be employed in this experiment for homogeneity. They will be classified by hand size, if the experiment is continued.

Materials and Apparatus:

Gloves. Commercially available Paraderm™ gloves will be employed in this study.

Blood flow. Blood flow will be measured using non-invasive means. The blood flow will be measured using the impedance technique routinely employed by Dr. Les Montgomery of the EVA lab. The impedance is measured by applying a .1milliamp 50KHz constant current to the end of digit 3 and measuring the impedance through surface electrodes Nicolet™ miniature (20mm dia) silver/silver chloride disposable electrodes (NI019-764900). The impedance will be measured in the medial and proximal phalanxes of digit 3, near the middle of the third metacarpal, and along the midline of the forearm. A four channel UFI, Inc (Model 2994) tetra-polar impedance plethysmograph (IPG) will be used to measure the blood flow. This system will be used to measure the blood flow in the fingers, hand and forearm of each subject. In addition,

EKG will be monitored (a Lead I EKG) on all subjects using a UFI, Inc (Model 2121) EKG Bioamplifier and three additional disposable EKG electrodes. This procedure has been utilized several times by bye personnel in the EVA lab for such applications as brain and scalp blood flow, etc.

All impedance and EKG data will be recorded on a portable IBM-compatible computer using the CODAS (by DATAQ, Inc.) data acquisition system for post-test analysis. Each of the recorded channels of information will be digitized at a rate of 250Hz using a 12bit A/D conversion board. The data will be collected every 15 minutes.

Temperature. Temperature will also be monitored non-invasively using copper constantan thermocouples that are attached to the skin using surgical tape. The thermocouples will be monitored every fifteen minutes and the results recorded via A/D conversion (A/D with Workbench by Strawberrytree, Inc.) on a Macintosh computer.

The hand will be exposed to a cooler temperature than ambient air to more closely simulate EVA conditions. The cooling will be localized hand cooling using the Sub-Zero™ cooler in the EVA lab, which has been adapted with arm holes and sleeves to allow hand access to the cooler environment. The ambient temperature in the cooler will be 45 degrees Fahrenheit. The subject will have his hands through the arm holes (lined with an insulatory sleeve up to the wrist crease) once with no glove for a 30 minute period and once with gloves for a 30 minute period. Between these cool exposures, the hands will be warmed to pre-cooled hand temperature.

Other Measures. Anthropometric dimensions will be recorded for segment volume including hand length, hand breadth, segment length, several segment circumferences for the fingers, hand, and forearm. In addition, height, weight, and subject age will be recorded.

Procedure:

After anthropometric dimensions are recorded, the subject will have the impedance and EKG electrodes attached to the right hand and the thermocouples attached to the left hand. Base line readings will be taken at time 0 and 15 minutes later. Both hands of the subject will be placed in the cooler and an immediate impedance and temperature reading taken, then repeated at 15 and 30 minutes after exposure. The hands are then removed from the box. An immediate impedance and temperature reading is taken, and one 15 minutes after the hands have been removed from the cooler. If the hands are not at the pretrial temperature, the subject is allowed to warm them or sit until they have regained the pretrial temperature. After the hands are rewarmed, another baseline impedance and temperature is taken.

The gloves are then donned on both hands and immediate blood flow and temperature readings are taken in the ambient temperature. Readings are taken once every 15 minutes for the 30 minutes the gloves are worn.

The glove is removed and immediate readings are taken, as well as readings 15 minutes after doffing the glove at ambient temperatures for another baseline reading.

The glove is donned again and the hands placed in the cooler. Immediate readings of blood flow and temperature are recorded. Readings are taken every 15 minutes for a total of 30 minutes after donning the glove and placing the hands in the glove box. The hands are then removed from the cooler and immediate readings are taken, as well as a final control 15 minutes after the hands are out of the cooler. This concludes the trial. The total duration of the experiment is approximately 2 hours, performed during one session.

RESULTS:

The initial subject's data are plotted on the graph, shown on the next page. The left y-axis is temperature, while the right y-axis is bloodflow, with the x-axis as the trial condition. Since these are discrete measurements, there should be just a scatterplot, but for ease of reading, a line graph was employed to plot the data.

DISCUSSION:

For finger, hand, and forearm temperatures, the results were as expected. The further from the deep body core, the more extreme the cooling. The gloved hand in the ambient (70F) temperature condition also performed as expected showing no difference in temperature. The no glove/cold only condition showed the most peripheral cooling, but the difference between the

gloved and ungloved condition in the cold was not as large as expected, they only differed by about 5 degrees F for both the medial and proximal phalanges. However, this gloved versus ungloved temperature difference was more pronounced for the hand than the fingers. The forearm temperature (outside the cooler) did not vary much.

For bloodflow, the decrement in the fingers was about the same in the cold only and gloved/cold conditions. Lesser decrement was found in the gloved only condition. It was believed that the cold and glove conditions would be synergistic, but in this case it was not found to be true. The hand bloodflow for the cold only and gloved/cold conditions were similar, with lesser bloodflow reduction than in the gloved only case. The forearm bloodflow, like the forearm temperature did not change appreciably.

The reduction in bloodflow lagged behind the temperature decrement by about 1 time unit (15 minutes), as graphed. This time unit was arbitrarily determined; thus, in further experimentation smaller increments could be used to determine more closely how the bloodflow and temperature decrements are related.

In conclusion, the surface pressure from the glove in ambient temperatures reduces bloodflow, but doesn't affect finger and hand temperature. However, gloved and ungloved conditions in the cold environment do not differ greatly on the tested subject for both temperature and bloodflow. This suggests that the glove reduced bloodflow, but the greater factor in bloodflow reduction was hand temperature.

Unfortunately no more subjects will be run. The EVA branch where I was working will be closed on October 1, 1996 and this research is a casualty of the closing. The research could have yielded novel information about relationship among bloodflow, temperature, and subjective "coldness", but with the demise of EVA research these relationships will remain unexplored.

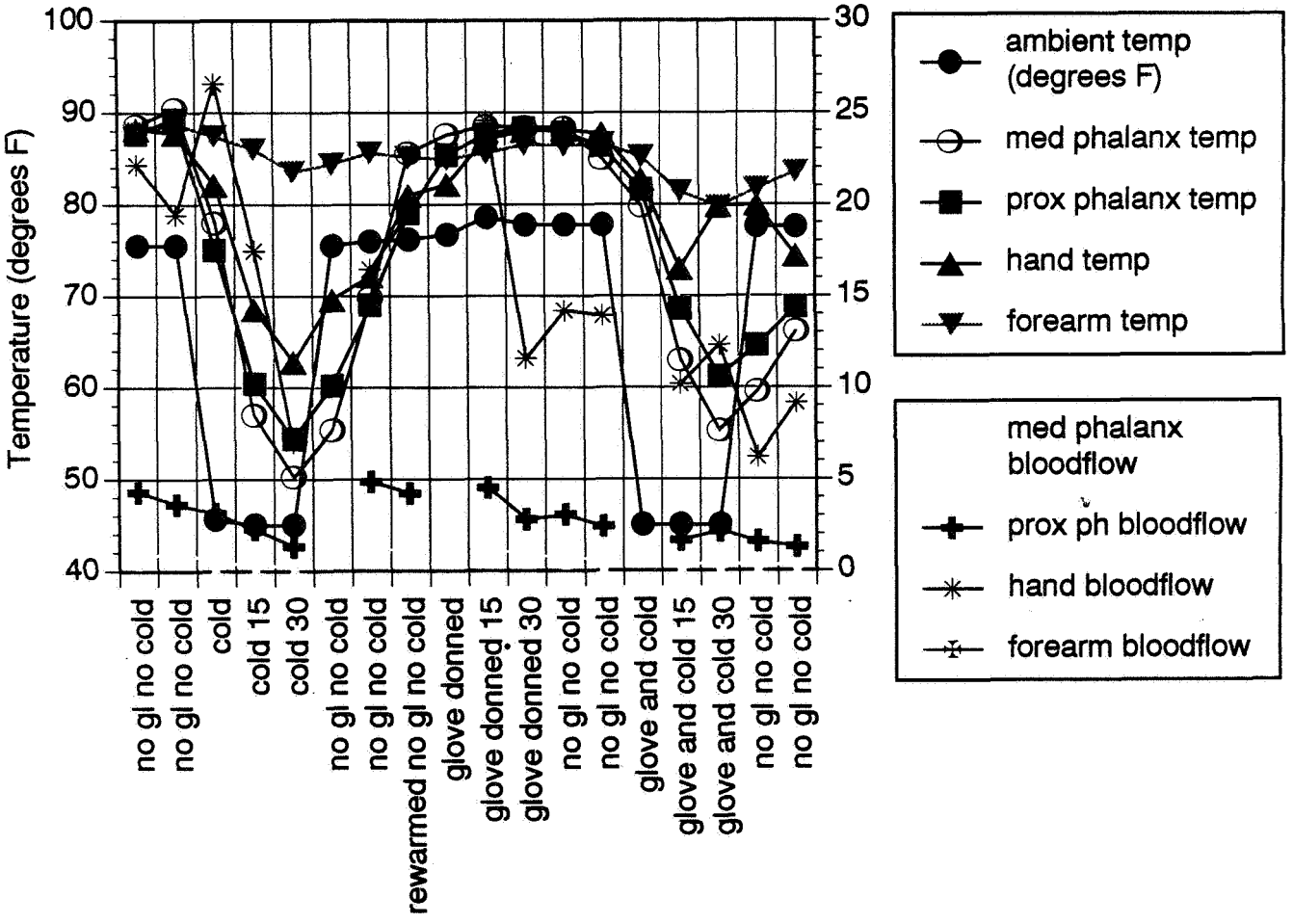

1995,6 NASA-ASEE-STANFORD SUMMER FACULTY FELLOWSHIP FINAL REPORT

Further Study Of 'Pop-Up' Vortex Generators

By
Dr. David Manor
Tenured Professor of Aerospace and Mechanical Engineering
Parks College Of St. Louis University

INTRODUCTION

My June - August , 1995,6, NASA-DFRC Summer Fellowship enabled me to interact and work with several colleagues, among them, Bob Curry, Dave Fisher, Tim Moes, Glen Gilyard, Dr. Whitmore, David Neufeld, Al Bowers, and Lisa Bjarke, to name a few, and on a variety of flight-test projects:

(1) The drag-reduction and frost-effect projects on the L-1011, (my Library-Search revealed a report by a major aircraft manufacturer showing that the test was accomplished some years earlier. No one was aware of the test, including the manufacturer. I am pleased to say that my discovery saved Much time and money) --- Tufts were applied to the upper wing surface, flow patterns were analyzed during side-slip and stall maneuvers.

(2) The Aerospike Tests on the SR-71 --- where abnormal pitch-down and more than elevator power were found in wind tunnel tests. I proposed water tunnel tests to investigate the vortical flow. The water tunnel model was built and tested. I was to correlate the water and wind tunnel data, thereby help the analyses and corrections before flight testing.

(3) I have also participated in flight testing of the F-18 HARV (High Angle of Attack Research Vehicle) checking the performance of its strakes.

(4) My main project, however, was testing my patent-pending 'pop-up' vortex generators (See attached Figures and Ref. 1-3) using an ultra-light model. The model is a replica of a modified MAX-103 kit aircraft that our Parks College of St. Louis University Student Design Group built and modified from a tail wheel to a tricycle configuration. A model was tested in the Parks College low-speed wind tunnel. I hope to initiate flight-testing upon my second return to St. Louis. The combined data using wind tunnel, water tunnel, RC, flight-testing and analytical results will be very valuable for assessing the correlation between the different methods of analyses, since at present it is almost impossible to accurately predict flight characteristics from anything but in-situ tests. Unfortunately, political/financial reasons dictated using a generic wing rather than a specific model in the NASA-DFRC water tunnel.

CONCLUSIONS AND FUTURE DIRECTIONS

My plans are to combine my test-piloting experience with my vortical flow background to improve the performance of the MAX-103 as well as to find the relevant correlation(s) between theory, experiments, and in-situ flight testing.

I was instrumental in linking my colleagues at MDA who invented the Pressure Sensitive Paint (PSP) with NASA-DFRC personnel. I was encouraged (NOT instructed) by my NASA-DFRC colleagues to attend an AIAA Technical conference where two papers were scheduled to be presented on the PSP subject. Drs. Marty Morris and John Donovan came to NASA-DFRC and presented a technical briefing on the subject. The Seminar was very successful and was well attended by scientists and engineers from both NASA-DFRC and ARC. A flight test using PSP was initiated due to my persistence. A more elaborate test is scheduled for next year. I will probably continue my involvement in this interesting and challenging project. In addition, I am pleased to report that my friend and colleague, DR. Fred ROOS, is also coming to NASA-DFRC to initiate flight testing of micro blowing, made possible by my work. Micro blowing was used successfully to control vortex asymmetry in water tunnel tests. The method uses 2-3 orders of magnitude lower mass flow rates that translate to 0.1 LB/sec -- a very low power source is needed.

Finally, although there were several incidents of inconsiderate behavior on the part of some colleagues, I think the ASEE-NASA-Stanford Fellowship program is an excellent idea. More preparation, open mind, and good will on both sides will justify the sacrifices and the hardship associated with uprooting and coming to NASA-DFRC and the desert. I hope that the work done these past two Summers will lead to more collaborative work between NASA-DFRC and Parks College of St. Louis University with or without my participation.

REFERENCES

'Pop-Up' Vortex Generators -- Patent is pending

1. Dima, C., Manor, D.: "Further Study of Vortex Generators' Effects on Lift and Stall Angle of Attack", AIAA paper #94-0625.
2. Manor, D, Dima, C., Schoch, P. and Polo, J.: "Using 'Pop-Up' Vortex Generators on the Wing Surface to Greatly Increase the Lift and Stall Angle of Attack," AIAA paper # 93-1016.
3. Manor, D., Lozano, R .S. N., Merino, J. C.: "High Angles of Attack Aerodynamics of Delta Wing Planform Using 'Pop-Up' Vortex Generators," AIAA paper #93-3497.

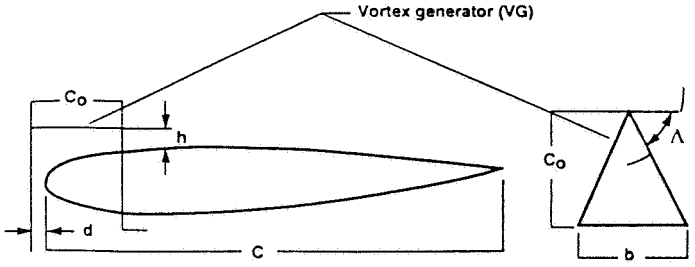

Fig. 1. Design parameters.

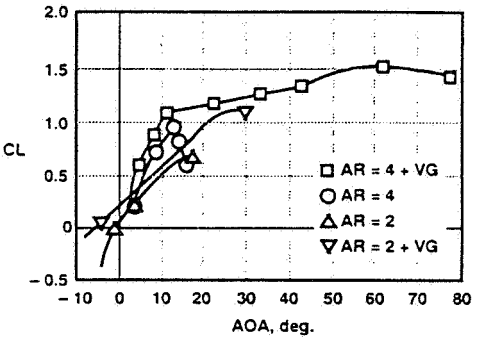

Fig. 4. CL vs. AOA VG effect on AR = 2 and 4.

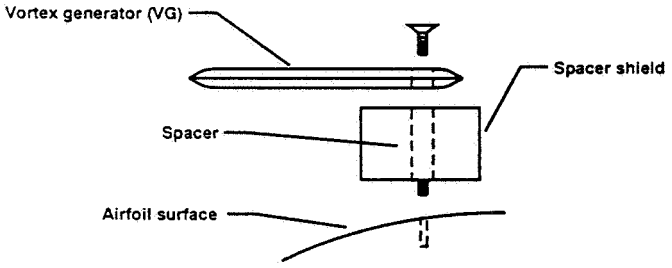

Fig. 2. Mounting system.

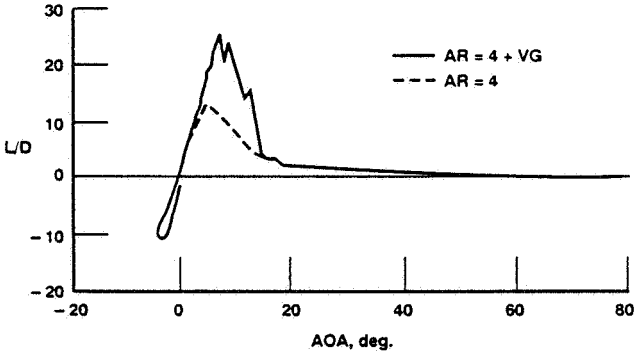

Fig. 4. L/D vs. AOA with and without vortex generators.

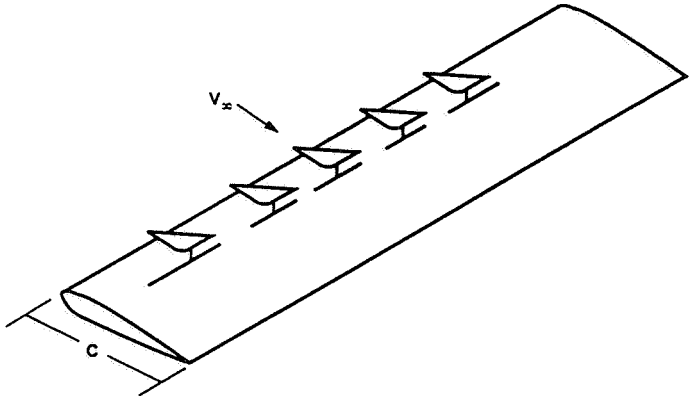

Fig. 3. Wing model with vortex generator.

NASA-ASEE-Stanford Summer Fellowship 1995- Final Report

A System for Automatically Generating Scheduling Heuristics

Robert Morris, Computer Science Department, Florida Institute of Technology
Melbourne Fl. 32901

1 Introduction

The goal of this research is to improve the performance of automated schedulers by designing and implementing an algorithm for automatically generating heuristics for selecting a schedule. The particular application selected for applying this method solves the problem of scheduling telescope observations, and is called the Associate Principal Astronomer (APA) (Drummond, Swanson and Bresina, [1]), developed at NASA Ames. The input to the APA scheduler is a set of observation requests submitted by one or more astronomers. Each observation request specifies an observation program (sequence of telescope movements and instrument commands) as well as scheduling constraints and preferences associated with the program. The scheduler employs greedy heuristic search to synthesize a schedule that satisfies all hard constraints of the domain and achieves a good score with respect to soft constraints (preferences), expressed as an objective function established by an astronomer-user.

The system for automatic heuristic generation described in this report, called *genh*, is demonstrably *fast*, *accurate* (converges to a solution faster than existing techniques), *robust* (solves a wide range of problem instances), *simple* (is based on a simple algorithm easily integrated into the scheduling process), and potentially *generalizable* to other problem domains.

2 Adaptive Telescope Observation Scheduling

The motivating idea for adaptive scheduling is the idea that the heuristics underlying the search for a good schedule vary among different problem instances. In the telescope observation domain, for example, a strict adherence to the advice of a particular heuristic policy may result in a good schedule on underloaded nights, but fail to produce the best schedule on overloaded nights. It should be possible to *derive* the best heuristic for a given problem instance, evaluated against a particular objective function, from information about the problem instance, or the objective function. The challenge is to derive the best heuristic effectively and efficiently. The telescope observation domain has both a large class of problem instances (one for each night of the observing season) and an infinite heuristic space, so enumeration of the set of possible heuristics is impossible.

The *genh* method for exploring a space of heuristics requires the following factors to be specified:

$h = seed$;
$best = score(h)$;
Until some terminating condition is met do
    $h' = Tune(h)$;
    $hscore = score(h')$;
    if $hscore \leq best$ then
      $h = h'$
      $best = hscore$ **endif**
Return h

Figure 1: Algorithm for Searching a Space of Heuristics

1. a way of scoring the *utility* of a candidate heuristic;
2. a *seed* to initialize the search;
3. a *tuning procedure*, based on
    - a *transformation* function $T : H \rightarrow H$ for selecting the next candidate heuristic in the space of heuristics;
    - An *ordering* of the heuristic components which establishes the order in which the transformations are to be applied; and
    - a *granularity function*, which determines the "minimal distance" between the result of any single application of a transformation function;
4. a *termination condition* for the search.

The pseudo-code for an abstract heuristic selection algorithm based on these factors is displayed in Figure 1. The variable h holds the result of the search; it is initialized to the seed. The heuristic component of the best problem solver is retained, as well as the score achieved by the best problem solver. The function *Tune* returns the result of updating the candidate heuristic as the result of applying a transformation operation.

3 Experimental Results on the Telescope Observation Domain

Subsequent to designing and implementing *genh*, most of the research effort consisted of devising and running experiments testing the ability of *genh* to improve the performance of the APA scheduler. Specifically, we wished to show an improvement in the following ways:

- **accuracy**: the scheduler should identify higher quality solutions than previously used approaches;
- **robustness**: the APA should be less sensitive to differences in problem instance characteristics;
- **simplicity**: *genh* should be easy to implement and integrate with the current scheduler; and
- **speed**: *genh* should not prohibit the scheduler from generating high quality solutions in the required time.

One important class of experiments on *genh* tested robustness by comparing how the automatic generation process fares when the problem instance is varied with respect to night or objective function specification. There are two independent factors determining the robustness of *genh*: changes in night conditions, including the contention (overloaded, under-loaded, balanced) among groups; and secondly, changes in the objective function, e.g., as the result of multiple astronomers using the APA for scheduling. Therefore, to test robustness, we designed two separated experiments. The first tested the ability to find a good schedule across a wide range of night conditions, and the second tested the ability to find a good schedule across a wide range of objective function settings. In both cases, *genh* produced heuristics which produced good schedules. Robustness of the approach was confirmed.

Finally, we compared the results of automatic generation to, first, employing the dispatch policy of the telescope controller devised by astronomers; and second, employing a heuristic which uses the same attributes and weights as the objective function. The results of this experiment (published in a technical report presented to the IC Division at NASA Ames) show that *genh* outperforms the other approaches on nearly every night, sometimes dramatically.

4 Summary and Conclusion

This paper has reported on the results of developing and testing a simple, fast, robust, and accurate method for adaptive problem solving in the telescope observation scheduling domain. The success of the *genh* system to improve the performance of the APA resulted in its currently being an operational part of the APA. Future work will consist in future experiments and refinements of the system.

Reference

1. Drummond, M., Swanson, K., and Bresina, J. Robust Scheduling and Execution for Automatic Telescopes. In *Intelligent Scheduling*, M. Fox and M. Zweben, eds., (1995).

NASA-ASEE-Stanford Summer Fellowship 1996 - Final Report

THE ROLE OF RISK IN PILOTS' PERCEPTIONS OF PROBLEM SITUATIONS

Thomas E. Nygren, Ph. D., Associate Professor of Psychology,
Ohio State University, Columbus, OH

During the next decade, a number of dramatic changes are planned for the commercial aviation system. These changes will encompass both operational and technological advancements. One planned operational change of great potential significance is referred to as Advanced Air Traffic Technology (AATT) or "free flight" -- an advancement, which, when in place, will give airlines and flight crews more freedom in choosing and dynamically changing their optimal travel routes. Although free-flight has the stated goal of more flexibility of operations for commercial airlines while maintaining the highest levels of safety, it will necessarily require a much greater sharing of responsibility for safe use of airspace on the part of airline flight managers, air traffic controllers, and aircraft flight crews. The increased flexibility of free-flight suggests that flight crews may be faced with higher levels of workload and may be required to make more complex sequential and time-constrained dynamic decisions. With this increase in both number and difficulty of decisions comes the potential for decision related problems for commercial flight crews.

Flight-related problems that require some kind of crew decision making are already being reported with high frequency as incident reports to the Aviation Safety Reporting System (ASRS). These ASRS incident reports are extremely valuable because they can suggest situations or circumstances that are potentially problematic from a safety perspective and which might require operational changes on the part of the FAA, ATC, the airlines, or the flight crews. A significant number of these incidents appear to have high enough levels of safety risk or time pressure associated with them to produce difficulty in pilot decision making.

Research Efforts.

The effects of time pressure on decision making in flight settings, although not completely understood, has been the subject of a large amount of research in recent years and is an important component of models relating perceived workload to task performance. Perceived risk and its role in crew decision making, on the other hand, is not very well-defined and has not been systematically examined. The first summer of my fellowship was spent developing ways in which research in more traditional areas of decision making might be applied to aviation. This led to the re-analysis of data from an aviation decision making study that was conducted several years ago by NASA Ames personnel [1]. That re-analysis project has been completed this summer and will be summarized below. It will also be presented as a paper at the *Human Factors and Ergonomics Society Meetings* in September, 1996. A second project that examined pilots' perceptions of their most difficult flight decisions is also near completion. A third project under way is an in-depth analysis of 284 ASRS incident reports dealing with risky decisions and will be continued over the next year.

Summary of Project 1.

My colleague, Dr. Judith Orasanu, of the NASA Ames AFO Branch is one of a few researchers who have recently recognized the importance of perceived risk in pilot decision making and she has incorporated the construct into her model of aviation decision making. The study of risk poses some special problems for dynamic decision environments like flight, however. In a recent paper, Orasanu and NASA colleagues [1] examined whether perceived risk and time pressure, two important components of Orasanu's [2] model, are in fact relevant to pilots judgments. Participants in their studies sorted a representative set of 22 scenarios, taken from ASRS reports, into piles according to their similarity as decision problems. Using

an algorithm based on alternating least-squares multidimensional scaling (MDS) methodology, Fischer et al. [1] showed that, when pilots were asked to make this kind of undirected sorting, they differentiated between the decision problems on the basis of an "immediacy of potential risk" dimension and a "time pressure" dimension.

I wrote a computer program to re-analyze the data for each individual pilot separately and then attempted to compare the MDS scaling solution obtained from the directed sort of a second group of pilots' evaluations of the scenarios with respect to perceived riskiness, with the scaling solution that was based on the original group's undirected sort of the decision problems. It was hypothesized that if these two scaling solutions, one specific and one general, were to match, then there would be evidence to suggest that it is, in fact, perceived risk that primarily drives pilots' perceptions of flight decision problems, and that perceived risk is primarily a function of immediacy of potential risk and time pressure.

Method

Subjects. Two groups of twenty-eight pilots each from two major American airlines had served as volunteer participants in this study. The participants included approximate equal numbers of captains, first officers, and flight engineers.

Stimuli and Procedure. The same twenty-two brief scenarios were sorted by both groups of pilots. The scenarios were chosen to cover all aspects of flight; three scenarios were associated with pre-flight, two each with taxiing and descent, and four each with the takeoff, climb, and cruise phases of flight. One group of pilots was asked to make an undirected sort of the 22 scenarios by sorting them into as many or as few piles as necessary, such that those incidents that involved the same kind of major decision should be grouped together. Pilots were given no other instructions about using any specific criteria. In contrast, in the second study participants were asked to sort the scenarios specifically in terms of their perceived riskiness.

Results and Discussion

In the original aggregate group analyses done by Fischer et al. [1], a two dimensional MDS solution was obtained for captains, first officers, and flight engineers separately. Results indicated some group differences, but two primary dimensions emerged -- a time pressure dimension and a potential risk dimension with three categorical levels of risk -- no risk, immediate risk, and potential future risk.

We hypothesized that the directed sorting data for risk for the second group of pilots would match the undirected sorts of the first and this hypothesis was supported. A graphical picture of the two most important dimensions from the pilots' directed risk sort is shown in Figure 1 along with brief descriptions of the associated incidents. Dimension 1 was labeled "potential risk" and clearly resembled the comparable dimension found in the earlier study. Incidents were grouped as "no or low risk" incidents, incidents with risk immediacy (e.g., engine stall, smoke in the cabin, etc.), and incidents which have more future potential risk (e.g., landing gear problem detected while in cruise stage of flight). The second dimension seemed to indicate a distinction between high and low time pressure and matched very closely the time pressure dimension found in the undirected sort group's data.

The similarity of the observed two-dimensional cognitive maps for the two groups of pilots suggests that the categorization and evaluation of flight decision problems are heavily influenced by the perceived riskiness of the situation, and that risk, in turn, is to a large extent a function of the immediacy of the potential risk in the problem and time pressures associated with solving the decision problem. These results are important for aviation decision research for several reasons. First, they provide legitimacy to the inclusion of risk in models of aviation decision making. Second, they suggest that the construct of risk in dynamic decision tasks is not the same as in simple static decisions like those studied in gambling paradigms. Risk appears to be much more multidimensional in dynamic tasks. Future efforts will attempt to

look at pilots' perceptions of risk in more detail. We will continue to focus on the multidimensional nature of risk, the different types of perceived risk (e.g., professional, safety, economic), the impact of time constraints on risky decisions, and the impact of perceived risks on crew decision making.

References

[1] Fischer, U., Orasanu, J., and Wich, M. (1995). Expert pilots' perceptions of problem situations. *Proceedings of the Eighth International Symposium on Aviation Psychology, April 24-28, 1995.* Columbus, Ohio.

[2] Orasanu, J. (1994). Shared problem models and flight crew performance. In N. Johnston, M. McDonald, and R. Fuller (Eds.), *Aviation psychology in practice.* Avebury Technical.

Figure 1: Group Stimulus Space for Dimensions 1 (X-axis) and 2 (Y-axis).

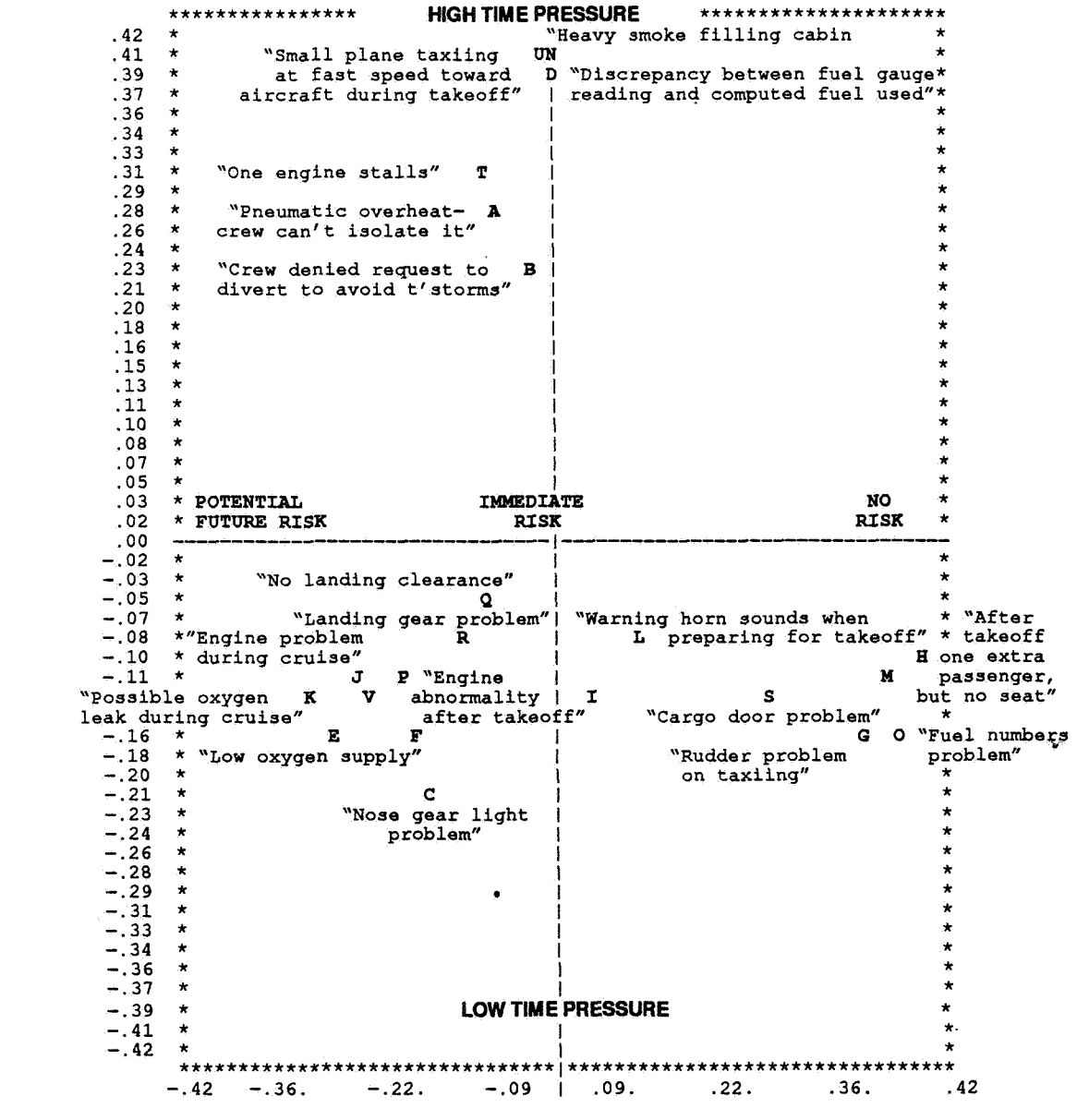

1996 NASA/STANFORD-ASEE SUMMER FELLOWSHIP FINAL REPORT
Absorption Spectroscopy of Polycyclic Aromatic Hydrocarbons Under Interstellar Conditions

Bradley M. Stone
Associate Professor of Chemistry
San Jose State University

I. INTRODUCTION

The presence and importance of polycyclic aromatic hydrocarbons (PAHs, a large family of organic compounds containing carbon and hydrogen) in the interstellar medium has already been well established (see, for example, Ref. 1). The Astrochemistry Laboratory at NASA Ames Research Center (under the direction of Louis Allamandola and Scott Sandford) has been the center of pioneering work in performing spectroscopy on these molecules under simulated interstellar conditions, and consequently in the identification of these species in the interstellar medium by comparison to astronomically obtained spectra.

My project this summer was twofold:

1. We planned on obtaining absorption spectra of a number of PAHs and their cations in cold (4K) Ne matrices. The purpose of these experiments was to increase the number of different PAHs for which laboratory spectra have been obtained under these simulated interstellar conditions.
2. I was to continue the planning and design of a new laser facility that is being established in the Astrochemistry laboratory. The laser-based experimental set-up will greatly enhance our capability in examining this astrophysically important class of compounds.

In addition, I attended the "Complex Organics in Space" session at the COSPAR '96 conference in Birmingham, England in July.

II. ABSORPTION SPECTROSCOPY

a. Experimental. Absorption spectra were obtained this summer using the UV/VIS absorption spectrometer/matrix isolation setup in the Astrochemistry Lab in N-245. Details regarding this experimental station have been given elsewhere[2]. Essentially, the setup consists of an ultrahigh vacuum system in conjunction with a cell designed to be coupled to a cryostat. The cryostat is used to cool down a sapphire window to liquid He temperature (4K). Typically the PAH being studied is heated to give it a significant vapor pressure, which subsequently condenses on the cold window. Simultaneously, a rare gas (typically Ne) is flowed into the cell to be simultaneously deposited along with the PAH. In principal the PAH molecules are then completely isolated from one another by being surrounded by the Ne matrix. Light from a tungsten lamp (visible) or a deuterium lamp (ultraviolet) can then be imaged through the window (and deposited sample) and subsequently into a spectrometer, where the light is detected by means of a CCD

(charge-coupled device). Photolysis of PAH molecules is accomplished by irradiation of the matrix with the Lyman-alpha line of hydrogen, by means of a microwave driven hydrogen lamp.

b. Results. Due to a number of experimental difficulties, our plans to generate spectra from a number of PAH molecules and cations did not come to fruition. Spectra from two molecules were attempted: fluoranthene and benzo(k)fluoranthene. The fluoranthene proved to be a difficult molecule for us to work with in terms of forming a "good matrix" with Ne. We then switched to benzo(k)fluoranthene, which promised to be a better candidate to work with. Several attempts were made to form Ne matrices with this compound. In all cases but the first trial, we had difficulty forming a Ne matrix, apparently due to temperature fluctuations in the cryostat, which did not seem to maintain constant liquid He temperature. An apparent heat leak raised the temperature of the window a few degrees periodically, thereby causing a loss of Ne. Also, difficulty with a shutter that is used in conjunction with the CCD detector and monochromator made spectral observations in subsequent trials impossible. During the first set of experiments, a PAH/Ne matrix was formed, and ultraviolet spectra of the benzo(k)fluoranthene were obtained (see Fig. 1. The bottom spectrum resulted from deposition of the PAH for a few minutes, overlaying spectra resulted from subsequent further deposition of PAH). However, after irradiation with vacuum ultraviolet, the matrix exhibited no evidence of cation absorption bands in the visible/near-infrared region of the spectrum. The matrix-isolated benzo(k)fluoranthene shows clear evidence of absorption from the ground electronic state to three excited electronic states: S_1, 350nm - 400nm; S_2, 250nm - 300nm; and S_3, 180nm - 200nm.

III. LASER LABORATORY IMPLEMENTATION

I have continued to work this summer on the design and preparation of the new laser laboratory in the Astrochemistry Lab. This laboratory will be centered around a flashlamp-pumped alexandrite laser, capable of being tuned about a fundamental wavelength range of 715nm - 800nm. This summer I have helped identify the following peripheral items to be ordered for completion of the laboratory: second and third harmonic generators with autotracker, oscilloscope, Raman cells, optics, power meter, laser safety goggles, HeNe laser, a fast photodiode, mounts, etc. I have worked closely with Robert Walker, the technician in the Astrochemistry group, in the design of the laboratory. Mr. Walker has been instrumental in implementing the necessary facilities requirements and changes in order to accommodate this new equipment. The new laser will arrive late September and will be installed at that time.

IV. FUTURE PLANS AND STUDIES

Our plans are for me to continue on with my collaboration in the Astrochemistry group. I will continue with participating in the following projects during the academic year:

1. Installation of the new laser/establishment of the laser lab. We plan to have the laser lab fully operational by the beginning of next summer, so that laser fluorescence studies of PAHs in rare gas matrices can proceed.
2. Absorption spectroscopy of PAH cations - a continuation of this summer's project to amass spectra of additional members of molecules in the PAH family will be carried out.

In addition, I plan to begin to apply to granting agencies, such as the American Chemical Society's Petroleum Research Fund and the National Science Foundation, to attempt to establish my own source of support to continue on with this work.

V. ACKNOWLEDGEMENTS

I would like to thank Dr. Farid Salama for the generous giving of his time this summer in helping me to learn this (often finicky) experimental technique. Thanks also to Bob Walker for his expertise and professionalism in helping us to design and maintain the Astrochemistry facilities. Thanks to my research colleagues Drs. Max Bernstein, Scott Sandford and Doug Hudgins for many useful discussions and interactions, and especially to Dr. Lou Allamandola for his enthusiasm for having me participate in the group.

REFERENCES:

1. F. Salama, "Low Temperature Spectroscopy: From Ground to Space", from Low Temperature Molecular Spectroscopy (R. Fausto, ed., Kluwer, 1996).

2. F. Salama and L.J. Allamandola, "Electronic Absorption Spectroscopy of matrix-isolated polycyclic aromatic hydrocarbon cations. I. The naphthalene cation ($C_{10}H_8^+$). J. Chem. Phys. 94 6964 (1991).

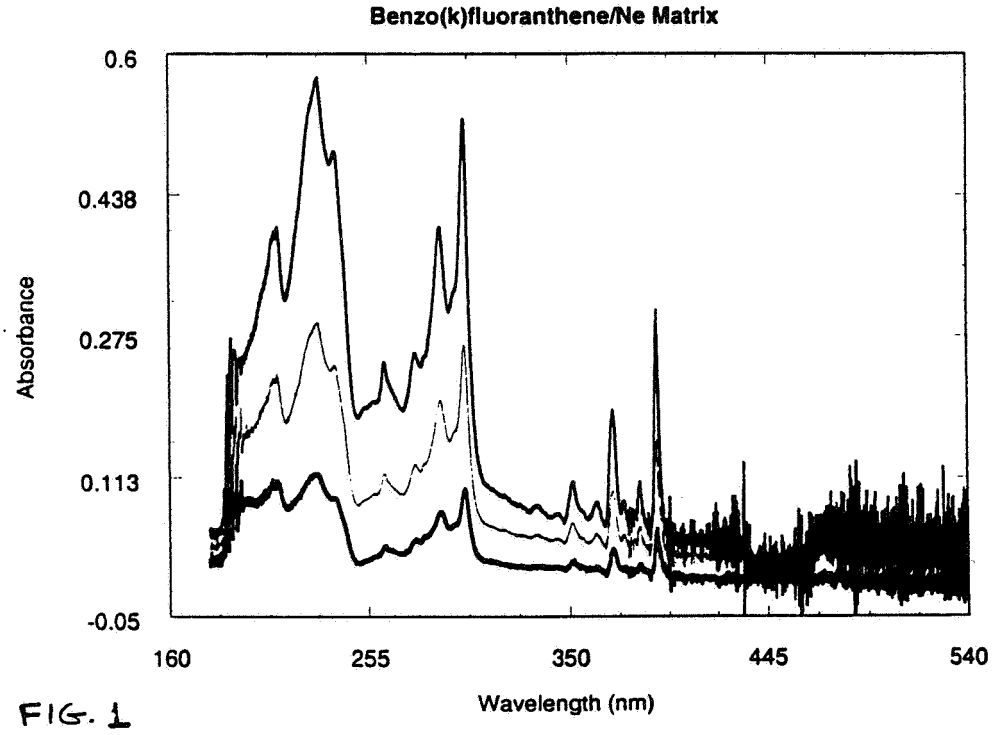

FIG. 1

NASA-ASEE-Stanford Summer Fellowship 1996-Final Report

H. William Wilson, Professor of Chemistry, Western Washington University, Bellingham, WA, 98225

Introduction

Several reduced sulfur compounds are produced in the terrestrial boundary layer and emitted into the atmosphere as part of the sulfur cycle, probably the least understood of all of the elemental atmospheric cycles. The group includes hydrogen sulfide, H_2S, carbon disulfide, CS_2, carbonyl sulfide, OCS, methyl sulfide, $(CH_3)_2S$, and dimethyl disulfide, $(CH_3)_2S_2$. Of these, only carbonyl sulfide, OCS, is inert enough to exist in the atmosphere for relatively long periods of time. Various estimates of the residence time of the compound range from about 1 year to 10 years (1).

Ultimately, the fate of OCS is oxidation to CO and $SO_4^=$ by singlet D oxygen atoms O (^{1}D) or OH radicals, both of which are produced by photochemical reactions. It has been proposed that much of the sulfate loading of the stratosphere results from the oxidation of OCS (Crutzen). Because of its important potential role as a S tracer, OCS has received considerable interest from spectroscopists involved in atmospheric measurements from airborne platforms (2).

There are several methods by which analytical data for OCS loading can be obtained. They include such classical techniques as whole air sampling and gas chromatography but each, however, is a relatively slow method and the amount of information that can be obtained from a flight is severely limited. Tunable diode laser (TDL) spectroscopy offers a viable alternative with many advantages (3-5).

Present day spectrometers are compact, light weight, and capable of accumulating 10 - 30 spectra/second with a resolution of under 10^{-4} cm^{-1}. The net result is that a large number of spectra can be obtained in a short time and co-added to give S/N ratios in excess of 1000:1. At Doppler limited resolution, a TDL spectrometer is capable of isolating individual rotation/vibration lines in complex atmospheric spectra. In the 5 μm atmospheric window region for instance, the ν_3 band of OCS and its rotational fine structure can be differentiated from its own isotopic species and hot bands, and from fine structure due to other compounds in the atmosphere, including CO, CO_2, and H_2O (Figure 1). Our TDL has been shown capable of isolating as many as 10 -15 OCS R- and P-branch transitions that show no evidence of occluded structure from other species nor nearby isotopic transitions. Fried et al (6) have shown that a TDL absorption spectrometer (TDLAS) equipped with a long path infrared cell (117 m) can theoretically yield OCS measurements accurate to the 10 part per trillion (pptv) level. OCS mixing ratios of about 500 pptv are typical at ground levels, so the TDLAS and long path cells offer an attractive alternative to GC or whole air sampling.

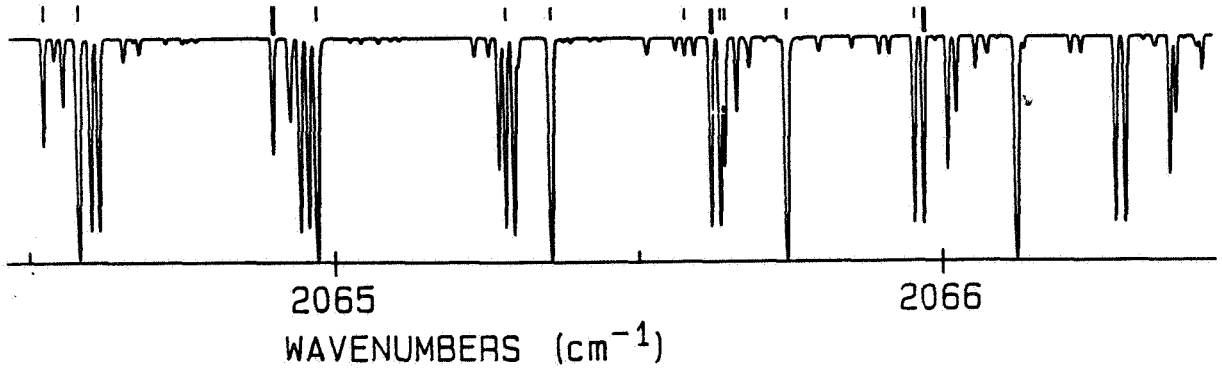

Figure 1. Section of high resolution spectrum of OCS showing variety of isotopic and hot bands.

The goal of this summer's work with our colleague, Dr. Max Loewenstein of NASA Ames, was to examine rotation vibration features in the ν_3 band of OCS and select transitions that can be utilized to measure OCS concentrations from an airborne platform with a TDLAS /long path length cell combination. Once suitable OCS rotational fine structure transitions are identified, nitrogen and oxygen pressure broadening coefficients for OCS can be determined at various temperatures with standard non-linear least squares by fitting hybrid Voigt profile bandshapes to the rotational fine structure features. Information necessary for utilizing the TDLAS instrument in the lower stratosphere to measure OCS concentrations can be obtained. at temperatures that span the region from 180K to 298K and broadening gas pressures in the range from 20 torr to 120 torr.

Instrumentation

The particular optical system for the study was assembled at the NASA Ames Space Sciences laboratory of our colleague, Dr. Max Loewenstein. The core of the TDLAS instrument consisted of a lead salt ($PbS_{1-x}Se_x$) laser tuned to a central frequency of 2060 cm^{-1} by Laser Photonics. It was operated in sweep integration mode (7) with an InSb detector cooled to LN2 temperatures and controlled with a Laser Photonics laser control module. Data was digitized on a Keithley 1600F A/D board and collected on an IBM 386 PC dedicated to the project. The laser had been characterized in 1995 during an ASEE/NASA/Stanford summer fellowship and 14 lines including transitions in the P and R branches of the ν_3 OCS band were selected for study. The sample cell was a 30-cm cold cell that has been described previously (8). Briefly, it consists of an an oxygen-free 30-cm copper cell thermally interfaced with a LN2-cooled copper block. Temperatures are controlled from about 80K to room temperature with 1- to 5-W bucking heaters. They can be maintained to within +/- 2K. Commercial OCS samples were used without further purification. The cell is illustrated in Figure 2.

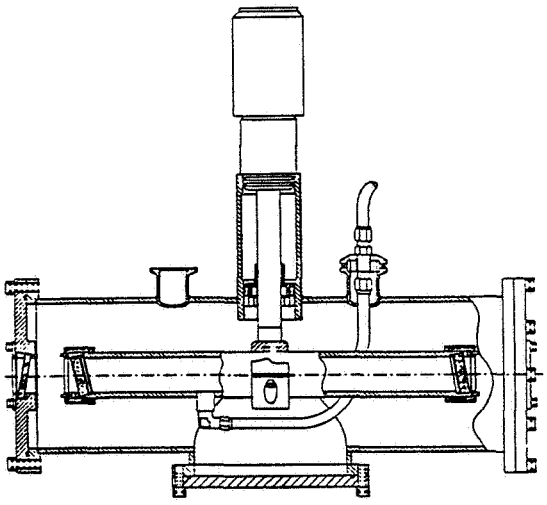

Figure 2. Cutaway of cold cell assembly used for measuring foreign gas broadening coefficients at subambient temperatures as low as 85 K.

Accomplishments

Fourteen separate rotational transitions were scanned in 2 different laser modes. They included the P(10), P(11), P(12), P(13), and P(14) features and the R(23), R(25), R(26), R(27), R(28), R(30), R(31), R(32), and R(33) rotation/vibration fine structure bands. The measurements were made at 4 different temperatures; 296 K, 250K, 225K, and 182K. Values using N_2 and O_2 as the foreign broadening gases have been obtained for all of the lines at all of the temperatures listed. Most researchers accept a linear combination of the N_2 and O_2 values as valid for the calculation of broadening due to air.

As far as we can find, the literature contains no information on the latter three temperatures. Data is available on broadening coefficients at 200K and at 170K, but the values are dated and appear to need revisions based on more recent software resources. Our newest measurements indicate that the 1980s information is about 10% too high. We plan to publish our results as soon as possible.

Future Work

In view of the complexity of the OCS spectrum, it is difficult to single out individual transitions whose intensities and widths are due solely to single lines. With current computing software, it is possible to deconvolve sets of overlapping lines under certain circumstances. In an effort to test the ability of a commercial software to deconvolve spectral features, we have measured a series of OCS lines at room temperature. They sets include both fundamental transitions and a nearby isotopic set that converges on and passes through the fundamental sequence of lines as the J quantum numbers increase. . We have been able to record spectra in which we can begin with well separated lines and gradually observe the coalescence and subsequent slow separation of lines as higher and higher J values are accessed. We plan to return to our home institution and use our own TDLAS to continue with room temperature measurements of this type. If we are successful, we would plan to return to Ames to repeat the deconvolution calculations at subambient temperatures with Dr. Loewenstein's cold cell system.

Bibliography

1. P.J. Crutzen, "The Possible Importance of CSO for the Sulfate Layer of the Stratosphere," Geophys. Res. Lett. 1976, 3, 73.
2. N.D. Sze and M.K.W. Ko, "Photochemistry of COS, CS_2, CH_3SCH_3, and H_2S: Implications for the Atmospheric Sulfate Cycle," Atmos. Environ. 1980, 14, 1223.
3. M. Loewenstein, J.R. Podolske, K.R. Chan, and S.E. Strahan, "Nitrous Oxide as a Dynamical Tracer in the 1987 Airborne Antarctic Ozone Experiment," J. Geophys. Res. 1989, 94, 11,589.
4. D.R. Hastie, G.I. Mackay, T. Iguchi, B.A. Ridley, and H.I. Schiff, "Tunable Diode Laser Systems for Measuring Trace Gases in the Troposphere," Environ. Sci. Technol. 1983, 17, 352A.
5. C.R. Webster, R.D. May, C.A. Trimble, R.G. Chave, and J. Kendall, "Aircraft (ER-2) Laser Infrared Absorption Spectrometer (ALIAS) for In-situ Stratospheric Measurements of Hcl, N_2O, CH_4, NO_2, and HNO_3," Appl. Optics 1994, 33(3), 454.
6. A. Fried, J.R. Drummond, B. Henry, and J. Fox, "Versatile Integrated Tunable Diode Laser System for High Precision; Application for Ambient Measurements of OCS," Appl. Opt. 1991, 30(15), 1917.
7. D.E. Jennings, "Absolute Line Strengths in ν_4, $^{12}CH_4$: a Dual Beam Diode Laser Spectrometer with Sweep Integration," Appl. Opt. 1980, 19, 2695.
8. Max Loewenstein and H.W. Wilson, "Line Width Temperature Dependence of Selected R-branch Transitions in the ν_3 Fundamental of $^{14}N_2{}^{16}O$ Between 135K and 295K. Spectrochim. Acta. 1992, 48A, 434.

NASA-ASEE-Stanford Summer Fellowship 1996 - Final Report

CALCIUM BALANCE IN MATURE RATS EXPOSED TO A SPACE FLIGHT MODEL

Ira Wolinsky, Ph.D., Dept. Human Development
University of Houston, Houston, TX

Introduction. Negative calcium balances are seen in humans during spaceflight [1] and bed rest [2], an analog of space flight. Due to the infrequency and costliness of space flight and the difficulties, cost, and restraints in using invasive procedures in bed rest studies, several ground based animal models of space flight have been employed. The most useful and well developed of these models is hind limb unloading in the rat [3]. In this model the hind limbs are non-weight bearing (unloaded) but still mobile; there is a cephalad fluid shift similar to that seen in astronauts in flight; the animals are able to feed, groom and locomote using their front limbs; the procedure is reversible; and, importantly, the model has been validated by comparison to space flight [4].

Several laboratories have studied calcium balance using rats in hind limb unweighting. Roer and Dillaman [5] used young male rats to study calcium balance in this model for 25 days. They found no differences in dietary calcium intake, percent calcium absorption, urinary and fecal excretion, hence indicating no differences in calcium balance between control and unloaded rats.

In another study [6], employing 120 day old females, rats' hind limbs were unloaded for 28 days. While negative calcium balances were observed during a 25 day recovery period no balance measurements were possible during unweighting since the researchers did not employ appropriate metabolic cages. In a recent study from this laboratory [7], using 200 g rats in the space flight model for two weeks, we found depressed intestinal calcium absorption and increased fecal calcium excretion

(indicating less positive calcium balances) and lower circulating 1,25-dihydroxyvitamin D.

The above studies indicate that there remains a dearth of information on calcium balance during the hind limb unloading rat space flight model, especially in mature rats, whose use is a better model for planned manned space flight than juvenile or growing animals. . With the aid of a newly designed metabolic cage developed in our laboratory [8] it is now possible to accurately measure urinary and fecal calcium excretions in this space flight model.

The purpose of this study, then, was to extend and enlarge our previous findings [7] viz: to measure calcium balances in mature rats exposed to a space flight model.

Results. To determine the effect of the space flight model on calcium balance in mature rats, we exposed six month old males weighing 492±12 g to the model for four weeks and compared calcium in the diet, urine, feces and 1,25-dihydroxyvitamin D in unweighted rats and controls. Rats were fed diets containing sufficient calcium (0.1%) to satisfy metabolic needs, but not to cause deficiency over the experimental period. At the end of four weeks, there was a five percent weight loss in the space flight model animals, but not in the controls. There were no differences in dietary, urinary or fecal calcium in hind limb unloaded and control rats. Net calcium absorption (0.1 vs. 2.7%), 1,25-dihydroxyvitamin D (50±16 vs. 47±14 pg/ml) and calcium balances (-1.8±4 vs. -1.0±2.9 mg/day) were similar in control and unweighted rats. Urinary calcium loss was added to the experimental model by inducing this calciuria with eight percent salt diets. A four-fold increase in urinary calcium excretion in both controls and space flight model animals was transiently higher in unloaded animals than controls after one week. After four weeks, loss in body weight was greater in hind limb unloaded rats than in controls,

calcium absorption was higher in controls than in space flight model rats (32±10 vs. 3.5±16%, $p<0.05$), 1,25-dihydroxyvitamin D greater in unloaded rats than in controls (98±15 vs. 79±14 pg/ml, $p<0.05$) and calcium balance loss in unloaded rats than controls (-5.2±4 vs. -1.7±2 mg/d, $p<0.05$).

Thus it has been shown that calcium balance in the mature rat is unaffected by the space flight model unless calciuria intervenes and reveals the failure of the intestine to enhance calcium absorption and compensate for urinary calcium loss.

References

[1] Whedon, G. D., Lutwak, L., Rambaut, P., Whittle, M., Reid, J., Smith, M., Leach, C., Stadler, C. and Sanford, D. (1976) Mineral and nitrogen balance study observation: the second manned Skylab mission. Aviat. Space Environ. Med. 47: 391-396.

[2] LeBlanc, A., Schneider, V., Spector, E., Evans, H., Rowe, R., Lane, H., Demers, L. and Lipton, A. (1995) Calcium absorption, endogenous excretion and endocrine changes during and after long-term bed rest. Bone 16: 301S-304S.

[3] Morey-Holton, E. and Wronski, T. J. (1981) Animal models for simulating weightlessness. Physiologist 24: S45-S48.

[4] Morey-Holton, E. R. and Arnaud, S. B. (1991) Skeletal responses to spaceflight. Adv. Space Biol. Med. 1: 37-69.

[5] Roer, R. D. and Dillaman, R. M. (1990) Bone growth and calcium balance during simulated weightlessness in the rat. J. Appl. Physiol. 68: 13-20.

[6] Lutz, J., Chen, F. and Kasper, C. E. (1987) Hypokinesia-induced negative net calcium balance reversed by weight-bearing exercise. Aviat. Space Environ. Med. 58: 308-314.

[7] Navidi, M., Wolinsky, I., Fung, P. and Arnaud, S. B. (1995) Effect of excess dietary salt on calcium metabolism and bone mineral in a spaceflight rat model. J. Appl. Physiol. 78: 70-75.

[8] Harper, J. S., Mulenburg, G. M., Evans, J., Navidi, M., Wolinsky, I. and Arnaud, S. B. (1994) Metabolic cages for a space flight model in the rat. Lab. Anim. Sci. 44: 645-647.

RECOMBINATION RATES OF ELECTRONS WITH INTERSTELLAR PAH MOLECULES

NASA-ASEE-Stanford Summer Faculty Fellowship
1996 Final Research Report

Jorge Ballester, Dept. of Physics, Emporia State University, Emporia, KS

Introduction. The goal of this project is to develop a general model for the recombination of electrons with PAH molecules in an interstellar environment. The model is being developed such that it can be applied to a small number of families of PAHs without reference to specific molecular structures. Special attention will be focused on modeling the approximately circular compact PAHs in a way that only depends on the number of carbon atoms.

The Space Science Division at Ames has been and continues to be a world leader in theoretical and experimental investigations of interstellar polycyclic aromatic hydrocarbons (PAHs). The hypothesis that PAHs are present in interstellar space was motivated by the general agreement of PAH infrared spectra with the "unidentified" infrared emission bands.[1,2] This widely accepted PAH hypothesis has led to the suggestion that PAHs may play a role in other important astrophysical processes. For example, PAHs are expected to be particularly efficient at transferring UV photon energy to the interstellar gas by photoionization.[3] PAHs have also been suggested as carriers of the as yet unexplained diffuse interstellar absorption bands.[4]

Refinement of the PAH hypothesis is needed in several areas and progress can be made by theoretical modeling and laboratory simulation. One important issue is the experimental characterization of the properties (e.g. UV and IR spectra) of PAHs individually or within families. Furthermore, comparisons of PAH properties with observations must consider which charge states are most probable within a given environment. The relative abundances of the various charge states are determined by the rates of the fundamental processes which add or remove charge. The charge balance between the neutral and cation states can be expressed as

$$f(0)\cdot J_{pe}(0) = f(+1)\cdot J_{e}(+1)$$

where $f(Z)$ is the fraction of the PAHs with charge Z, $J_{pe}(0)$ is the rate of photoemission from the neutral and $J_e(+1)$ is the rate of electron recombination with the cation. $J_{pe}(0)$ is proportional to the product of the interstellar UV flux F_{UV} and the photoemission cross section σ_{pe}. $J_e(+1)$ is given by $n_e \cdot \langle v_e \cdot \sigma_e \rangle$ where n_e is the ambient electron density, v_e is the electron velocity, σ_e is the electron capture cross section, and the average is taken over a Boltzmann distribution of velocities.

Recent experimental results[5] indicate that the recombination rates of PAHs are considerably smaller than expected from the existing theoretical models[6]. One specific result expected from our project is the calculation of electron-PAH cation recombination rates. We have separated this calculation into several tasks. First we have investigated the nature of the interaction between electrons and PAHs, and are building an appropriate model potential. Next we will formulate a general description of the capture process combining classical and quantum principles. Then we will carry out analytical and numerical calculations to determine the capture cross sections and recombination rates.

In practice, the electron-PAH recombination problem is constrained in electron energy and PAH charge state. We are primarily interested in the diffuse interstellar medium with T~100K. The relevant PAH charge states depend on the electron recombination rate, so in principle we should begin by considering all possible states. However, for small PAHs electron recombination should take place primarily with PAH cations and, in regions of high electron density, neutral PAHs. We do not expect this basic conclusion to change with an improved model. In the case of large PAHs it will be necessary to consider multiple charge states.

Electron-PAH Potential. The part of the capture process in which the electron and PAH are separate entities is governed by an electron-PAH potential energy function which must be constructed from fundamental physical principles. The method by which we are building this potential is based on the *ab initio* distributed multipole analysis (DMA) of Price[7] and the electron-benzene potential of Baum, et al[8] in the context of simulating electron solvation in liquid benzene. We are constructing a potential which assigns appropriate multipoles and other properties to each carbon site.

The Coulomb attraction (i.e. monopole) between an electron and a PAH cation is the dominant interaction for large separations. In their calculations of electron recombination rates Verstraete, et al[6] use a pure Coulomb potential centered at the origin. However, distributed charges located at each carbon site will give a more accurate representation of the potential at smaller separations. Considering that in a classical description of the electron capture process the potential at the capture surface is important, the use of distributed charges may provide a more appropriate representation of the potential. We have identified several plausible ways in which the cation charge can be distributed among the carbon atoms. One possibility which we have developed is to use classical charged disc electrostatics suitably modified by the results of Huckel molecular orbital calculations.

Due to their symmetry, PAHs have no permanent dipole moment perpendicular to their plane and in general they have little if any in-plane moment. The quadrupole moment, the next multipole which must be considered, is relatively large for π-electron systems. Its contribution to the electrostatic potential drops as $1/r^4$, so it is not significant at large distances. However, distributed quadrupole moments can make a significant electrostatic contribution at short range. There are two major contributions to the total PAH quadrupole moment. The distribution of π-electrons above and below the molecular

plane generate an axial (i.e. linear) quadrupole at each carbon site. The in-plane polarization of peripheral C-H bonds generates localized dipoles which result in a net quadrupole moment with little or no residual total molecular dipole. We have found that suitably chosen axial quadrupoles at each carbon site and dipoles at each peripheral carbon site generate an acceptable model potential.

Additional terms in the potential must account for polarization, and quantum exchange and exclusion. Polarization is included in our potential via a localized polarizability at each carbon site. The effects of exchange and exclusion are included using the appropriate density functional expressions in terms of the electron density. The problems associated with applying density functional results to the open shell electronic structure of the cation is not yet resolved.

Capture Simulations. For each model potential, we will numerically integrate the equations of motion for the electron and determine the classical trajectory. The lack of spherical symmetry will make it necessary to consider different directions for the initial velocity as well as magnitudes and impact parameters. Considering the closest approach of the electron to the PAH, we will apply a capture criterion which determines whether or not the electron is captured. The minimal distance at which electron capture can take place is not clearly defined, therefore we will have to consider this point in greater detail. The capture cross section will be determined for each velocity and direction. We will then perform the appropriate averaging procedures to obtain recombination rates.

References

1. Leger, A., & Puget, J. L. 1984, *Astronomy & Astrophysics*, **146**, 81

2. Allamandola, L.J., Tielens, A. G. G. M., & Barker, J. R. 1985, *Astrophysical Journal*, **290**, L25

3. Bakes, E. L. O., & Tielens, A. G. G. M. 1994, *Astrophysical Journal*, **427**, 822

4. Salama, F., Bakes, E. L. O., Allamandola, L. J., & Tielens, A. G. G. M. 1996, *Astrophysical Journal*, **458**, 621

5. Abouelaziz, H., Gomet, J. C., Pasquerault, D. and Rowe, B. R. 1993, *Journal of Chemical Physics*, **99**, 237

6. Verstraete, L., Le'ger, A., d'Hendecourt, L., Dutuit, O. and De'fourneau 1990, *Astronomy and Astrophysics*, **237**, 436

7. Price, S. L. 1985, *Chemical Physics Letters*, **114**, 359

8. Baum, J., Cruzeiro_Hansson, L. and Finney, J. 1990, *Physica Scripta*, **T33**, 71

S1562

NASA-ASEE-Stanford Summer Fellowship 1996 - Final Report

007911

WEBPRESS: An Internet Outreach from NASA Dryden

Daniel J. Biezad, Ph.D., Professor, Aeronautical Engineering
Cal Poly State University, San Luis Obispo, CA. 93407

957775

p3

Introduction. The Technology and Commercialization Office at NASA Dryden, under the leadership of Mr. Lee Duke, has developed many educational outreach programs for K-12 educators. This project concentrates on the internet portion of that effort, specifically focusing on the development of an internet tool for educators called Webpress. This tool will not only provide a user-friendly access to aeronautical topics and interesting individuals on the world wide web (www), but will also enable teachers to rapidly submit and display their own materials and links for use in the classroom.

To understand the motivation for this project, it is important to understand three powerful underlying forces that are currently shaping the internet. The first is the enormous infusion of resources onto and into the internet, which is far outstripping the rate of increase in capability of the individual computing workstation. The downside of these growing pains are the proliferation of "home pages" and trivial (or worse) information which contributes to what has been called the "world wide wait" on the internet. In reality, however, much of the information is vital, immediate, and changing the way we do business, from submitting resumes to signing up for classes at the local university. The resource base available to any internet user is awesome and growing.

The second phenomenon shaping the web is that enormous talent is contributing to and is available on the internet. Educational institutions traditionally rely on the innovation and motivating power of their home grown faculty, and that will continue. However, that faculty's impact can be greatly extended by augmenting it with the uniquely talented contributors who are available on the internet. To do this the individual teachers must be able to use and to control web technology--they must be able both to access the talent and to implement it effectively in their own classroom scenarios.

Finally, it is vitally important for educators to realize that the emerging presentation and interactive educational power of a web browser is potentially independent of the hardware and software configurations (including the operating system) residing in their computers. By tapping into the virtually unlimited hardware and software capabilities of the internet, they can be relatively free from the limitations of the personal computer in their classroom. These capabilities are in their infancy now on the internet, and new internet languages like "Java" promise to exploit this new technological territory in the future.

Webpress is designed to provide a home for teachers on the internet who are interested in math and science as presented and illustrated with aeronautical themes. The primary emphasis of Webpress is the development of educational material using as a base the science of aeronautics. Webpress will provide basic links to NASA research centers and to K-12 web sites with aeronautical themes, identify other educators with similar

interests and their projects, promote internet educational packages and programs in progress, and provide an opportunity for "hands on" interactive educational experiences. Webpress for an individual educator includes directory space for his or her internet files on a server provided by Cal Poly State University, San Luis Obispo. Each educator can then be an author as well as a "web surfer" whose work will be available within a few days of submission on the internet.

Project Goals. The following goals were proposed for the Webpress project:

1. Develop a cooperative and productive relationship between NASA Dryden, Cal Poly (San Luis Obispo), and K-12 educators interested in producing their own educational material on the internet with aeronautical themes.
2. Identify and cooperate with K-12 educators to enable them to participate via the internet in ongoing projects at Cal Poly which are supported by NASA.
3. Assist in developing NASA training programs for educators which includes an introduction to and demonstration of the Java programming language.
4. Setup a procedure for teachers to develop and promote their own educational materials on the internet with rapid turnaround time, adequate storage, and an indefinite term of use.

WEBPRESS Description. The internet address for Webpress is

http://daniel.aero.calpoly.edu/webpress/webpress.html

which provides the following six hyperlinks: NASA, K-12 Education Center, Internet Instruction, Cal Poly (SLO), Teacher's Lounge, and Other Links (with aeronautical themes). The best way to become familiar with the Webpress is to experiment with the home page and then to submit your own Webpress by double-clicking on the link asking if you want to "make your own web page." This will establish you on the Cal Poly server with your own directory for html file storage. Subsequent files can then be sent to Cal Poly electronically and the URL internet address will be returned via e-mail.

The appendix shows the screens as they appear to the Webpress user. Webpress includes options for "text only" to increase the access time on the internet.

Accomplishments.

The Webpress link for educators is operational. They may submit and create their own customized home page which will be displayed indefinitely on a server operating at Cal Poly State University. Educators have their own directory for file storage on that server and enjoy full control of the contents submitted. Cal Poly system administrators, operating through the Aeronautical Engineering Department, review the contents at the time of submission and establish security checks so that the files will not be tampered with in the future. New web pages may be submitted at any time.

Educators were contacted in the Bakersfield area of Kern Country and in the Atascadero and Arroyo Grande areas of San Luis Obispo County. They were queried about their exposure to and their needs related to the internet. A few were recruited to

assist NASA in its ongoing efforts to produce course material. A major input from these educators was the need for control of their own internet materials in a timely manner.

A Java application has been planned involving an interactive experience of flight suitable for use in high school classrooms. A flight design portfolio will permit the student to select a wing shape, engine, elevator deflection, and weight location (center of gravity). The aircraft design equations will then be programmed to determining whether or not flight will occur, and an animated graphic will display the results to the student interactively. If problems occur the program will provide simple advice("move the center of gravity, choose a larger engine, etc."). The goal is to both illustrate the power of Java to educators and to provide an interactive educational experience to the student. At this time the application is in development.

Recommendations and Future Activities. It is recommended that the Webpress project be continued beyond the termination of the Fellowship to determine the level of teacher interest in this resource. If the interest remains high then a way to permanently implement the Webpress should be investigated.

It is further recommended that the Java application program be delivered to NASA for evaluation when it is completed. It may be possible to develop course materials at Cal Poly with aeronautical themes suitable for K-12 educators that are fully illustrated on the internet. They may contain Java application programs for animation and for interactive modes of use.

References.

[1] Lemay, L., and C.L. Perkins, Java in 21 Days, Sams Net Press, 1996.

[2] Gilder, G., "The Coming Software Shift," Forbes Magazine, August 28, 1995.

[3] Business Section, The Economist, October 14, 1995, pp. 75-76.

[4] Brock, C., "An Introduction to the Internet," NASA Dryden FRC (no date).

Welcome to Webpress!

What is Webpress?

Webpress is a World Wide Web page that is designed for K-12 teachers. The primary emphasis of Webpress is the science of aeronautics, and the page includes many links to various NASA facilities as well as many other scientific organizations.

Webpress has many features of interest to K-12 educators:

NASA Links- see what is going on at NASA facilities around the country. Learn how you and your students can get involved with ongoing aeronautical projects.

Teacher's Lounge- this is a place to "hang out" and exchange ideas with other educators.

Make Your Own Webpage- this feature will let you easily make and post your own Webpage as part of Webpress.

Education Links-We've searched the Web for other sites that we thought would be of interest to you as educators. Webpress offers summaries of some of the best sites on the Web and links directly to them.

Internet Instruction- Webpress offers information to help you learn more about the Internet. Learn where Internet classes are being held in your area.

And many other features. Come and explore!

Why is Webpress Different from other Webpages?

Although there are several other Websites dedicated to K-12 education, Webpress is different.

Quality Filter- The content of Webpress has been carefully screened for quality education sites and information. Even if you are new to the Web, you will not be overwhelmed by masses of information. Instead, we offer you the best of the best.

Rapid Publishing of Your Material- Webpress offers to educators the unique opportunity to rapidly design your own Webpage. You can quickly share your ideas with your peers as well as rapidly create tools for your students.

Interaction- Webpress fosters interaction between K-12 educators. In addition, through Webpress, you and your students will be able to actually participate in ongoing scientific projects all over the world.

How Do I Make a Webpress Webpage?

1. In your Internet browser, go to the following address (Webpress URL):

   http://daniel.aero.calpoly.edu/webpress/webpress.html

2. Scroll to the bottom of the page and click on Make your own Webpage.

3. Fill in the fields with the information requested. You may leave any field blank.

4. At the bottom of the page, click on "Submit Query".

5. In a few days, check to see your new Webpage! Start at the Webpress URL above, then click on Teacher's Lounge. Next, click on Meet the Teachers. Find your name on the list and click. Welcome to your new page!

Send comments and questions to dbiezad@oboe.calpoly.edu
Daniel J. Biezad, Ph.D.

Make Your Own Webpress Webpage!

Hi! This screen will let you establish your own Web page on our system! Just fill in the information requested and click the submit button. Your Web page will be established in a few days.

To check out your new page, start at the Webpress Homepage, follow the link to Teacher's Lounge, and click on Meet The Teacher's. Your name and a link to your own Web page should appear in the list. Have fun!

Your Information

Your First Name:

Your Last Name:

Your E-mail Address:

Your School:

Do you have any comments for other teachers?

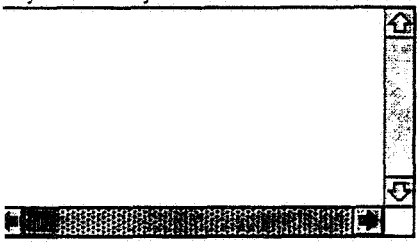

Thank you! Now just send in your responses by clicking on the the *submit* button.

Submit Query

ASEE FINAL REPORT:

A COMPARISON OF THE PHYSIOLOGY AND MECHANICS OF EXERCISE IN LBNP AND UPRIGHT GAIT

BODA W.L.*,WATENPAUGH D.E., BALLARD R.E., CHANG D.
LOOFT-WILSON R., HARGENS A.R.

Gravitational Research Branch (239-11), NASA Ames Research Center,
Moffett Field, CA 94035-1000.

INTRODUCTION

Bone, muscular strength, aerobic capacity, and normal fluid pressure gradients within the body are lost during bed rest and spaceflight (1). Lower Body Negative Pressure (LBNP) exercise may create musculoskeletal and cardiovascular strains equal to or greater than those experienced on Earth and elucidate some of the mechanisms for maintaining bone integrity (2,3). LBNP exercise simulates gravity during supine posture by using negative pressure to pull subjects inward against a treadmill generating footward forces and increasing transmural pressures. Footward forces are generated which equal the product of the pressure differential and the cross-sectional area of the LBNP waist seal. Subjects lie supine within the chamber with their legs suspended from one another via cuffs, bungee cords, and pulleys, such that each leg acts as a counterweight to the other leg during the gait cycle. The subjects then walk or run on a treadmill which is positioned vertically within the chamber. Supine orientation allows only footward force production due to the negative pressure within the chamber.

The purpose of this study was to determine if the kinematics, kinetics, and metabolic rate during supine walking and slow running on a vertical treadmill within LBNP are similar to those on a treadmill in a 1-g environment in an upright posture.

MATERIALS & METHODS

Eight healthy subjects (5 males and 3 females; age, 30 ± 2 years; height, 169 ± 8 cm; and weight, 67.76 ± 12 kg; mean ± SD) participated in the study after giving their informed written consent.. Reflective markers were placed on the shoulder, hip, knee, ankle, and 5th metatarsal for video analysis. A neoprene waist seal was selected such that one body weight of footward force was produced at a LBNP of 50-60 mm Hg as measured by a force insole inserted in the left shoe. The force produced by the insole

was calibrated using a force plate at a sampling rate of 500 Hz. The clear acrylic LBNP chamber allowed subjects to be videotaped during exercise. The exercise protocol consisted of 5 minute stages at self-selected walking and running speeds. Subjects were videotaped and force data were collected during the third minute of each stage. Force data were collected at 500 Hz and video data were collected at a frame rate of 60 Hz using a VHS camcorder to obtain five strides of a left sagittal view. The video data were digitized using a Peak Performance motion analysis system.

Oxygen consumption was analyzed from the 5th minute of each stage using computerized turbine volumetry and gas analysis. Heart rate was measured using electrocardiography. This protocol was approved by the NASA Human Research Institutional Review Board. Statistical differences were assessed using a repeated measures ANOVA with Newman-Keuls post-hoc tests and an α level of 0.05.

RESULTS

Many variables were essentially equivalent in supine LBNP and upright gait. There were no significant differences between footward forces integrated over each stride, rate of force development, VO_2, and heart rate in the upright versus LBNP exercise. Peak impact forces were not significantly different between LBNP and upright walking.

Some variables were different between upright and LBNP gait. Peak push-off forces were significantly less in LBNP than upright for both walking (646.7 ± 53.6 N and 774.4 ± 57.8 N, respectively; mean ± SE) and running (1,141.8 ± 284.3 N and 1,348.5 ± 334.8 N, respectively). Maximum rise distance of the foot was significantly higher during upright running (0.10 ± .004 m) than running in the LBNP chamber (0.08 ± 0.006 m). Step frequency was faster for running in the LBNP (1.34 ± 0.02 Hz) than upright running (1.29 ± 0.02 Hz) and slower for walking in the LBNP (0.87 ± 0.08 Hz) than walking upright (0.91 ± 0.05 Hz). Stance time was longer in the LBNP (0.55 ± 0.03 sec) than upright gait (0.53 ± 0.03 sec). Knee and hip flexion during swing phase were less in LBNP (67.6 ± 1.7° and 25.2 ± 0.7°, respectively) than upright gait (79.2 ± 1.7° and 28.4 ± 1.0°, respectively). Knee flexion during stance phase was also less during exercise in the LBNP chamber (35.8 ± 8.2°) than upright exercise (39.8 ± 8.3°).

DISCUSSION

Despite some differences in gait mechanics and force profiles between LBNP and upright gait, exercise within LBNP is physically demanding and remarkably similar to upright exercise against gravity. Integrated force data and rate of force generation within LBNP are not significantly different. Peak forces within LBNP are close to the

values produced during upright gait and could be increased by increasing the level of negative pressure within the chamber. Oxygen consumption and HR are not significantly different between LBNP and upright gait.

The kinematic differences observed during LBNP exercise such as the decrease in knee flexion, hip flexion and maximum rise of the foot during the swing phase of gait are probably due to the leg and back suspension system and the waist seal in the LBNP. As the leg extends through the pushoff phase, there is resistance against the bungee cords at the thigh and ankle holding up the leg. When one knee is flexed and the other extended there is maximal counter resistance within the bungee cord system. Many of these differences would disappear in microgravity because a suspension system would not be necessary.

This study suggests that LBNP exercise may provide sufficient musculoskeletal and cardiovascular strains during supine bedrest and in space to maintain aerobic capacity and bone density. LBNP exercise is also known to create transmural pressures within the body similar to upright standing in 1-g (1). The LBNP could also be used for the rehabilitation of patients at levels of 1/4 or 1/2 g for initial weight bearing during recovery from bedrest.

Accomplishments

Analysis of HR-143 bedrest data
Manuscript preparation of the data presented in this summary.

Future Activities We would like to study LBNP exercise within a KC-135 aircraft in order to determine if kinematic and kinetic changes within LBNP are due to the suspension system.

REFERENCES

1. Hargens et al. Acta. Physiol. Scand., 150, suppl 616,103-114, 1994.
2. Whalen et al.,Trans. Orthop. Res. Soc., 16:628,1991.
3. Hargens et al., Aviat., Space and Environ. Med., 62, 934-937, 1991.

Flow Field Measurements in a 3-D Separating Flow
Final Report for NASA-Ames - ASEE Summer Faculty Fellowship

Debora A. Compton
Aerospace & Mechanical Engineering, Boston University
16 August 1996

Summary

A combined experimental and computational effort to test the performance of turbulence models in prediction of three-dimensional separation is under way. The current phase of the project is the acquisition of flow field data using laser Doppler velocimetry. Accomplishments for summer '96 include development of the instrument and signal processing system and acquisition of mean velocity profiles.

Introduction

Predicting the onset of separation (and subsequently predicting reattachment) is a stiff challenge to turbulence models. Separation is characterized by the detachment of a boundary layer in the presence of adverse pressure gradient, with a layer of reversed flow beneath the shear layer. In the flow over a swept wing at angle of attack, the spanwise pressure gradient causes separation to exhibit three-dimensionality. Because three-dimensional separation greatly affects the performance of wings, it is critical in aircraft design to be able to predict separation accurately. Currently, most turbulence models fail in this area.

The overall approach of this project is to generate a relatively simple three-dimensional separation, to document the flow, and to test current turbulence models on the flow. The aim is eventually to develop improved turbulence models for the prediction of separation.

Experimental Setup

The three-dimensional separation is generated on the floor of an open circuit wind tunnel (in NASA-Ames Bldg. N-231) built especially for this project. The test section begins as 1.15m × 150mm, with a freestream velocity of 30 m/s. After a development length of 1.5m, the top wall boundary layer is removed via suction. The top wall then diverges over a length of 1.22m, and the exit height of the test section is 258mm. This diverging geometry causes the boundary layer on the bottom wall of the wind tunnel to be near separation. Removal of a small percentage of the mass flow from an elliptical hole on the top wall of the test section causes a three-dimensional separation. The tunnel walls are made of Plexiglas to allow for optical access, and the floor is instrumented with pressure taps in the separation region. Flack, Driver, and Schwarz (1996) found using surface oil flow techniques that the separation is symmetric about the tunnel centerline and that it exhibits "owl-face" skin friction line topology. Although the skin friction lines indicated a highly three-dimensional flow, the pressure field showed very little spanwise variation. The features of the flow which make it a good test case for computation are its simple well-defined boundaries and centerline symmetry. This test case is a more difficult flow to predict than flows with abrupt changes in geometry because the location of separation is not fixed by geometry.

To measure the velocity field in a reversing and highly sensitive flow, a non-intrusive instrument is required. Laser Doppler velocimetry is a logical choice. Johnson[1] has developed a strategy for building compact, essentially self-aligning, laser Doppler velocimeters with high spatial resolution. We developed

[1] private communication, 1996

a two-component laser Doppler velocimeter which would place an $80\mu m$ diameter measuring volume approximately 1m from the final lens. The instrument was mounted on a three-axis traverse system, with a computer-controlled stepper motor controlling motion in the wall-normal direction.

The system is shown in Fig.1. Light from an argon-ion laser is launched into a single-mode optical fiber. The output of the fiber is sent through a GRIN lens to generate a $370\mu m$ diameter waist about 200mm away. The beam is sent through a two-dimensional Bragg cell which serves to split and shift the beams. Three useful beams emanate: the reference beam, the U beam shifted by 40 MHz, and the V beam shifted by 42.5 MHz. The three beams all pass through a series of lenses which cause the measuring volume to be formed inside the wind tunnel. The interference fringe spacing in the measuring volume is approximately $20\mu m$. Scattered light from polystyrene particles passing through the interference fringes is captured by imaging the measuring volume onto the tip of a $600\mu m$ diameter fiber, viewing in sidescatter. The fiber feeds the signal into a photomultiplier tube. We developed a PC-based laser Doppler velocimetry signal processor. The signal from the photomultiplier tube is amplified, downmixed by 45MHz and filtered. The Doppler bursts then contain frequencies corresponding to the U velocity, centered on 5MHz, and the V velocity, centered on 2.5MHz. We use a high-speed A-to-D card (Gage Inc., model 2125, sample rate on one channel up to 250MHz with 8-bit resolution) to acquire series of Doppler bursts, using signal amplitude as the trigger criterion. In post-processing, we perform a fast Fourier transform on each burst and extract the frequencies corresponding to the two velocities.

Results

We present a series of mean velocity profiles along the centerline of the separation in Fig. 2. In this case, 6% of the mass flow is removed by suction from the top wall, and a separation bubble extends between $x = 59in$ and $x = 72in$. Within the separated region, the reversed flow (where $U < 0$) is quite slow compared to the external flow. Beyond $x = 80in$ the boundary layer reattaches.

For the same flow configuration, we have measured the skin friction using the Fringe Imaging Skin Friction method. We see that the skin friction reduces as is expected in the presence of adverse pressure gradient. In the region of separation the skin friction is only slightly negative, corresponding to the slow reversed flow encountered in the mean flow profiles.

We have also measured the mean velocity profiles for 8% suction. Those results are not shown here, but the separation bubble is significantly larger, with earlier separation, later reattachment, and larger displacement thickness.

Conclusion

We have measured the mean streamwise velocity at several locations in a three-dimensional separating flow. The next step in our study will be to compare computational solutions to these profiles to judge the computational results' ability to measure the displacement thickness of the separation bubble. Future work will include measurements of the turbulent shear stresses using the existing laser Doppler anemometer, and extension of the instrument to measure the spanwise velocity.

References

1. Flack, K.A., Schwarz, W.R., & Driver, D.M. (1996) "Experimental investigation of three-dimensional flow separation," ASME Fluids Engineering Division FED-Vol 237, pp 577–582.

2. Schwarz, W.R., Flack, K.A., Driver, D.M., & Jovic, S. (1995) "A combined experimental and computational study of pressure-driven three-dimensional separation in a turbulent boundary layer," Submitted to J. Exp. Thermal Fluid and Science.

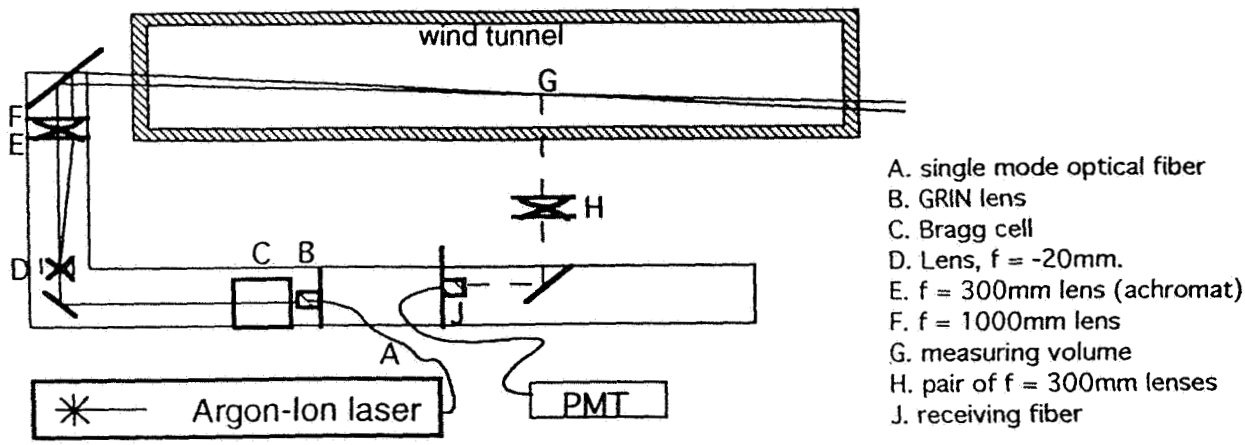

Figure 1. The laser Doppler anemometer.

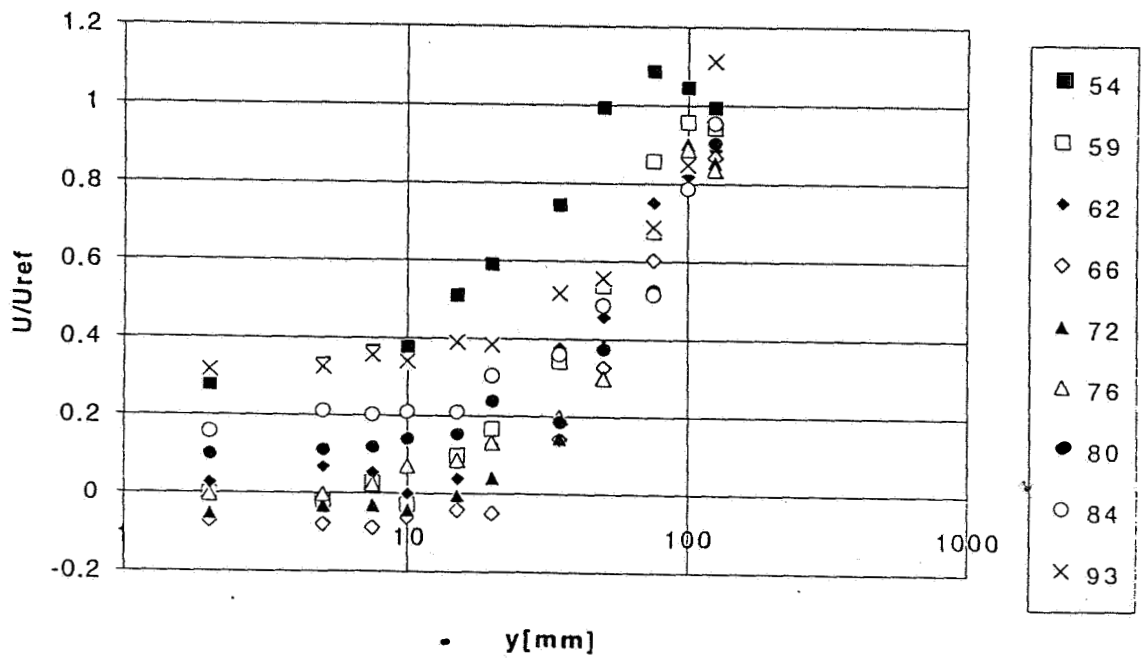

Figure 2. Mean velocity profiles along the centerline of separation, with 6% suction, normalized on a reference velocity. Each curve is for a different streamwise position.

Final Report
NASA-ASEE-Stanford Summer Fellowship Program
16 August 1996

John Crepeau
Department of Mechanical Engineering
University of Idaho

NASA Colleague:
Murray Tobak
Fluid Mechanics Laboratory

1 Center Manifold Work

The notions of dynamical systems theory in determining hydrodynamic stability have been around since Ruelle and Takens[1] proposed that the transition to turbulence consisted of a series of bifurcations in the flow. Since that landmark work, a number of papers have been written which contribute to the notions of dynamical systems and turbulence.

Determination of stability and transition in a boundary layer is an area of intense research. The linear stability results cannot accurately model fluid behavior when nonlinear effects dominate the flow. These effects include wall curvature, vortices, separation, and the onset of turbulent spots. The dynamical system approach to transition is based on the notion that instabilities are absolute within the flow field. There is a long history of using dynamical systems to analyze a boundary layer. Benjamin[2] describes bifurcations in Couette flow between rotating cylinders. End effects are taken into account, and he shows that as the Reynolds increases, these cause the smooth appearance of steady cellular vortex structures.

One objective in analyzing fluid motion using dynamical systems techniques is to reduce the infinite degrees of freedom inherent in fluid motion into a manageable number of modes. The concepts behind the center manifold are ideal for this purpose.

The equation that we started with was the Navier-Stokes equation where the velocity was decomposed into mean and fluctuating components. The fluctuating term was expanded in a fourier series, giving a system of ordinary differential equations,

$$\begin{aligned}\frac{da_i(\mathbf{k})}{dt} &= -\nu k^2 a_i(\mathbf{k}) - \frac{\partial U_i}{\partial x_l} a_l(\mathbf{k}) + 2\frac{k_i k_l}{k^2}\frac{\partial U_l}{\partial x_m} a_m(\mathbf{k}) \\ &\quad + i \sum_{\mathbf{k}'+\mathbf{k}''=\mathbf{k}} \left(k_i \frac{k_l k_m}{k^2} - \delta_{im} k_l \right) a_l(\mathbf{k}') a_m(\mathbf{k}'') \qquad (1)\end{aligned}$$

where the rate of change of the wavenumbers is,

$$\frac{dk_i}{dt} = -\frac{\partial U_l}{\partial x_i} k_l. \qquad (2)$$

The center manifold technique can reduce this equation in the following way. If the eigenvalues of the linear part of the equation are zero or negative, the stability of the system

can be reduced to a form,

$$\dot{\mathbf{y}}_c = \mathbf{J}_c(\mathbf{y}_c) + \mathbf{g}_c(\mathbf{y}_c, \mathbf{h}(\mathbf{y}_c)) \tag{3}$$

where $\mathbf{h}(\mathbf{y}_c)$ is the center manifold.

Approximately half of the summer was devoted to understanding the reduction technique and beginning to apply it to fluid problems. It provided the necessary foundation work for detailed study of the Blasius boundary layer and a precise description of stability within the flow field.

2 Flow Topology

Separated flow is an area of fluid mechanics that is of great practical interest, yet is very difficult to gain useful results using computational or theoretical tools. Experimental techniques using oil-streak methods have proven to be valuable, and describing the behavior of these streaks is important.

Topological arguments have been used to describe these streaks, with useful results. Patterns in these skin-friction lines can modeled in terms of nodes of attachment or separation, and saddles of attachment or separation. In a number of works, including Tobak and Peake[3], and Tobak and Coon[4], topological arguments were made to describe the behavior of juncture flows, especially flow impingement on a cylinder.

Roughly the other half of my summer was devoted to becoming familiar with the topological arguments and assisting my NASA colleague with proofing manuscripts and deriving necessary formula. Upon my arrival at NASA Ames, I described my work to Mr. Tobak. He was supportive of the center manifold ideas, but recommended that I look into his topological arguments. He assigned me the problem of determining the flow field for a wavy wall (see figure). This flow configuration is important because it can be useful in explaining the origin of disturbances in otherwise quiet windtunnels.

The flow topology studies dovetailed nicely into the center manifold studies, as the perturbations due to the vortices can lead to bifurcations farther downstream in the flow. The fluid dynamics laboratory has been working on explanations of vortices arising in the flow, and the topological studies have proven helpful in beginning to understand the phenomenon.

3 Future Work

I am grateful to my NASA colleague and the engineers at the Fluid Dynamics Laboratory for their helpfulness this summer. I found the research experience to be quite profitable, and it has laid the foundation for future work. This work will be carried on during the coming school year.
Future work includes:

- Employ the Blasius boundary layer and determine the eigenvalues of governing equations. Use center manifold techniques to determine stability at increasing Reynolds

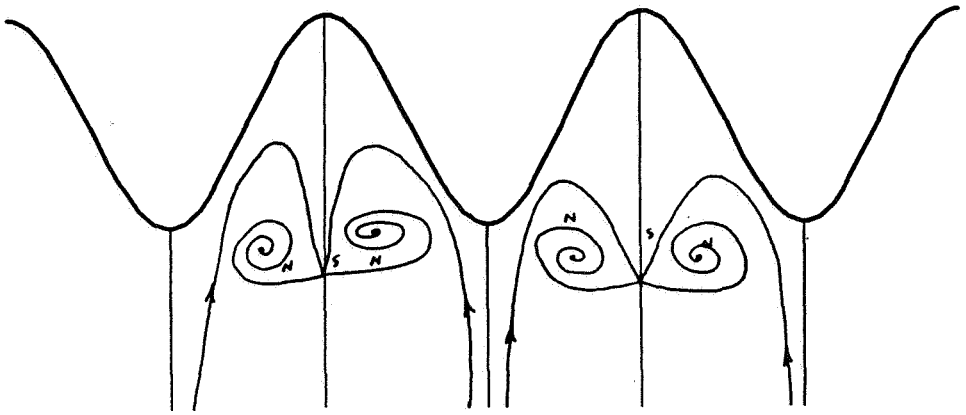

Figure 1: Nodes and saddles created by flow impinging on a wavy wall.

numbers and different locations above the plate, and construct resulting bifurcation diagram.

- Perform reductions with a two-dimensional flow, and then with a small crossflow component.
- Use center manifold techniques on other reduced equations, for example, Aubrey et al.[5] and Bertolotti et al.[6], and compare results.
- Formulate the mathematical constructs of the pressure variations and vorticity lines for flow impinging on a wavy wall, and for flow on a leading edge with small imperfections.

References

[1] D. Ruelle and F. Takens, Comm. Math. Phys. **20**, 167 (1971).

[2] T. B. Benjamin, Proc. R. Soc. Lond. A, **359**, 1 (1978).

[3] M. Tobak and D.J. Peake, Ann. Rev. Fluid Mech., **14**, 61 (1982).

[4] M. Tobak and M.D. Coon, AIAA Paper 96-0319, (1996).

[5] N. Aubrey, P. Holmes, J. L. Lumley, J. Fluid Mech., **192**, 115 (1988).

[6] F. P .Bertolotti, Th. Herbert, P. R. Spalart, J. Fluid Mech. **242**, 441 (1992).

NASA/ASEE Summer Faculty Program 1996 - Final Report

Emission Spectral Measurements in the Plenum of an Arc Jet Wind Tunnel

Jim Donohue, Santa Clara University, Department of Mechanical Engineering
NASA colleague: Doug Fletcher, NASA AMES, STA

Introduction Arc jet wind tunnel facilities are used to evaluate thermal protection system materials for re-entry vehicles. The high speed, high temperature flowfield generated by the arc jet can simulate the extreme aerodynamic heating environment experienced during re-entry so that the survivability of heat shield materials and performance of various designs options can be tested. Although the re-entry heating environment can be approximated in the arc jet facility, the flowfield only partially simulates the actual re-entry flight conditions. Reynolds numbers are not matched so that surface shear stress distributions and mass transfer rates due to ablation or other mechanisms are not modeled correctly. Unlike flight conditions the arc freestream air is in non-equillibrium because of the rapid expansion that occurs in the supersonic nozzle. To properly study the actual re-entry flow environment, computational fluid dynamics, computational chemistry and radiation models must be used. Arc jet tunnel tests serve to validate these models. To perform accurate simulations inlet and boundary conditions are needed, which come from measurements of the flowfield. The present study is concerned with measurements in the plenum region an arc heater. In the past, conditions in the arc heater flowfield have been predicted using simulations[1] since conventional measurement techniques could not be used in the harsh extremely high temperature environment. The present study is part of a recent push to utilize optical techniques to help better characterize the arc jet flowfields. Emission measurements have been made in the shock layer and the constrictor section of the arc heater[2] to determine temperatures and species number densities. LIF measurements have been made in the free stream to determine temperature and velocity.

Experimental Set-up Figure 1 shows a schematic of the facility to be used in the present study, the AHF conical nozzle arc jet tunnel at the NASA Ames Research Center. Air is injected into a constrictor type arc heater which is powered by a 20 MW DC power supply. The electric discharge heats the air which is passes through a plenum/settling chamber section and is then expanded through a supersonic nozzle. The flow passes over the test model and into the diffuser section. The test chamber is maintained at low pressure conditions by a steam ejector system located downstream of the diffuser.

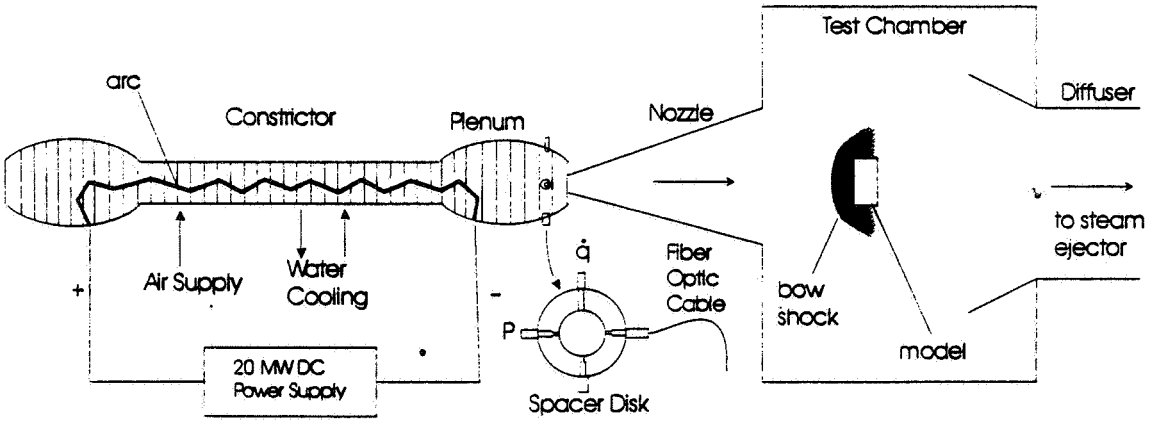

Figure 1 - Arc jet wind tunnel schematic

The arc heater assembly is composed a stack of over two hundred water cooled copper disks whose inside surfaces form the flow path inside the heater. Some disks are used as electrodes for the arc while others contains pathways to inject test gases. For the measurements to be made here, one of the spacer disks in the plenum region has been replaced with a specially instrumented disk. This disk contains ports to gain optical access, to make surface heat flux measurements and to make static pressure measurements as shown in Figure 1. The emission from the hot gases in the plenum (perhaps 10,000-15,000 K) is collected with a fiber optic cable and sent to a monochrometer in an adjacent room. The monochrometer is scanned to measure the emission spectrum from approximately 300-900 nm. A PMT is used to measure light intensities and the MACLAB data acquisition system is used to record the data. Deuterium and tungsten lamps are used to calibrate the measured intensities due to variations in the spectral response of system optical components. A mercury lamp is used to calibrate the wavelength scale.

Since the proposed technique is a line-of-sight technique and the properties inside the plenum are expected to vary radially, the emission spectra collected give measurements averaged through the flowfield. If several lines of sight are measured an Abel inversion can be used to make measurements across the flowfield. Because pressures in the arc heater are relatively high (50 - 100 psi) the emission in the plenum region may be optically thick for many wavelengths, considerably complicating the interpretation of the measurements.

Simulated emission spectra The arc jet facilities have been undergoing an overhaul recently and are expected to be operational in the near future. Since measurements are not presently available a calculated emission spectra from NEQAIR[3] was used to 1) gain familiarity with the kind of results that are expected, 2) to begin developing data reduction schemes and 3) to evaluate possible sources of error in the measurements. Figure 2 - shows the simulated data.

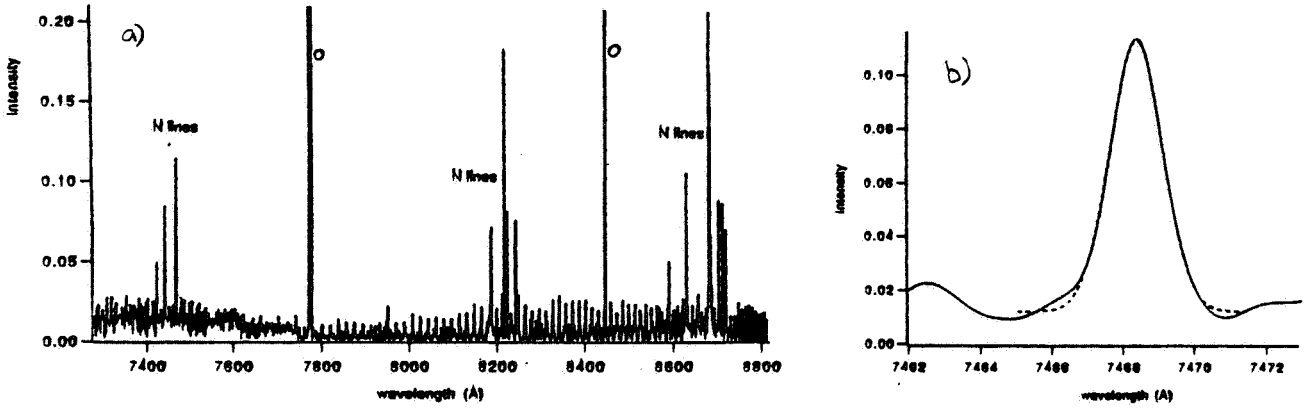

Figure 2 - a) Emission spectra of equilibrium air at 7000 K, simulated data using NEQAIR. b) Closeup of a spectral line with a Gaussian curvefit used to determine the line strength.

Excitation Temperatures from Emission Spectra If a flowfield is in equilibrium the intensity of a spectral lines can be modeled as[3]:

$$I = C_1 \frac{A_{ul} g_u}{\lambda} e^{\frac{E_u}{kT_e}}$$

Here I is the intensity of line, A_{ul} is the Einstein transition probability, g_u the degeneracy of upper state, λ the wavelength of emission, and E_u the energy of the upper state. The terms can be rearranged to give:

$$\ln(\lambda I / A_{ul} g_u) = (-1 / kT_e) E_u + C_2$$

A Boltzmann plot is made by plotting, for several lines, the log term against the upper state energy. The slope of the line determines the electronic temperature of the species, assuming the flow is in equilibrium. Line intensities are measured by integrating over the line shape. Figure 3 gives an example of this kind of plot made for several of the N lines in the spectra shown in Figure 2.

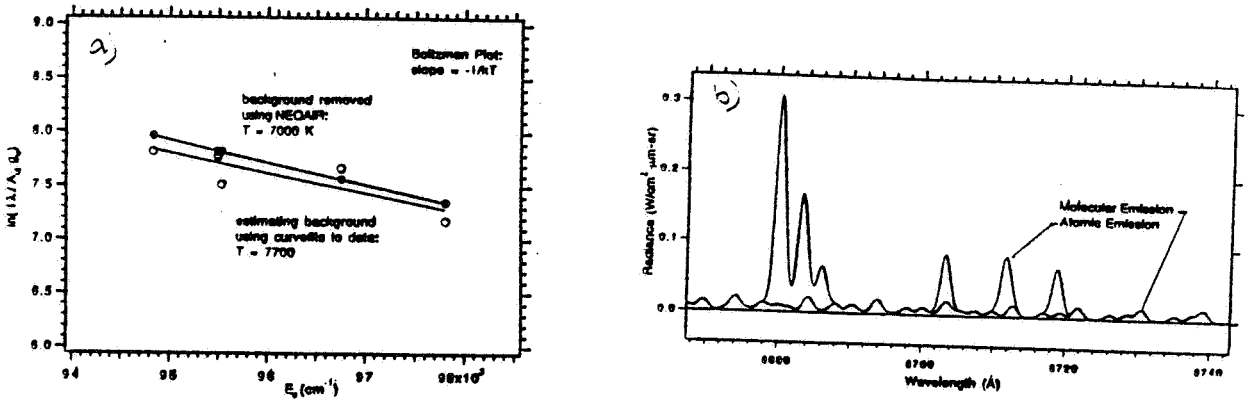

Figure 3 - a) Boltzmann plot to determine electronic temperature of atomic nitrogen using simulated spectra from NEQAIR. Correct line strengths found by taking only N contribution to spectrum, b) Emission contribution due to several atomic lines of interest for Boltzmann plot and background emission from molecular species.

The figure shows that in a measured spectra emmision will be due to both molecular and atomic transitions. While it is easy to separate these contributions out in a calculated spectra, as was done here, in an experimental spectra a method for determining the contribution form a single species must be developed. Here a curvefit using a gaussian with a DC offset is made throughthe region near the spectral line. The DC offset is used as an estimate of the background level. Using this method with the simulated data shows a 10% error in the electronic temperature determined.

Summary and Future Plans Emission in the plenum region of an arc jet heater is to be measured using a manochrometer/fiber optic set-up. Hardware to make the measurement is in place and upgrades to the optical setup, including fiber optic cables and holographic gratings for the spectrometer, are planned. Atomic electronic temperatures can be determined from Boltzmann plots assuming equilibrium conditions exist. Eventually a measurement using multiple lines-of-sight will be needed to account for radial variations in conditions. The measurements have been delayed due to arc jet facility problems. NEQAIR simulated data has been used to allow data reduction techniques to be tested and to study sources of measurement errors. The measurements will be used to determine plenum temperatures, species concentrations, and enthalpy which can be used as inlet conditions for simulations of the nozzle, shock layer and surface flow around TPS materials being tested in the arc jet facilities.

References

1. Arc Flow Code W.E. Nicolet, Analytical and design study for a highpressure, high enthalpy constriction heater, AEDC TR-75-47, Aertherm Division / Acurex Corp., July 1975.
2. I. Terrazas-Salinas, C. Park, A.W. Strawa, N.K.J.M. Gopaul and J.S. Taunk, Spectral measurements in the arc column of an arc jet wind tunnel, AIAA Paper 94-2595 (1994).
3. C. Park, Nonequillibrium and equillibrium air radiation (NEQAIR) program: users manual, NASA TM-86707, July 1985.
4. H.R. Griem, Plasma Spectroscopy, McGraw-Hill, New York, (1964).

S21-42
007929
25781
p4

A Within-Leaf Radiative Transfer Model with Anisotropic Scattering

B. D. Ganapol, Professor, Departments of Hydrology and Water Resources and Aerospace and Mechanical Engineering, University of Arizona, Tucson Arizona

Introduction

The relatively new discipline of earth system science is concerned primarily with the dynamic evolution of our planet. Unlike in the past, the scientific focus is now on the Earth as an integrated system of land, oceans, ice, atmosphere and vegetation rather than the traditional limited view given by the investigation of only one subsystem. The goal of the earth scientist is to understand earth dynamics from first principles on a global scale. Specifically, the major challenge facing the earth science community is to reliably predict changes in the earth's climate over the next decade. In particular, the question of whether the observed and predicted changes are natural in origin or humanly induced must be addressed. Possibly, the greatest challenge is how best to communicate the scientific knowledge gained to world political and economic leaders so that sound environmental decisions can be made based on today's needs without compromising the environment and future prosperity. NASA has played and will continue to play a prominent role in addressing this challenge through its prodigious scientific enterprise "Mission to Planet Earth" (MTPE). The unique element of NASA sponsored scientific investigations of earth is the global perspective provided by earth-orbiting satellites. The centerpiece of MTPE is the Earth Observing System (EOS) which is a series of planned satellites to be launched during the next ten years. These satellites are expected to provide 15 year coverage of the earth beginning with the AM launch in 1998. NASA's responsibility will be to acquire, archive, process and distribute global data sets to interested researchers in order to answer relevant environmental questions facing the earth's population. Specific issues concerning land-cover and land-use, agricultural productivity and ecosystem vitality will be addressed as well as the potential causes for seasonal to interannual climate variation. Modeling from first principles is anticipated to contribute significantly to the MTPE activity. Using global or regional data, models will generate the underlying terrestrial state variables through inversion. With this knowledge, a model can subsequently be applied in the forward mode to interpolate and extrapolate new data characterizing new scenarios. In this way, predictions in faster than real time can be made. The research to be described here concerns the

development of a within-leaf radiative transfer model for application to satellite remote sensing of terrestrial vegetation.

Remote Sensing of Vegetation

To reliably interpret an optical signal from vegetation detected on -board a space platform, signal distortion caused by the atmosphere as well as the vegetation canopy cover must be removed. This is accomplished by theoretically specifying how photons interact with molecules in the atmosphere and within the canopy. Photons undergo both deflection and absorption as the travel along their trajectories. In addition, photons interact within the canopy leaves and therefore contain information concerning the leaf biochemical content. In order to extract this information, which is useful in predicting the health status of a canopy, a leaf radiative transfer model simulating how these interactions occur is required. In the remainder of this presentation, the development of such a model is described.

A Within-Leaf Radiative Transfer Model

The photon/leaf interactions to be modeled concern both deflection and absorption of photons. A photon can be initially scattered by small structures on the leaf surface which also tend to polarize the scattered light. Photons entering the leaf interior experience diffuse "volume scattering" either within the cell walls or through the variation of the index of refraction as the photons alternatively pass through cell tissue and entrapped water or air. Some photons will be absorbed by the pigments in the visible and by the water in the near infrared wavebands. Absorptions produce atomic and vibrational excitations of the molecules constituting the leaf biochemicals.

For modeling purposes, the leaf is assumed to be a homogeneous plane parallel medium which is infinite in extent in the transverse dimensions. Thus, only vertical spatial variation will be accommodated. In addition, an anisotropic law of deflection (or phase function) will be specified which is a departure from the initial model developed [1] where only isotropic scattering was assumed. A radiative transfer equation can therefore be formulated under these assumptions. A balance of photons in a spatial/directional phase space is constructed accounting for scattering, absorption and streaming between collisions. The resulting equation specifies the radiance which is a measure of the number of photons in a differential volume around any given position traveling in a differential cone of angles about a specific direction. The physical data required for this model are the coefficients characterizing scattering and absorption interactions ($\Sigma a, \Sigma s$), the medium thickness and the phase function. The

desired quantities, are the exitances at the top (reflectance) and bottom (transmittance) of the leaf and the exiting radiances.

Model Inversion and Demonstration

The value of the within-leaf radiative transfer model is in the inversion to obtain information concerning the biochemical content of the leaf. An exact inversion has been devised in which experimentally measured exitances are equated to those obtained via the model. This results in two highly non-linear equations which can be solved by a Newton-Raphson root solver to obtain the scattering and absorption coefficients at each wavelength.

As a demonstration, an inversion was performed using measured exitances from a representative leaf of the LOPEX [2] data set. To observe the effect of an isotropic versus anisotropic scattering law on the retrieved absorption profile, two case were investigated -- a forward peaked anisotropic "fog" and an isotropic phase function. As shown in the accompanying figure for the visible wavelengths, the affect on the

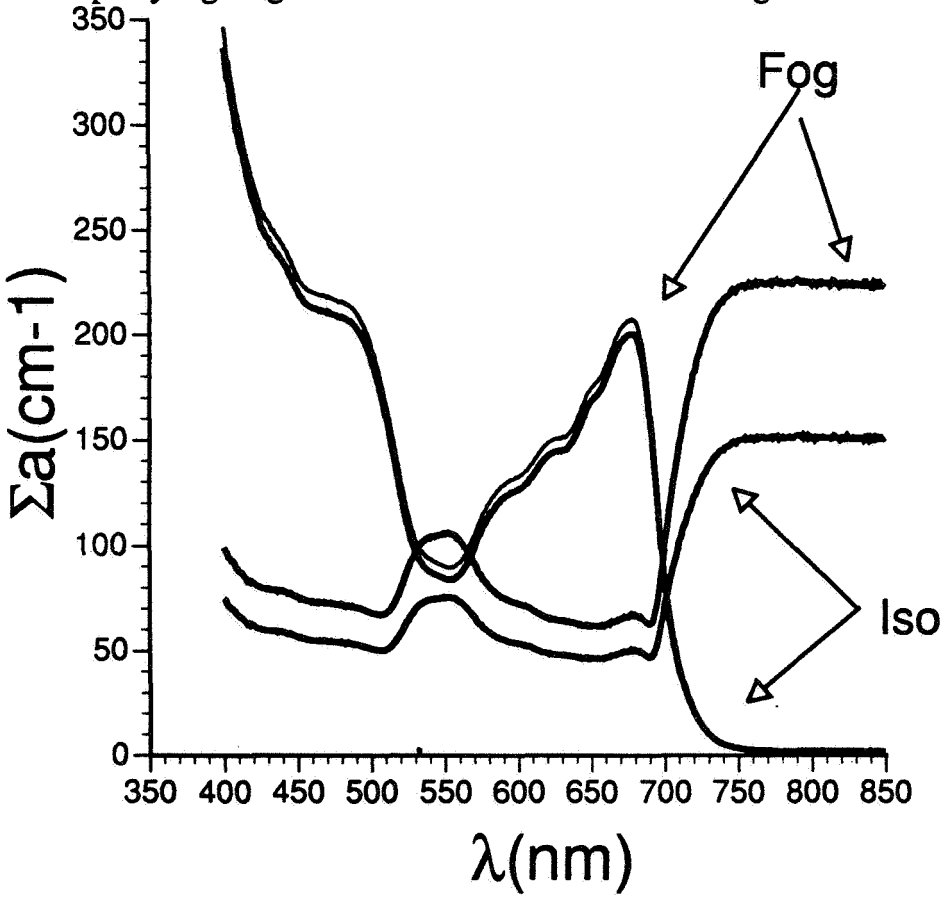

retrieved absorption profile is minimal. The reason is that since scattering and absorption are essentially separate physical effects, the distribution of scattered photons does not directly influence the medium properties. To maintain the desired reflectance spectrum for different phase functions therefore, the scattering coefficient merely adjusts itself appropriately.

References

[1] Ganapol, et. al., IGARSS94, Firenze, Italy, (1994).

[2] Hosgood, et. al.,LOPEX93, European Commission, Joint Research Center, Institute for Remote Sensing, Ispra, Italy, Report EUR-16095-EN(1994).

NASA-ASEE-Stanford
Summer Faculty Fellowship Program
1996 - Final Report

Effect of +Gz acceleration on the oxygen uptake-exercise load relationship during lower extremity ergometer excercise

Catherine G. R. Jackson, Ph. D., Professor, Kinesiology,
University of Northern Colorado, Greeley, Colorado

Long term spaceflight and habitation of a space station and/or the moon require that astronauts be provided with sufficient environmental and physiological support so that they can not only function in microgravity but be returned to earth safely. As the duration of habitation in microgravity increases, the effects of the concomitant deconditioning of body systems becomes a concern for added exercise in space and for reentry to Earth gravity. Many countermeasures have been proposed to maintain proper functioning of the body, but none have proved sufficient, especially when the cost of crew time spent in these activities is considered. The issue of appropriate countermeasures remains unresolved.

Spaceflight deconditioning decreases tolerance to +Gz acceleration, head to foot, the direction which is experienced during reentry; the result is that the crew member is more prone to becoming pre-syncopal or syncopal, thus exacerbating the orthostatic intolerance. All ground-based research using microgravity analogues has produced this same lowered G tolerance.

When intermittent exposure to +1 to +4 Gz acceleration training was used, some alleviation of orthosatic intolerance and negative physiological effects of deconditioning occurred. Exercise alone was not as effective; but the added G force was. The physiological responses to acceleration added to exercise training have not been clearly shown.

We will test the hypothesis that there will be no difference in the exercise oxygen uptake-exercise load relationship with added +Gz acceleration. We will also compare oxygen uptake during graded exercise-acceleration loads in the human-powered short arm centrifuge with those from normal supine exercise loads. The human-powered short arm centrifuge was built by NASA engineers at Ames Research Center (Figure 1).

During this summer we did preparatory work for this study with human volunteers. The centrifuge was refined as we concomitantly prepared for data collection. The analysis of oxygen and carbon dioxide which is necessary for the experiment was originally proposed to be attached to a platform on the centrifuge next to the subject. The equipment is bulky, has multiple units, and would be a safety problem should a piece of equipment break loose. As a

result we procured and evaluated two small, compact metabolic analyzers which could be used to collect the data.

The centrifuge has been set up and all preparations are being completed for the data collection phase. I will continue to collaborate on the project and hope to return for the actual experiment which will be conducted in a few months.

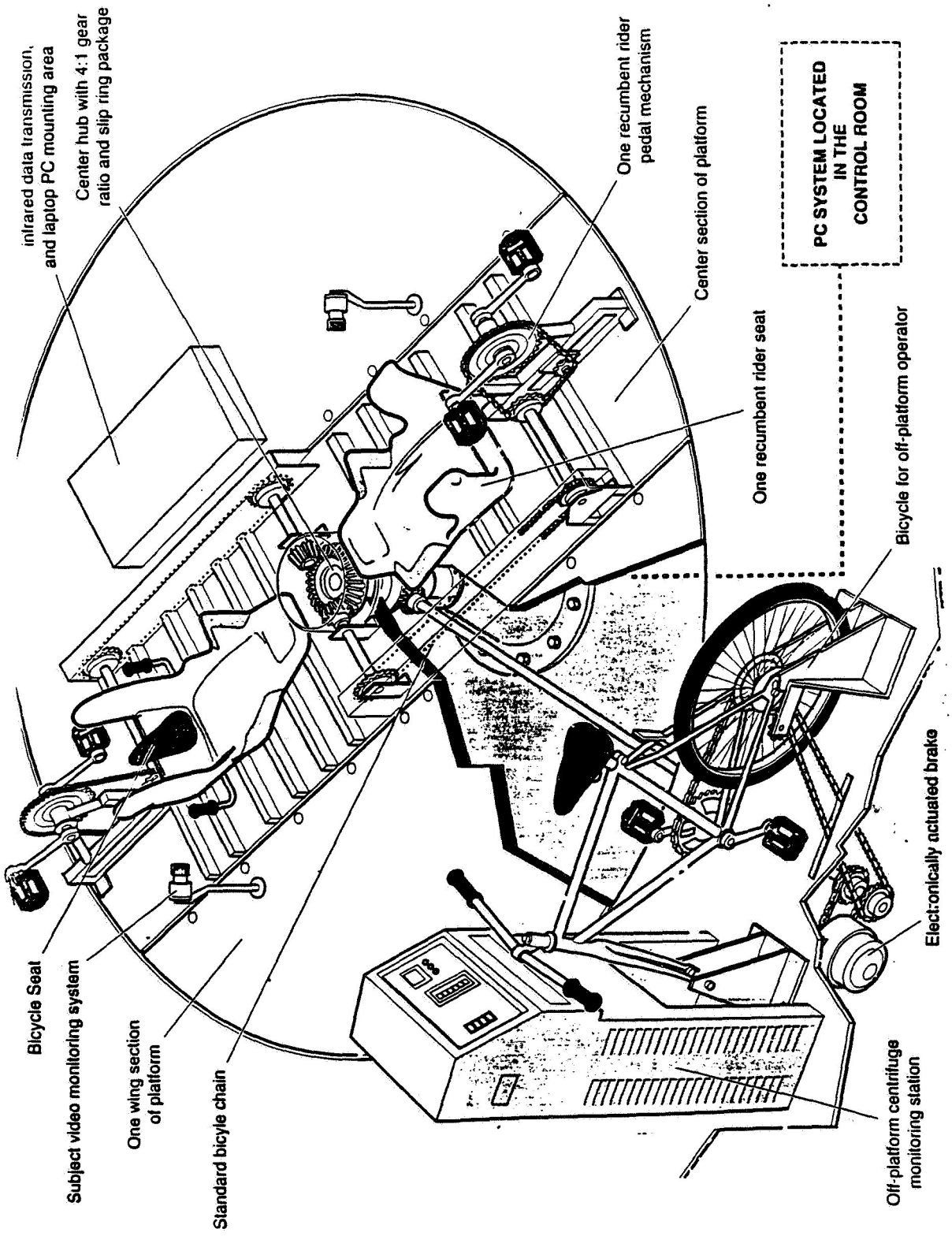

FIGURE 1

REFERENCES:

1. Burton, R.R. A human-use centrifuge for space stations: Proposed ground-based studies. Aviat. Space Environ. Med. 59: 579-582, 1988.
2. Burton, R.R., and L.J. Meeker. Physiologic validation of a short-arm centrifuge for space application. Aviat. Space Environ. Med. 63: 476-481, 1992.
3. Greenleaf, J.E. Letters to the editor (The metabolic "cost" of physical exercise training by astronauts in microgravity). Aviat. Space Environ. Med. 63: 150, 1992.
4. Greenleaf, J.E., R.F. Haines, E.M. Bernauer, J.T. Morse, H. Sandler, R. Armbruster, L. Sagan, and W. Van Beaumont. +Gz tolerance in man after 14-day bedrest periods with isometric and isotonic exercise conditioning. Aviat. Space Environ. Med. 46: 671-678, 1975.
5. Kumer, K.V., and W.T. Norfleet. Issues on human acceleration tolerance after long-duration space flights. Johnson Space Center, Houston, TX: NASA Tech. Memo 104753, 1992. 48 p.
6. Shulzhenko, E.B., I.F. VilVilyams, E.A. Aleksandrova, and K.I. Gogolev. Prophylactic effects of intermittent acceleration against physiological deconditioning in simulated weightlessness. Life Sci. Space Res. 17: 187-192, 1979.
7. Shulzhenko, E.B., I.F. VilVilyams, M.A. Khudyakova, and A.I. Grigoryev. Deconditioning during prolonged immersion and possible countermeasures. Life Sci. Space Res. 14: 289-294, 1976.
8. VilVilyams, I.F., Ye.B. Shulzhenko. Functional state of the cardiovascular system under the combined effect of 28-day immersion, rotation on a short-arm centrifuge and exercise on a bicycle ergometer. Kosm. Biol. Aviakosm. Med. 14: 42-45, 1980.
9. White, P.D., J.W. Nyberg, L.M. Finney, and W.J. White. Influence of periodic centrifugation on cardiovascular functions of man during bed rest. Santa Monica, CA: Douglas Aircraft, Co., Inc., Report DAC-59286, 1966. 47 p. (NASA Contractor Rept. 65422).
10. White, W.J., J.W. Nyberg, P.D. White, R.H. Grimes, and K.L. Finney. Biomedical potential of a centrifuge in an orbiting laboratory. Santa Monica, CA: Douglas Aircraft, Co., Inc., Report SM-48703, 1965. 120 p. (Air Force Space System Div. Rept. SSD-TDR-64-209-suppl.).
11. Zborovskaya, B.I. Use of short-arm centrifuge to prevent deconditioning when immersed in water (according to H-reflex). Kosm. Biol. Aviakosm. Med. 13: 78-79, 1979.

1996 NASA-ASEE-Stanford Summer Fellowship
Final Report

Collagen Gel Contraction by Fibroblasts: The Role of Myosin II and Gravity Effects

Dr. Barbara P. Johnson-Wint
Associate Professor, Department of Biological Sciences
Northern Illinois University, DeKalb, IL

NASA Colleagues:
Dr. Alexandre Malouvier
Dr. Emily Holton
Life Sciences Division
Ames Research Center, Moffett Field, CA

Introduction

Several lines of evidence suggest that collagen organization by connective tissue cells is sensitive to force. For instance, in flight experiments on rats the collagen fibrils which were produced under weightlessness and which were immediately next to the tendon fibroblasts were shown to be oriented randomly around the cells while the older fibrils right next to these and which were produced under 1G, were highly organized (1).

In a previous study we tested the hypothesis that this can be explained because connective and supportive tissue cells respond to external force by exerting their own force on collagen either 1) directly through integrin-actin-myosin and/or 2) by cell-cell attachments involving N-cadherin-actin-myosin which squeeze fluid out of the collagen, in both cases, making the extracellular collagen dense enough to resist the external force (2). We used a model system involving cells seeded in Type I collagen gels in culture to test this hypothesis. We found that cells from different tissues and species had different intrinsic force generating characteristics. Collagen was contracted fastest on a per fibroblast basis by: (rabbit skin=rat skin)>(rat tail tendon=rabbit cornea)>rat cornea>rabbit foot tendon>>>mouse L-cells=0. Collagen was not degraded in these studies. Fibroblasts that contracted collagen slowly (rabbit and rat cornea, rabbit foot tendon) responded to rotational force (30-50 RPM) and to increased gravitational force up to 5G by contracting collagen more rapidly. Drugs that disrupt the cytoskeleton interfered with cellular collagen contraction. Cytochalasin D, colcemid and acrylamide at maximum effect inhibited 100%, 10-50% and 10-74% respectively of cellular collagen contraction depending on cell type. Integrin binding site peptides GRGDTP and KDGEA, and N-cadherin binding site peptide LRAHAVDVNG, respectively inhibited 0-43%, 43-100% and 0-36% of cellular collagen contraction depending on cell type. L-cells which have no N-cadherin, could not contract collagen gels. These results suggest interacting combinatorial roles for the cytoskeletal and transmembrane components examined here in collagen contraction by cells.

The purposes of the present study were 1) to test the role of myosin II in our hypothesis, and 2) to examine in more detail the effect of hypergravity on cellular collagen contraction.

Materials and Methods

Suspensions of fibroblasts and osteoblasts were seeded into culture medium containing native rat tail tendon Type I collagen in solution and 100 ul aliquots of the mixture applied as a 1 cm diameter drop onto an agarose coated tissue culture dish. At 37° C the collagen rapidly

polymerized into native fibrils forming a three dimensional gel in the shape of a disk with cells suspended throughout it. These cell gels easily detached from the floor of the culture dish with the addition of culture medium, and formed floating cell-bearing disk shaped collagen gels. The floating collagen cell gels were then cultured either 1) with increasing concentrations (0.01mM to 100mM) of 2,3-butanedione monoxime, a myosin kinase inhibitor to knock out myosin II function or 2) at 1G or with the additional physical forces of 4G to 6G in the Hypergravity Facility for Cell Culture (HyFaCC). Cell mediated physical remodelling of the collagen fibers in the gel (contraction) was followed by measuring the diameter of the cell containing collagen gel at appropriate time intervals and converting this data to area for comparisons.

Results and Conclusions

Myosin action to slide actin microfilaments was found to power collagen contraction by corneal fibroblasts. In a dose dependent fashion, the myosin kinase inhibiting drug, 2,3-butanedione monoxime, inhibited collagen contraction by corneal fibroblasts. The effective concentration range of 2,3-butanedione monoxime was 1mM-50mM (Fig. 1). The other cell types were not tested.

Study of four 1G control incubators, two with one fan motor and two with two motors (a fan motor and an air pump), revealed that vibration induces cellular collagen contration. Cell populated collagen gels in the two-motor incubators contracted collagen more rapidly than those in the one motor incubators.

Hypergravity at 5.6 G began to inhibit the ability of rabbit corneal fibroblasts to contract collagen gels (Fig. 2). Full inhibition of collagen contraction by these cells is predited to occur at 11 G. Hypergravity at 5.6 G did not inhibit the ability of rabbit skin or tendon fibroblasts, or rat fetal calvarial osteoblasts to contract collagen gels. Their inhibitory G range is predicted to begin higher than 5.6 G.

Future Directions

The following future experiments will be conducted:

1. Establish the specific full range of "G inhibition" of collagen contraction for corneal, skin and tendon fibroblasts and osteoblasts.

2. Use agents that inhibit polymerization or function of cytoskeletal elements to determine which elements are failing under increased G.

3. Examine collagen contraction by vibration isolated cultures.

References

(1) S.B. Doty, E.R. Morey-Holton, G.N. Durnova and A.S. Kaplansky. (1992). Morphological studies of bone and tendon. *J. Appl. Physiol.* 73: 10S-13S.
(2) B.P. Johnson-Wint, R. Grymes and A. Malouvier. 1995. Collagen contraction by corneal, skin and tendon fibroblasts: mechanisms and force effects. Biorheology 32: 175-176.

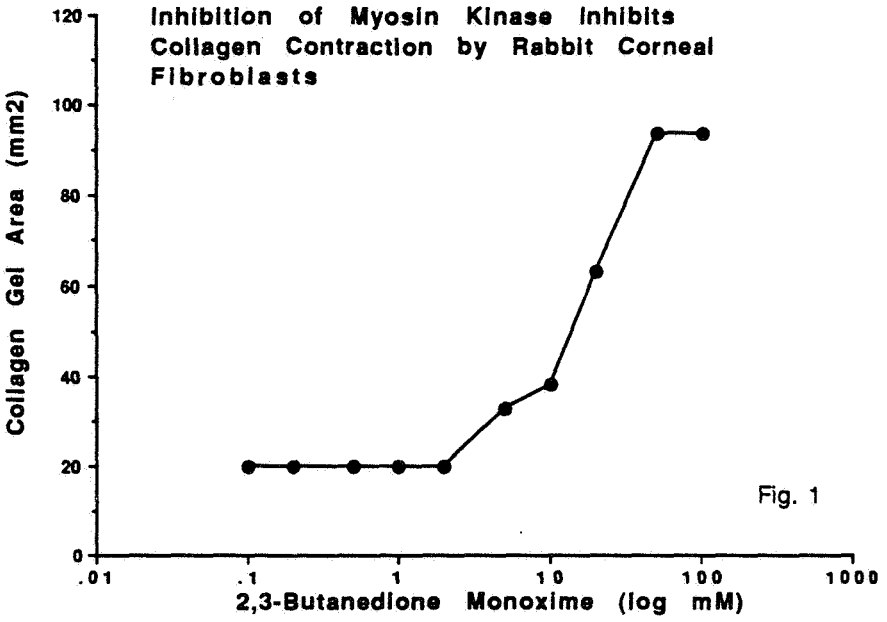

Fig. 1

Collagen Gel Contraction (8 hrs.) by Rabbit Corneal Fibroblasts is Impeded Above 4.4G

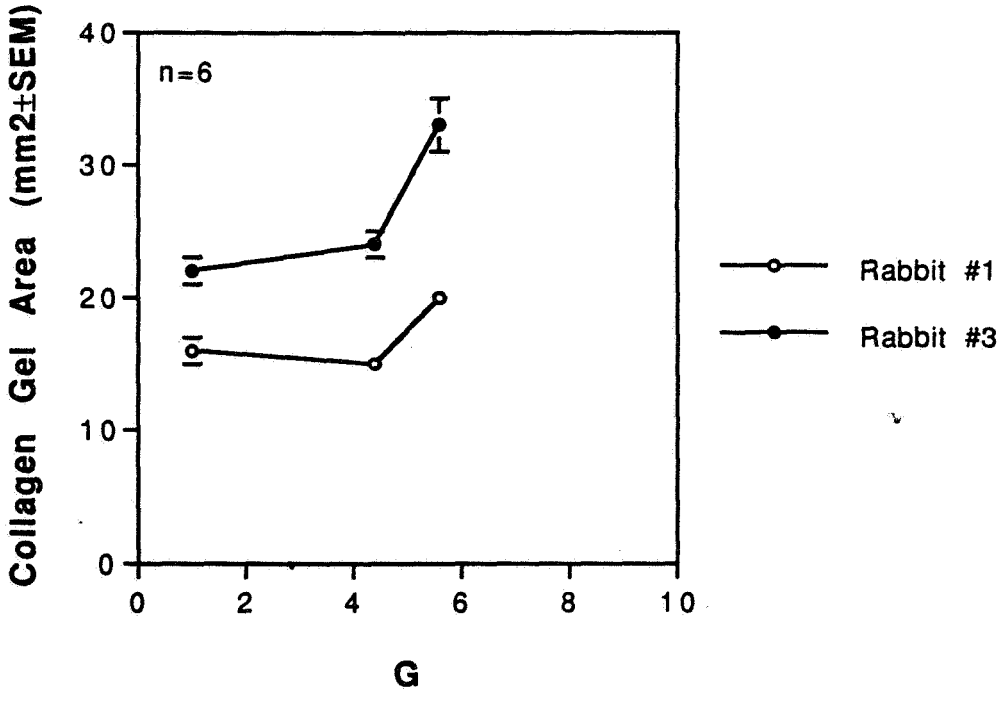

Fig. 2

ASEE-Stanford Summer Faculty Fellowship 1996-Final Report

PERFORMANCE OF SOVIET NK-321, MIXED STREAM, TRIPLE SPOOL, AUGMENTED TURBOFAN ENGINE

Fazal B. Kauser, P.E. Professor, Air Breathing Propulsion, Department of Aerospace Engineering, California State Polytechnic University, Pomona CA-91768

INTRODUCTION. In 1960's it became clear to the Russian that subsonic Strategic bomber "Tu-95 Bear" had only a limited life in term of their ability to penetrate modern air defense systems. Thus, there was a need for a new, large bomber with variable sweep wings, which would make it possible to have an efficient and economical subsonic cruise in combination with a supersonic dash capability at high altitudes and near sonic dash capability at tree-top altitude. The design studies led to the development of Tu-160 long range strategic bomber with the NATO code name "Blackjack".

Blackjack made its public debut at Tushino in august 1989, when one took part in the "Aviation Day" fly-past. Despite this public presentation, very little information has been released about this aircraft and its propulsion system. The interesting point to note is that external aerodynamic shape of the Blackjack closely resembles Rockwell International B-1. Blackjack is, however, much bigger than American B-1-A or B-1-B.

The objective of this research is to estimate the performance of Soviet NK-321 engine using NASA/Navy Engine Simulation Program "NNEP89" briefly described below. Owing to lack of information on some of the key design parameters, the author has to rely on his own experience and speculate a base-line engine to perform off-design cycle analysis of the Soviet NK-321 engine.

ENGINE DATA. NK-321 engine is a triple spool, mixed stream, medium bypass, after-burning, turbofan developed by Soviet Samara State Scientific & Production Enterprise. It is claimed to be the largest existing military engine in the world. Work on the NK-321 engine began in late 70's and batch production started in early 80's.

AVAILABLE DATA		UNAVAILABLE DATA
Turbine Inlet Temperature	2934 R	
Max Air Mass Flow Rate(T.O., SSL)	805 lb/sec	Fan Pressure Ratio
Inlet Diameter:	57.51 in (4.79 ft)	Pressure Ratio, Intermediate Comp
Weight (dry):	7296 lb	Pressure Ratio, Hi pressure
MILITARY Thrust (T.O., SSL, dry)	30,805 lb	Max Afterburner Temperature
Thrust (T.O. SSL, Full A/B)	55,116 lb	Performance Maps, Comp/Turbine
		Level of Technology

The fan pressure ratio was fixed by identifying the three critical phases of the Blackjack's mission profile namely Take-off, penetration at Mach 2 at 60 K altitude, and Sea level penetration at Mach 0.95. ONX-OFFX Computer Code[3] predicted following values for fan pressure ratios:

	FPR
■ Take-off	2.403
■ Supersonic penetration	1.283
■ Transonic Dash-SL	1.798

Key design parameter of some of the low to medium bypass ratio engines built during late 70's are summarized below:

Mode No	BPR	FPR	TIT (R)	OPR	APPLICATION
F100-PW-100	0.630	2.80	3026	24.80	F-15, F16
F101-GE-100	1.910	2.00	3010	27.00	B-1-B
TF30- P -11	0.730	2.43	2515	21.80	F-111

A fan pressure ratio of 2.40 was selected for the NK-321 engine based upon the above analysis.
Knowing that high pressure compressor of a mixed stream, low to medium bypass ratio turbofan should not be less than 4.0, the author was able to calculate a reasonable value for the low pressure compressor.

NEPP89 ENGINE SIMULATION CODE

.The ""NNEP89" computer code is written in standard FORTRAN 77 and is capable of performing one dimensional, steady state, thermodynamic analysis of turbine engine cycles. The code is very flexible and can simulate almost any turbine engine configuration that the user could imagine including the multi-mode engine configuration over various portions of the flight regime. The code utilizes a set of standard engine components that are connected at execution time to simulate almost any turbine engine configuration. Off- design performance is performed through the use of component performance maps. The code incorporates a chemical equilibrium model to predict dissociation as well as model any fuel. The code is also capable of estimating installation losses with reasonable accuracy.

In general, two separate input files are required to run the code. The first contains input that tells the code what components will be used and how these components are configured to form a specific engine model. Detailed inputs for each of these components describe the desired component model. Also included in this input file are global inputs which control program input/ output, execution, optimization, turbine cooling, thermodynamic property calculations and installation effects calculations. The second input file contains all the performance map tables which are used to model off-design performance of components such as compressor and turbine. For the on-design performance analysis, the engine component map table are usually not required. In addition, the code automatically ensures that continuity of mass and speed/RPM between components. For off-design points, the continuity of mass and energy are not automatically met. The user must determine which components will have a potential mismatch or "error" in mass flow and energy. NEPP89 code has five control components namely Variable Control, Variable Optimization Control, Variable Limiter, Variable Scheduling, and Conditional Control. All the controls are rarely used in a cycle analysis. A comprehensive detail of these controls is given in the User'sManual[10]. Determining the engine errors, choosing a set of free variables to be used and writing the variable control component inputs is one of the most difficult tasks when using NNEP89, particularly for a novice engine performance analyst. As a result, an automatic control formulation option is available . this option is invoked by setting ACTL to one or two. The code will then determine the engine errors and will choose a set of free variables to eliminate these errors. It is recommended that the user should read the "User's Manual" thoroughly to get acquainted with the code format. The manual contains examples of five sample engine cycle analyses which are invaluable aids in understanding the code.

RESULTS Off-design performance plots of the Soviet NK-321 engine are shown below.

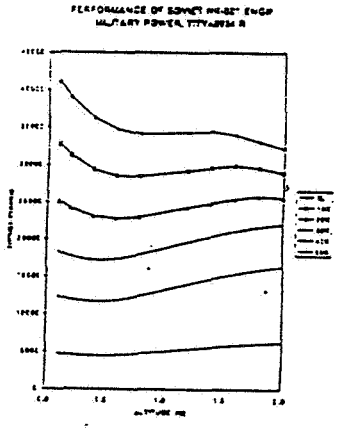

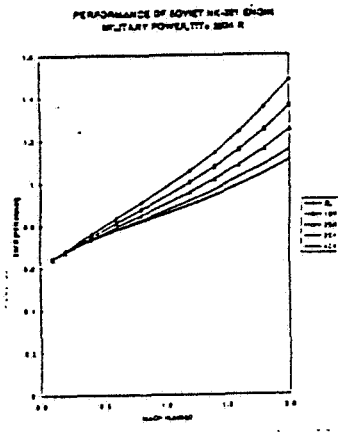

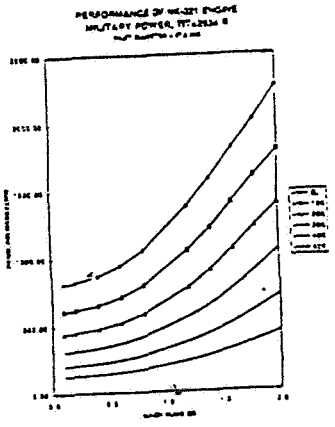

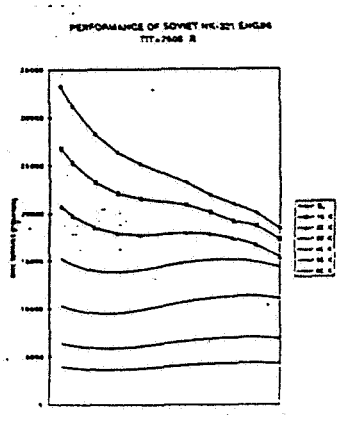

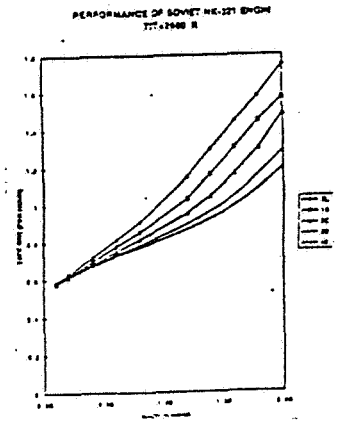

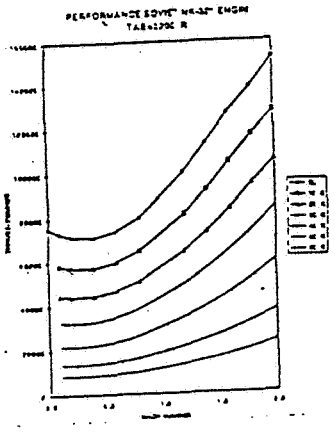

DISCUSSION OF RESULTS: NEPP89 Engine Simulation Code predicted a dry, max, SSE, up-installed thrust value of 39000 lb versus manufacturer's value of 30804 lb under the same operating conditions for TIT=2934 R. Knowing that TIT has a profound effect on the thrust of a low bypass engine, The Code was run with decreasing values of TIT. A TIT value of 2600 R yielded a dry thrust value of 31,145 lb- within 3.5% of the manufacturer's value.

As no $T_{MAX)A/B}$ value for NK-321 engine was known, the code was run for $T_{A/B}$ values of 3200R , 3600 R and 4000 R. The NEPP89 code predicted very large values of up-installed thrust ranging from 57,657 lb to 82,372 lb. A TIT value of 3200 R yielded thrust value which fell with 4.6% of the manufacturer's values of 55,077 lb with full after-burning.

The calculated maximum air mass flow at take-off was compared with the manufacturer's value. A discrepancy of 27.4% was found in the calculated value. This is probably due to the fact that during take-off, blow-in doors are used to meet the air mass flow requirements at take-off.

POSSIBLE SOURCES OF ERROR

- Turbine blades cooling technology incorporated in the NEPP89 code is probably far more advanced that used on NK-321 high pressure spool.
- Compressor and turbine maps used by the NEPP89 code probably belong to the state of the design and may not be appropriate for NK-321 engine built in late 70's.
- To the engine model simple, no additional load was allowed for auxiliary power unit.
- Customer bleed air requirements were not specified.
- Probably higher components adiabatic efficiencies were assumed in the engine model.

CONCLUSIONS:

- NEPP89 Engine Simulation Code is highly versatile and flexible. It allows an accurate one dimensional, steady state thermodynamics analysis of triple spool configuration.
- Setting the Control Variables for the off-design performance analysis of NK-321 engine offers the greatest challenge to the novice user.
- A more comprehensive simulation of the NK-321 engine is possible including installation losses provided additional time and engine data is made available to the researcher.
- NK-321 engine performance claims made in the literature should be viewed with caution due to significant difference in the NK-321 engine performance was predicted by the NEPP89 Engine Simulation Code.

REFERENCES:

1. Jack D. Mattingly, "Elements of Gas Turbine Propulsion", McGraw-Hill Publishing Co. 1996
2. Jack Mattingly, William Heiser, Daniel H. Daley " Aircraft Engine Design", AIAA Education Series 1987
3. Jack D.Mattingly, "On-Design and Off-Design Aircraft Engine Cycle Analysis Computer Programs", AIAA Education Series, January, 1990
4. Bill Sweetman, "Blackjack- Air Defense Challenge for the 990's" , Interavia Volume 43, October, 1988
5. Roy Braybrook, "The Tupolev Tu-160 Blackjack", Air International volume no. 1, January, 1991
6. Bill Sweetman, Graham Warwick, " Blackjack: Soviet B-1 or Better?", Flight International, Number 3840, Volume 122, December 11, 1982
7. Paul Jackson, Kenneth Munson, John Taylor, "Jane's All the World Aircraft" 1993-94"
8. Leo c. Francisus " Supersonic Fan Engines for military Aircraft", Aircraft Design Systems and Operations Meeting, Fort Worth October 17-19, 1983
9. Karl A. Geiselhart, Michael J. Caddy, & Shelby J. Morris " Computer Program for Estimating Performance of Air-Breathing Aircraft Engines", NASA Technical Memorandum 4254, 1991
10. Robert M. Plencner, Christopher A. Snyder "The Navy/NASA Engine Program(NNEP89), A User's Manual", NASA Technical memorandum 105186, August, 1991
11. Fazal B. Kauser, "An Overview of Gas Turbine Propulsion Technology" , Paper 94-2828, 30th AIAA/ASME/ASEE Joint Propulsion Conference, June 27-29, 1994/ Indianapolis, Indiana.

NASA-ASEE-Stanford Summer Fellowship 1996 - Final Report

ATMOSPHERE MODELS FOR THE BROWN DWARF GLIESE 229 B AND THE EXTRASOLAR GIANT PLANETS

Mark S. Marley, Assistant Professor, Department of Astronomy, New Mexico State University, Las Cruces, New Mexico

Introduction. Brown dwarfs inhabit a realm intermediate between the more massive stars and the less massive planets. Their thermal infrared emission is powered by the release of gravitational potential energy as regulated by their atmospheres. Long known only as theoretical constructs, the discovery of the first unimpeachable brown dwarf, Gliese 229 B [1], has opened up a new field: the study of brown dwarf atmospheres. The subsequent discovery of numerous extrasolar giant planets circling nearby stars [2], further demonstrated the need for a comprehensive modeling effort to understand this new class of jovian atmospheres. Although no spectra are yet available of the new planets, the next generation of groundbased and spacebased telescopes will return such data. Here I report on my effort with Ames collaborator Dr. Christopher McKay to better understand these new atmospheres.

Background. The past year has seen the dramatic discovery of the brown dwarf Gl229B [1] and eight extrasolar giant planets [2]. To interpret observations of the brown dwarf and to prepare for future observations of the giant planets, atmosphere models for these objects are required. Given a specified atmospheric composition, gravity, and effective temperature, a radiative-convective equilibrium model solves for the variation of temperature with pressure in the atmosphere. This temperature profile can be used as a boundary condition for evolutionary calculations and to synthesize a model spectrum for the object. Here I report on work to adapt an existing atmosphere model to the conditions appropriate for the atmospheres of the brown dwarf and the extrasolar giant planets.

A radiative-convective equilibrium atmosphere model originally developed for the atmosphere of Titan [3] was adapted by Marley to explore the atmospheres of Uranus and Neptune [4]. Over the six months prior to the ASEE fellowship, the model was further developed to explore the atmosphere of the brown dwarf Gliese 229 B. Specific modifications included an expanded spectral range, expanded temperature range, and numerous improvements in the radiative transfer algorithms. The goal for the 10 week summer program was to further improve the implementation of the model for the brown dwarf environment, explore a greater realm of brown dwarf parameter space, and make further modifications to the code to adapt it to the atmospheres of the extrasolar giant planets.

Current observations of the extra-solar giant planets generally constrain only the minimum mass of these objects. However, a statistical "most probable" mass can be calculated for each object. While this approach is fraught with uncertainty, it does provide a guide to the relative masses of these objects. In the analysis presented here, we assume this mass for the objects listed in Table I. Table I does not present a comprehensive list of the new planets, just those with estimated effective temperatures below about 700 K. The effective temperatures in the table are computed by assuming an albedo and age for the planet and accounting for the incident stellar flux. The range is indicative of the uncertainties in this calculation.

Results. Figure 1 shows the resulting computed temperature-pressure profiles for the new planets, Jupiter, Uranus, and the brown dwarf Gl 229 B. The temperature profiles for 70 Vir b, 47 UMa b, and Gl 229 B self-consistently include the stellar insolation. The Jupiter and Uranus curves are taken from data. The remaining profiles are for radiative-equilibrium conditions with the effective temperature taken from the midrange of Table I. We are working to produce self-consistent temperature profiles for each of the atmospheres in Table I.

The figure also illustrates two other characteristics of the models. At high temperatures thermochemical equilibrium favors molecular N_2 over NH_3. As shown in the figure the atmospheres from Figure 1 are generally sufficiently cool that NH_3 dominates over N_2. However at depth N_2 will

Table I: Selected Planets and Brown Dwarfs

Object	Primary	a (AU)	M (MJ)	Teff (K)
70 Vir b	G4	0.45	10.4	345-430
47 UMa b	G0	2.11	1.4	65-165
Gl 411 b	M2	2.33	0.9	90-110
55 Cnc c	G8	5 - 10	1.25	640 - 740
HD 114762 b	F9	0.41	14	425 - 770
Gl 229 B	M1	> 44	30 - 55	890 - 1030
Jupiter	G2	5.2	1	124

dominate in Gl 229 B, HD 114762 b, and 70 Vir b. If there is substantial vertical mixing, the perturbation to the atmospheric ammonia abundance may be detectable.

The appearance of Jupiter is dominated by clouds. Clouds condense when the relative humidity of the condensable species exceed 100%. Figure 1 illustrates the condensation curve for water; clouds will form where the computed temperature profile crosses the condensation curve. Ammonia and methane will condense at lower temperatures. Water clouds will form in the atmospheres of all the modeled planets with the exception of HD 114762 b and the brown dwarf. Ammonia will also condense above the water cloud in most of the atmospheres. Thus we can expect that most of the planets shown in Figure 1 will have an appearance very similar to that of Jupiter or Saturn

Figure 2 illustrates the observed reflected and emergent fluxes from Jupiter and the model predictions for Gl229B, 47 UMa b, and 70 Vir b. This work represents an important improvement over previous extrasolar giant planet model spectra which assumed the planets radiated as blackbodies. The blackbody emission is shown as the solid line for each object. In every calculation and at Jupiter, the emitted flux in the 4 to 5 μm region is significantly larger than the blackbody flux. This region is bright for very different effective temperatures (from 100 to 1000K) because both methane and water are the main absorbers in this region. Methane opacity has a minimum around 5 μm. Water opacity has a minimum around 3.5 μm.

Summary. In conclusion, we find that the cooler atmospheres among the newly-discovered planets (those listed in Table I) will have visible atmospheres consisting of H_2, He, NH_3, CH_4, and H_2O, presumably in approximately solar abundance. Clouds will condense in most of the atmospheres and the emergent planetary flux will exceed the blackbody flux in the 4 to 5 μm spectral range. Thus this spectral region is advantageous for future detection efforts.

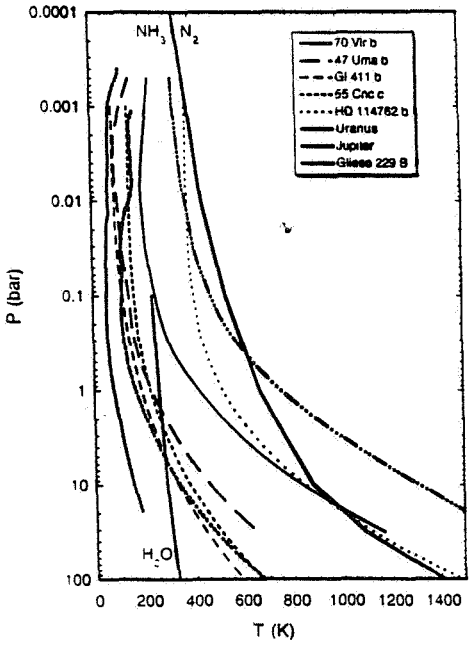

Figure 1: Derived temperature profiles for a selection of the newly discovered planets and Gl 229B. Observed temperature profiles are also shown for Uranus and Jupiter. The profiles of 70 Vir α and 47 UMa α self-consistently include the deposition of sunlight into their atmospheres. The other temperature profiles are more preliminary. The curved thick solid line denotes thermochemical equilibrium between NH_3 and N_2. Since the observable portion of these atmospheres lies to the left of this line, N will be present as ammonia. The lower solid line, labeled H_2O, denotes the condensation curve of water. Water clouds will form in the atmospheres where the temperature profile intersects this curve. Clearly such clouds will play an important role in most of the extrasolar atmospheres.

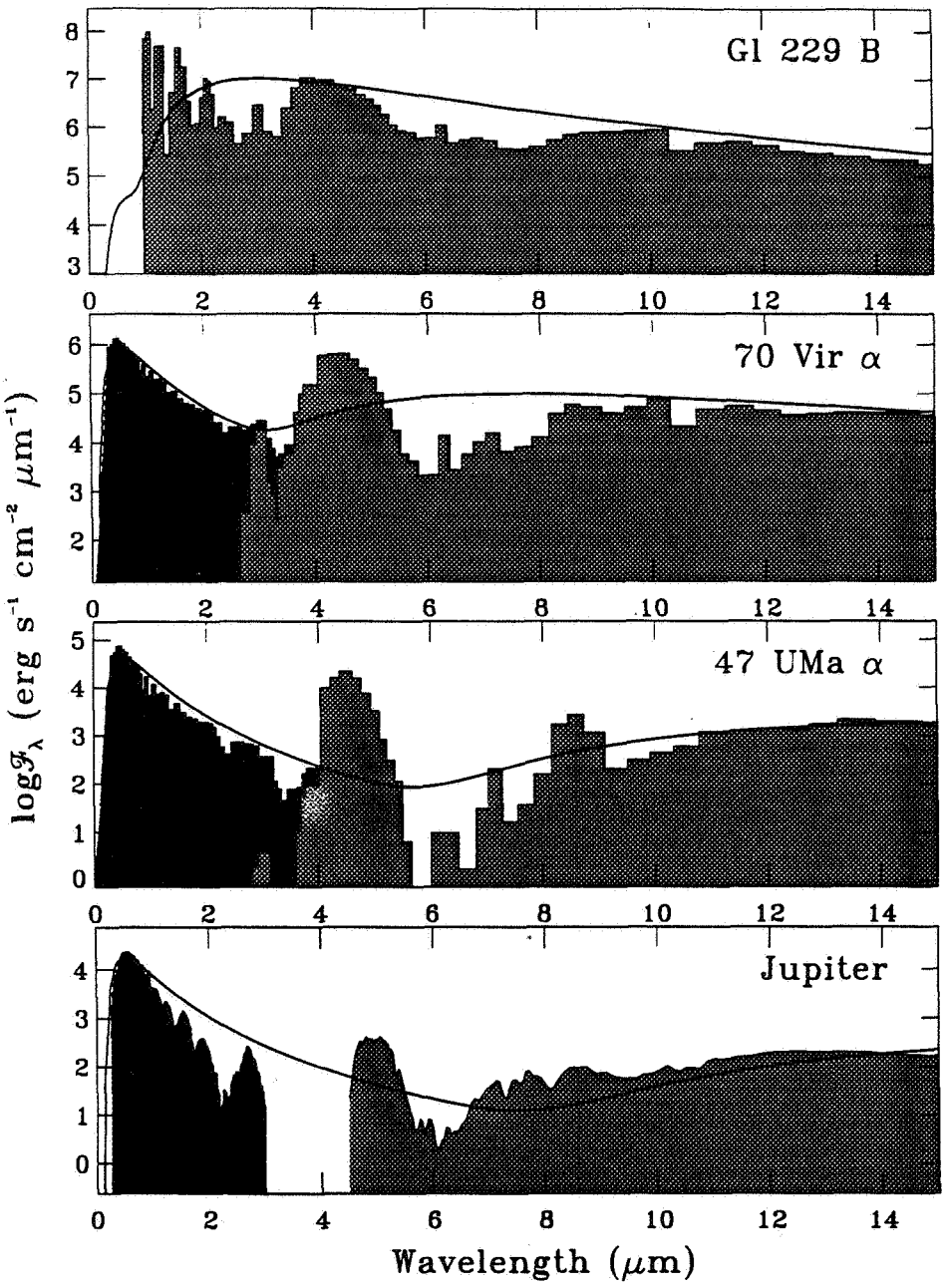

Figure 2: Theoretical spectra of Gl 229 B, 70 Vir α, and 47 UMa α, compared to an observed spectrum of Jupiter. The reflected part of the flux is shown in dark grey. The internal flux is shown in light grey. The line represents the flux of a black body at the same effective temperature, including the reflected stellar flux (assuming a blackbody at Teff = 5780 K). Although most of these calculations are preliminary, the presence of a strong flux in the 4 μm region is a robust conclusion.

References

[1] T. Nakajima et al., *Nature* **378**, 463 (1995)
[2] See `http://www.obspm.fr:90/departement/darc/planets/candidates.html`
[3] C. McKay et al., *Icarus* **80**, 23 (1989).
[4] M. Marley et al., *Icarus*, in press.

NASA–ASEE–Stanford Summer Fellowship 1996–Final Report

Dynamics of Nuclear Regions of Galaxies

Richard H. Miller
Associate Professor of Astronomy
University of Chicago

My research area is the dynamics of galaxies, which, along with Ames colleague Dr. B. F. Smith, we study by means of numerical experiments. Current research, carried out with the help of the ASEE-NASA Summer Faculty Program at NASA-Ames, is concentrated on the dynamics of nuclear regions of galaxies.

From a dynamical point of view, a galaxy is a collection of around 10^{11} stars like our Sun, each of which moves in the summed gravitational field of all the remaining stars. Thus galaxy dynamics becomes a self-consistent n-body problem with forces given by Newtonian gravitation. Strong nonlinearity in the gravitational force and the inherent nonlinearity of self-consistent problems both argue for a numerical approach. The technique of numerical experiments consists of constructing an environment in the computer that is as close as possible to the physical conditions in a real galaxy and then carrying out experiments, much like laboratory experiments in physics or engineering, in this environment. Computationally, an experiment is an initial value problem, and a good deal of thought and effort goes into the design of the starting conditions that serve as initial values. Experiments are run at Ames because all the "equipment" is in place—the programs, the necessary computational power, and good facilities for post-run analysis.

Our goal for this research program is to study the nuclear regions in detail, and this means replacing most of the galaxy by a suitable boundary condition to allow the full capability of numerical experiments to be brought to bear on a small region perhaps 1/1000 of the linear dimensions of an entire galaxy. This is an extremely delicate numerical problem, one in which some small feature overlooked can easily lead to a collapse or blow-up of the entire system. All particles attract each other in gravitational problems, and the $1/r^2$ force is (a) nonlinear, (b) strong at short range, (c) long-range, and (d) unscreened at any distance.

The goals for summer 1996 are to prepare computer programs for these studies. Progress has been made on two specific research problems, as follows:

Galaxy formation around a pre-existing supermassive black hole. Some of our recent work [1, 2] showed that the nuclear regions of galaxies are not static; the region of greatest density orbits around the galaxy's mass centroid. Workers in the field have shown considerable interest in this result, especially as concerns galaxies thought to have massive black holes near their centers.

We plan to address questions concerning the amplitude and velocity of black hole motions, and to investigate differences between galaxies that form around a supermassive black hole and "normal" galaxies (those that form otherwise). Studies like these are also important to the interpretation of Hubble Space Telescope (HST) observations of galaxies that may have supermassive black holes near their centers. These studies will also help to tell what form of peaked brightness distribution might provide an observational signature to distinguish whether there is a black hole present, when contrasted with our earlier work on the formation of a galaxy without any massive compact object [3].

Work on this project has progressed to the stage where we are now carrying out preliminary experiments to delimit interesting parameter ranges. Early results point out interesting directions for future research and warn of possible difficulties. Analysis of these results will enable us to sharpen designs for future research and to formulate additional questions to be studied. Computer programs are up and running, but we still want to enlarge the computation to use a larger computational grid.

Nuclear regions of galaxies. We have been working on methods to concentrate the full power of our $n-$body calculations in the nuclear regions of a galaxy (with or without a black hole). The goal of this work is to permit study of the nuclear regions without having to include the entire galaxy in the calculation, producing computations more efficient by factors of several thousand over present methods. We are hope to represent a rotating core region in this manner. These studies are important to the interpretation of HST observations of nuclear regions of galaxies, in particular to observations of the core of M31, which HST has shown to be double [4].

This effort brings up boundary conditions in a particularly fussy situation where any flaw can cause a lot of trouble. Successful developments in this area may well be of interest in other scientific areas, such as fluid dynamics.

Work on this project has progressed to the stage where we now have computer programs ready to link into full integration. Some preliminary tests showed places that needed more attention, and those weaknesses have been eliminated. However, substantial work remains to set up a full running program, and to test that it performs up to our expectations. That is a project for the coming winter and for the second year of this research under the ASEE program.

These examples represent challenging problems that we plan to follow up analytically and by remote (network) computer connections through the coming winter. We appreciate the opportunity the ASEE-NASA Summer Faculty Fellows Program has given us to work on this exciting problem.

References

[1] R. H. Miller and B. F. Smith.
Off-center nuclei in galaxies.
ApJ, 393:508–515, Fiche 122–B7, 1992.
includes a videotape.

[2] R. H. Miller and B. F. Smith.
Goings-on at the center of a galaxy.
In D. J. Benney, F. H. Shu, and Chi Yuan, editors, *Applied Mathematics. Fluid Mechanics, Astrophysics, a Symposium to Honor C. C. Lin*, pages 366–372, Singapore, 1988. World Scientific.

[3] B. F. Smith and R. H. Miller.
On the formation of galaxies with flat rotation curves.
ApJ, 309:522–543, Fiche 127–A1, 1986.

[4] Tod R. Lauer, S. M. Faber, E. J. Groth, E. J. Shaya, B. Campbell, A. D. Code, D. G. Currie, W. A. Baum, S. P. Ewald, J. J. Hester, Jon A. Holtzman, Jerome Kristian, R. M. Light, C. R. Lynds, E. J. O'Neil, and J. A. Westphal.
Planetary camera observations of the double nucleus of M31.
AJ, 106:1436, 1993.

Use of the Matching Pursuit Algorithm for Flight Flutter Test Data Analysis

Ronald E. Nelson
NASA-ASEE-Stanford Summer Faculty Fellow
Arkansas Tech University
Russellville, Arkansas

Research Colleague

Martin Brenner
NASA Dryden Flight Research Center
Edwards, California

August 11, 1996

Use of the Matching Pursuit Algorithm for Flight Flutter Test Data Analysis

Ronald E. Nelson

Introduction

The goal of flight flutter testing is to detect possibly destructive modes of aircraft vibration which may arise during flight from interaction of aerodynamic forces with structural dynamic properties of the airframe. This is typically accomplished by exciting the airframe with a time varying force and monitoring the response of the aircraft throughout its flight envelope. The data generated must be analyzed and presented so that the frequency and time of occurrence of excited modes are clearly and unambiguously displayed. Processing and display in near real time is also desirable.

Display of data in the time-frequency plane is a natural choice because it is a familiar and intuitive framework. The Matching Pursuit algorithm provides a time-frequency analysis with good adaptability to signal structure and good signal representation in the time-frequency plane. Improvements in efficiency are needed before the algorithm can be used in real time, however.

Objective

The research objective was to explore wavelet related techniques for analysis and display of flight test data in the time-frequency or time scale plane.

Accomplishments

The Matching Pursuit algorithm of Mallat and Zhang was identified as a promising method for time frequency analysis. Matlab code to implement the algorithm was written and documented, and will provide a convenient tool for further investigation. The software was tested by applying it to known signals, and was then applied to real flight test data with reasonable results. Areas for future investigation were identified.

Future Work

Continuing investigation is planned in the following areas:

1. Improvement of computation efficiency. Better criteria for terminating the decomposition (possibly entropy based) and parallel computation are possibilities.

2. Improved data display. A very wide dynamic range of data is present in the time-frequency range image. Image processing techniques may be applied to improve the visual effectiveness of the display.

3. Investigation of other functions for the signal expansion. Following Mallat and Zhang, real Gabor window functions were used in this work. Perhaps other functions would be better suited to flight flutter test data, and hence more efficient.

4. Investigation of possible cumulative processing, updating the time-frequency image as data points are added.

Conclusions

The Matching Pursuit algorithm is a promising method for analyzing and displaying data in the time-frequency plane. The algorithm allows the center frequency and width of the frequency window to be varied independently, yielding good absolute resolution at all frequencies. A false color plot of amplitude in the time-frequency plane provides an intuitive and easily interpreted display. The present implementation of the algorithm is not fast enough for real time analysis, but improvements in speed are possible and worth pursuing.

References

Mallat, Stephen G. and Zhang, Zhifeng , "Matching Pursuits With Time-Frequency Dictionaries," IEEE Transactions on Signal Processing , vol. 14, no. 12, pp 3397-3415, 1993.

NASA - ASEE - Stanford Summer Fellowships 1996 - Final Report

SUPERSONIC CHANNEL CONCEPT FOR ENHANCEMENT OF LIFT/DRAG RATIO

Dr. Stephen M. Ruffin
Georgia Institute of Technology
School of Aerospace Engineering
Atlanta, GA 30332-0150

Introduction

The concept studied during the summer NASA/ASEE Fellowship provides a means of lowering drag and a means for directional control of supersonic and hypersonic vehicles. Low drag and efficient directional control are essential for the success of aircraft, atmospheric entry vehicles, missiles, and other vehicles in supersonic and hypersonic flight. Drag reduction can result in increased vehicle range, increased speed, improved fuel efficiency, increased lift/drag ratio, and increased climb rate.

For high supersonic and hypersonic vehicles heat transfer considerations dictate the design of the nose and leading edge. The heat transfer to such vehicles is most severe at stagnation points which occur on the leading edges and nose of the vehicle. Theoretical formulations, experimental data, and semi-empirical formulas all agree in the fact that stagnation point heat transfer is inversely proportional to the square root of the nose or leading edge radius. Thus, the noses and leading edges of supersonic and hypersonic vehicles are typically blunted so that the heat transfer and structural loads will be manageable. However, much of the wave drag experienced by these vehicles is due to nose blunting.

Overview of Concept

Instead of significant blunting, the present concept allows for a hollow channel to exist in the nose of supersonic and hypersonic vehicles. The channel should extend from the nose to near the trailing edge of the vehicles with the freestream air flowing through the channel. This present concept can be applied to any supersonic vehicle but for simplicity is illustrated on a blunted diamond airfoil in Figure 1.

For a channel of a particular size (depends on Mach number and nose radius) a normal shock rests in front of the channel and the flow enters the channel subsonically. Computed static pressure contours at a blunt nose with a channel is shown in Figure 2. In this case the overall flow structure near the nose is similar to that of the no-channel case, i.e. an "effective blunt body" is generated. Without a nose channel the surface pressure in the stagnation region is very high and is responsible for much of the drag experienced by the vehicle. However with the nose channel concept the vehicle surface which experienced most of the high, near-stagnation pressure is removed. Thus, the wave drag with the nose channel is much lower than the no-channel case.

It is clear that the wetted area and thus the skin friction drag will be increased with use of a channel. However, when the channel is designed to operate at a choked condition the velocity and dynamic pressure inside the channel are significantly lower than the corresponding external flow quantities. Thus the friction drag on the internal walls is much less than the friction drag on the external walls for many flight conditions. The key question becomes: For what geometries and flight conditions will the decrease in wave drag be more than the increase in skin friction drag. The present study seeks to answer this question through numerical experiments for a wide variety of flight conditions.

In the present concept the entrance of the channel can either be placed symmetrically at the nose, as shown in Figure 1 or be placed somewhat off the symmetry axis. In practice, the vehicle would be designed so that the channel entrance can be opened, closed, and moved off center during flight. By moving the channel opening away from the center of the nose the direction of the vehicle can be controlled. Moving the channel opening upward results in increased pitch and moving the channel laterally induces yaw. Normally, control surface deflections are used for directional control. However, flow separation limits the effectiveness of these control surfaces and increases the surface heat transfer rate. Typical control surfaces are substantial in size and significantly increase drag. Conversely, use of the present nose channel concept provides excellent control authority while lowering the drag and often increasing the lift/drag ratio.

Approach

Over the summer a numerical study of the channel concept was performed using two numerical methodologies. Highly accurate, Navier-Stokes predictions of the flow were performed using GASP, a multi-block, finite volume solver that uses the Roe's flux split algorithm and an implicit 2 factor AF for time integration. The thin-layer formulation of the problem was solved for both laminar and fully turbulent flows. The Baldwin-

Lomax model was used to predict the effects of turbulence. The grids were generated using GRIDGEN and their size varied from 25,000 to 50,000 nodes. Over the summer, turbulent flow calculations with blunted airfoils at 0, 5 and 8 deg. angle of attack were performed. In addition, Mach 7 flow around an axisymmetric sphere-cone both with and without a channel were computed.

The second numerical methodology is less accurate than the Navier-Stokes procedure but is of particular value because of its computational efficiency. A numerical code was developed which models the geometry by 8 linear panels and computes the supersonic flow conditions behind oblique shocks and Prandtl-Meyer expansions generated by the panel junctions. Over the summer, compressible laminar and turbulent (using van Driest II) skin friction models were incorporated into the solver. A parametric study of channeled airfoil performance was conducted for hundreds of mach number/altitude combinations.

Results

Navier-Stokes calculations conducted over the summer of 5% thick blunted diamond airfoils with and without channels show that the total drag (including skin friction) decreases by over 30% for laminar flow and by over 20% for turbulent flow. The lift/drag ratios and drag breakdowns for the no-channel (NC) and various channel airfoil configurations (denoted by SNSC, RNSC, and RNDC) are shown in Figures 3, 4, and 5. The decrease in wave drag more than compensates for the increase in skin friction drag. The increase in lift/drag ratio is due to a reduction and drag and the channel has little effect on lift. The increase in lift/drag ratio afforded by the present concept can result in increased range, increased speed, improved fuel efficiency and enhanced performance. Navier-Stokes calculations also reveal that when the nose channel is employed the maximum heat transfer rate is lower than that for the baseline no-channel case. Thus the present concept results in significantly reduced wave drag, total drag (including skin friction drag) and heat transfer.

The linearized supersonic code with viscous model was utilized to conduct parametric studies of channeled and no-channel airfoils. Mach numbers from 1.3 - 7 and altitudes from sea level to 50km were analyzed to investigate the range of drag reduction afforded by the present concept. Figure 6 shows the results of analysis of a 5% thick blunted diamond channeled airfoil designed specifically for Mach 7. At Mach 7 a drag reduction of over 15% is observed at low altitudes assuming fully turbulent flow. At off design conditions with Mach numbers less than 7 a smaller but significant drag reduction is seen. For Mach numbers greater than Mach 7 the present airfoil will swallow the leading edge shock and the drag reductions will be even greater...however the heat transfer rate will also increase.

Accomplishments

The following specific objectives have been met during the 10 week fellowship period:

- Conducted turbulent Navier-Stokes simulations of channeled and no-channel airfoils at Mach 2.4 and at three angles of attack.
- Generated computational grid and conducted Navier-Stokes simulations of 17.5 deg., channeled and no-channel sphere cones at Mach 7.
- Developed and incorporated laminar and turbulent (using van Driest II model) skin friction models into a linearized supersonic flow code
- Utilized the linerized supersonic code with viscous model to conduct parametric studies of channeled and no-channel airfoils. Mach numbers from 1.3 - 7 and altitudes from sea level to 50km were analyzed to investigate the range of drag reduction afforded by the present concept.
- Began preparation of a proposal for a NASA Ames/University Consortium Grant to allow continuation of the project at Georgia Tech.

Future Activities

Collaboration with the Thermosciences Division will continue to experimentally validate the concept and evaluate the effect of the present concept on vehicle missions of interest.

- Conduct experiments (in ballistic range & wind tunnel) of models employing channel for proof of concept study.
- Develop and utilize aerodynamic database for channeled vehicles and couple with structural and thermal analysis for optimization study.
- Investigate effect of channel on performance on current vehicles of interest: XCRV, Re-Entry vehicles, X-33, supersonic cruise vehicles.
- Perform trajectory and mission analysis of optimized vehicles employing the channel concept - Quantify effects on range, fuel efficiency, and payload.

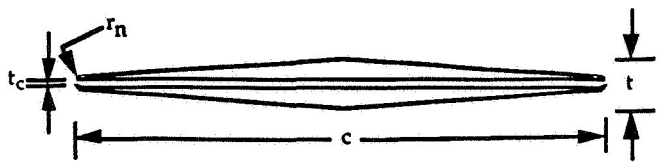

Figure 1. Schematic of supersonic channel airfoil

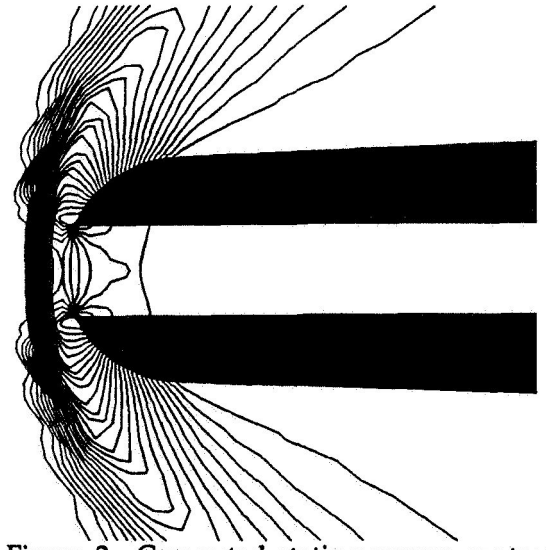

Figure 2. Computed static pressure contours at the nose of a vehicle employing a nose channel.

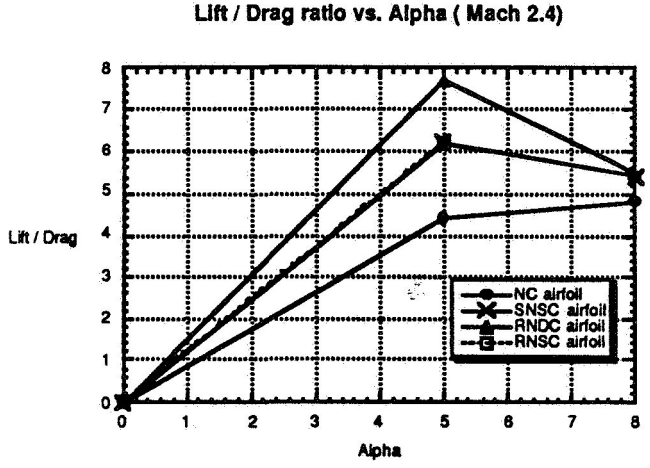

Figure 3. Lift/Drag ratio predicted by Navier-Stokes calculations assuming laminar flow around 5% thick airfoils. NC=No Channel Airfoil, SNSC, RNSC and RNDC denote channel airfoils with tc/c=0.004 and various leading edge geometries.

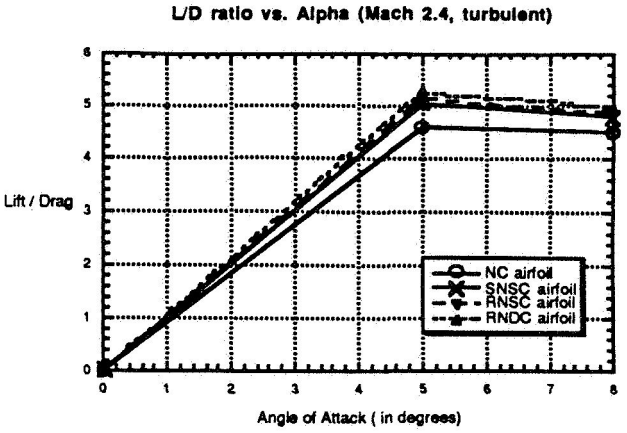

Figure 4. Lift/Drag ratio for fully turbulent flow

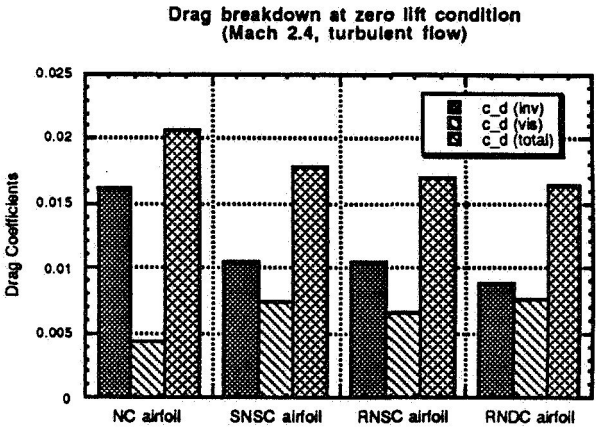

Figure 5. Drag breakdown for fully turbulent flow.

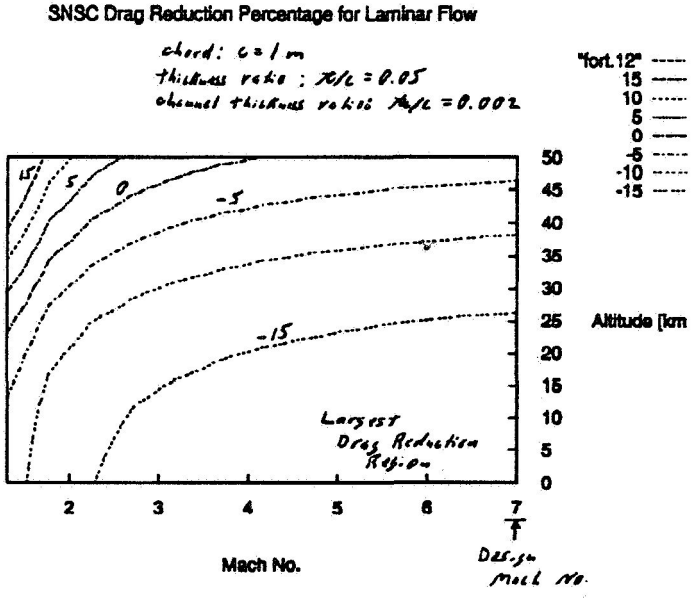

Figure 6. Predicted precentage drag reduction due to channel for 5% thick airfoil designed for choked flow at Mach 7.

NASA-ASEE-Stanford Summer Fellowship 1996 - Final Report

CURRICULUM DEVELOPMENT IN REMOTE SENSING AT CALIFORNIA STATE UNIVERSITY, MONTEREY, SEASIDE, CALIFORNIA 93955

Ravi Sinha, Ph.D., P. Geol., Professor of Geology, Elizabeth City State University

Introduction

The NASA-Ames Research Center and the California State University, Monterey Bay, California (CSUMB), have signed a Memorandum of Understanding (MOU) to develop and provide cooperative programs between the Ecosystem Science and Technology Branch of NASA (ECOSAT) and the University (CSUMB). The agreement is to carry out educational, research, and technology goals in ecological and environmental sciences and related disciplines, with particular emphasis on changing environmental and climatic conditions occurring worldwide due to the anthropogenic causes affecting the balance within ecological systems and the health and well-being of humans.

The preparation of the Curriculum for Remote Sensing at CSUMB was undertaken at the request of the Center as a result of the above agreement.

Curriculum Development in Airphoto Interpretation and Remote Sensing at California State University, Monterey Bay, CA

The Ecosystem Branch of NASA-Ames Research Center had discussions in the past with the CSUMB and were requested to develop a program on teaching Airphoto Interpretation and Remote Sensing at CSUMB. While some preliminary investigations were made, in the past, the whole program had to be developed from the grassroots. This included decisions regarding principles and objectives of the course, title of the course, assignment of credit hours, contact hours, lecture and lab sections for the course. A visit was made to the campus to review the lab equipment and facilities and, as a result of the visit, a number of recommendations were made to augment the lab. The curriculum, so developed, includes a detailed description of the lecture and lab assignments for each week by subject and title, with specific lab and homework assignments for each week.

The primary goal of the course is to familiarize students with examination and analysis of various types of imageries. The object is to teach students to learn techniques in detection, identification, and analysis of objects or features through the use of imageries from both high and low altitudes. These may be photographic images or electromagnetic radiation reflected or emitted from these objects. The visible, invisible, and microwave regions of the radiation receive primary attention. Particular attention is given to the use of imageries in field surveys, agriculture, forestry, military science, urban planning, and geosciences.

The course is designed as a one semester course for students majoring in geography/forestry or in areas of ecological studies. However, students majoring in other areas can also take the course to meet the requirements for the credit in a science course, as there are no prerequisites.

The course is aimed at students acquiring practical ability to interpret and analyze various types of imageries. Principles of photo interpretation focusing on photographic systems (black and white, color infrared) and the fundamentals of electronic sensors will be covered in the course. Students will learn about the unique features of different systems and their applicability in a wide range of Earth Systems including field surveys, agriculture, forestry, and other areas where applicable.

The course will include a lecture and a laboratory component. The laboratory will complement the lecture part and will be a hands-on study of understanding and interpretation of imageries. The syllabus submitted includes a recommended textbook and a breakdown of each week for lectures, labs, assignments, and tests.

Future Work

As a result of the above, I have been requested by NASA's Ecosystem Branch to develop a Curriculum for Advanced Remote Sensing and its Application in Environmental Areas as a next semester course.

NASA-ASEE-Stanford Summer Fellowship 1996 - Final Report

DEFORESTATION AND BIOGENIC TRACE GAS EMISSIONS FROM BRAZILIAN CERRADO

Ravi Sinha, Ph.D., P. Geol., Professor of Geology, Elizabeth City State University

Introduction. The overall goal of NASA's SCAR (Smoke, Cloud and Radiation) Program is to obtain physical and chemical properties of the smoke produced by biomass burning and the effects of the smoke on the earth's radiation balance and climate. It is a joint project with the Brazilian government and their organizations, including INPE (Instituto Nacional Pesquisas Espaciais) who actively participate in all activities. Appropriate estimates of the biomass burning in the tropics is therefore essential to determine its effect on the atmosphere and on climate. The SCAR series of experiments is designed with that purpose. The present study of evaluating the burnt-out areas is to augment the data collected to date to help evaluate the effect of biomass burning.

Rationale. Biomass burning in the tropics generate large quantities of trace gases and particulates into the atmosphere and is estimated to be responsible for 30% of the total net increase in the CO_2 emissions from 1950 to 1986 and for 23% of the current anthropogenic emissions of CO_2 (NASA '95). Biomass burning in the tropics may have global implications through its effect on the regional radiation budget. Changes in the regional circulation of the earth-atmosphere system, which can be brought about by the emissions from tropical forests, may also effect the global weather and climate.

The emissions from tropical forests is due to the burning which is being carried out on a large scale in Brazil to "clear out" areas for farming and for other developments. While emissions data are being collected aerially, it is important to have an estimate of the burnt-out areas so that a proper evaluation of the impact could be made. The present study is designed with that aim using landsat data.

The shape and size of the burnt-out areas, and the spectral reflectivity signature patterns, are the three main characteristics that have been observed to be useful in distinguishing the areas cleared out by burning (Fig. 1 & 2). Landsat MSS imageries of 1992 were used to estimate the aerial extent of the burnt-out areas. The data used was from the month of September which was immediately after the areas were burned.

Selection of Cerrado Area. The Brazilian Cerrado is a large region of essentially tropical Savannah in the southwest region of Brazil. The savannah area is extensively used by the locals for farming by clearing the land by burning the grasslands.

The region thus is believed to be a major source of smoke and associated gases on a local, regional, and global scale due to frequent and extensive burning of both natural and

agricultural areas. Thus, while large scale burning has taken place in the Cerrado area on an yearly basis, the major studies in the past were concentrated in the tropical areas around the Amazon. This study, therefore, consists of estimating the burnt-out areas in Cerrado, Brazil.

Observations and Discussions. The burnt-out areas were clearly discernable on the imageries. The shape, size, and spectral signatures were all used for the purpose. Cloud covers occasionally obscured the individual burned out patches completely or partially, but it is estimated that while data from certain areas are not attainable, some estimate of cloud coverage and the area under it however is desirable (Robinson '91) and will be made.

Flight Information. Biogenic gases from the area were collected for the National Center for Atmospheric Research (NCAR) by King Air airplane during September 2-22, 1992, in central Brazil including the Cerrado area. The timing of the data collection was perfect, as it was right after the fires. The landsat imageries of September '92 being used coincides with the timing of the flight.

Landsat MSS Bands Used for the Study. MSS Bands 1 to 4 were used for the study. The wavelength of these bands are:

1. •5 to •6 μm, 2. •6 to •7 μm, 3. •7 to •8 μm, 4. •8 to 1•1 μm

The corrected pixel resolution is 50 meters.

Spectral Reflectance. It was observed that the differences in spectral reflectance from different areas were enhanced in band 4 compared to bands 1, 2 and 3. Earlier, Pereira and Setzer ('93) had also concluded that TM channel 4 was the best to identify fire scars. This is because the reflectance from different types of vegitation enhances at the higher wavelengths.

Conclusions/Accomplishments. The ten weeks in summer provided an opportunity to complete Phase I of the program, which consisted of recognizing and isolating areas which have been cleared out by burning using landsat imageries. The shape, size, and the spectral signature patterns were the three main characteristics observed to be useful in distinguishing the areas cleared out by burning. These have been documented in detail in the report to the department.

Future Activities. The second phase of the activity will consist of estimating the area of the burnt-out region in the Cerrado and will be initiated as soon as possible. The final lphase of this study will consist of correlating the data on biogenic gases collected by the National Center for Atmospheric Research (NCAR), Colorado, with the burnt-out areas.

Acknowledgements. The research was done in cooperation with James Brass, Vincent Ambrosia, and Christine Hlavka of the Ecosystem Science and Technology Branch, NASA-Ames Research Center. I am thankful to all of them for their help and cooperation.

Selected References

(1) Brustet, J.M. (1993)

(2) Crutzen, P.J., Andreae, M.O. (1990) - Biomass Burning in the Tropics: Impact on Atmospheric Chemistry and Biogeochemical Cycles-Science, Vol. 250. pp. 1669-1978.

(3) Kaufman, Y.J., Tucker, C.J., Fung, I. (1990) - Remote Sensing of Biomass Burning in the Tropics - Jour. of Geophysical Research, Vol. 95, No. D7, pp. 9927-9939. June, 1990.

(4) Levine, Joel S. (1991) - Global Mass Burning: Atmospheric, Climatic and Biospheric Implications - The MIT Press. Cambridge, Massachusetts.

(5) Malingreau, J.P., Tucker, C.J. (1988) - Large-scale Deforestation in the Southeastern Amazon Basin of Brazil - Ambio, Vol. 17, No. 1.

(6) Nelson, R., Horning, N., Stone, T.A. (1987) - Determining the Rate of Forest Conversion in Mato Grosso, Brazil Using Landsat MSS and AVHRR Data - Intl Jour. of Remote Sensing, Vol. 8, No. 12. pp. 1767-1784.

(7) Pereira Jr., A.C., Setzer, A.W. (1993) - Spectral Characteristics of Fire Scars in Landsat-5 TM Images of Amazonia - Intl Jour. of Remote Sensing, Vol. 14, No. 11, pp. 2061-2078.

(8) Pereira Jr., A.C., Setzer, A.W., Santos, J.R. (1991) - Fire Estimates in Savanna of Central Brazil with Thermal AVHRR/NOAA Calibrated by TM/LANDSAT; 24th Intl Symposium on Remote Sensing of Environment, Rio de Janeiro, May 27-31, 1991.

(9) Robinson, J.M. (1991) - Fire from Space: Global Fire Evaluation using Infrared Remote Sensing - Intl Jour. of Remote Sensing, Vol. 12, No. 1.

(10) Setzer, A.W., Pereira, M.C. (1991) - Amazonia Biomass Burning in 1987 and an Estimate of Their Tropospheric Emissions - Ambio, Vol. 20, No. 1.

(11) Smoke, Clouds, and Radiation: Mission Plan (1995) - SCAR Project Office, NASA Langley Research Center, Hampton, VA.

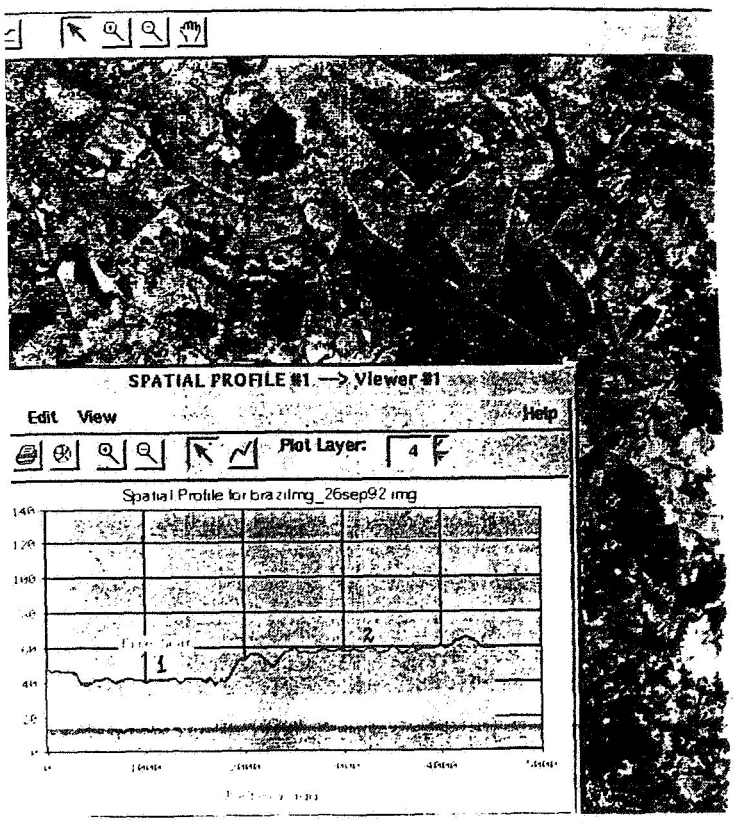

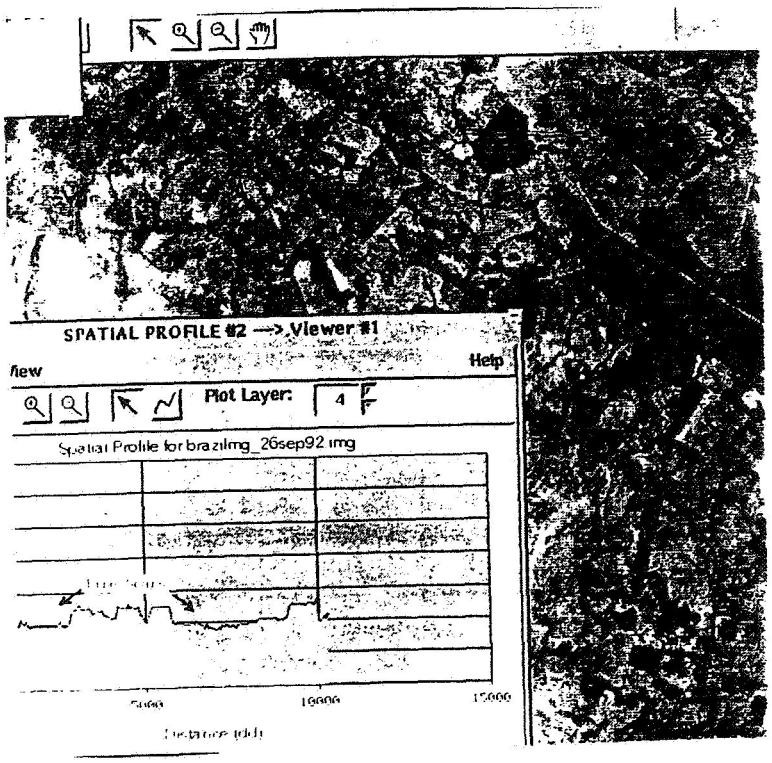

NASA-ASEE-Stanford Summer Fellowship 1996 - Final Report

INTERPLANETARY AND INTERSTELLAR DUST PARTICLES: REENTRY HEATING AND CAPTURE IN AEROGEL

Paul P. Szydlik, Department of Physics
State University of New York, Plattsburgh, New York 12901-2681

Introduction: Studies of interplanetary and interstellar dust can provide significant information on the evolution of the solar system or stars, respectively. However, for reliable analysis it is crucial to know how the particles have been modified during reentry (in the case of interplanetary dust particles, or IDP's) and impact into the capture medium. In the case of stratospheric capture, particles will be heated by atmospheric drag. Subsequent capture of the particles will result in heating, ablation, accretion of the capture medium and possible fragmentation. Modeling of these processes is a useful way of assessing their effects on the interpretation of the compositional data for these particles.

Previous work on reentry heating has shown that heat diffusion alone cannot adequately account for temperature gradients observed in IDP's. In fact, for any reasonable thermal parameters, calculations show the particles to be nearly isothermal. Here we extend those studies to include phase transitions. These preliminary results are promising and show a significant temperature gradient for a 100 μm (diameter) particle.

The actual capture of the particles in silica aerogel is being modeled using a comprehensive shock hydrodynamic code (called CTH). Various options of this code were investigated to attempt to make the most appropriate choice of methods of impact, equations of state, and processes of energy transfer from capture material to particle. The initial calculations with the code used only "reasonable" estimates for the physical parameters of silica aerogel. Through the literature searches and personal contacts with the knowledgeable scientists, the best possible mechanical and thermal data have been made available for these computations.

Reentry Heating of IDP's: A recent study [1] of fragments from a cluster IDP has shown that the primary particle was subject to a significant thermal gradient such that only the exterior surfaces were strongly affected during reentry. The variability of helium release temperature supports this interpretation. The low abundances of some volatile trace elements (e.g. zinc) also suggests that some fragments have been strongly heated, while other fragments retain chondritic levels of zinc. Previous calculations of the heating of IDP's which assumed only thermal diffusion as the heating mechanism [2] resulted in the particle's being isothermal for any reasonable value of thermal diffusivity. Bonny, et al. [3] proposed that the phase transition of an organic material might slow this thermal equilibration. The dehydration and decomposition of the hydrated silicates is strongly endothermic. Thus, hydrated IDPs contain a phase with the required properties.

The heat diffusion equation was modified to include a volume source term to account for the phase transition. The equation was then solved numerically using the Crank-Nicholson implicit method. The phase transformation energy ℓ_ϕ is treated as a fictitious temperature change which would occur if the energy inserted at a spatial node did nothing more than

increase the temperature at that node. This fictitious temperature change is given by $\Delta T_\phi = \ell_\phi / c_p$, where c_p is the specific heat.

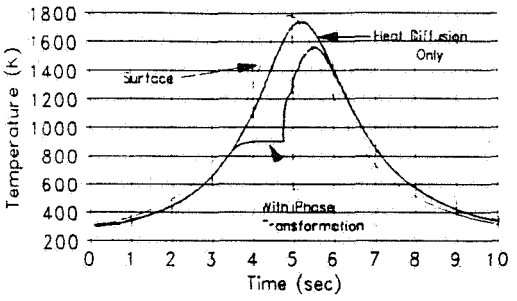

Figure 1. Temperature vs. Time for 50 micron (radius) particle. The solid line gives surface temperature. Heavy lines give the temperatures at a radial positionof 25 microns without and with a phase transformation. Particle at normalincidence: 15 km/s.

A preliminary result is shown in Figure 1 at the left. Surface temperatures were computed using the method of Flynn [5]. The assumed thermal diffusivity was 10^{-9} m^2/sec characteristic of lunar material; $c_p = 2$ cal/gm/K; $\ell_\phi =$ 600 cal/gm (a typical value for kaolinite) and the temperature of the transition was 900 K. Since the particles will not be 100% hydrated clays, the energy of the phase transition was reduced to 300 cal/gm. The results for a 50 μm (radius) spherical particle are shown in Figure 1. The phase transition produces a peak temperature drop of about 200 K. The effects of such a temperature difference are well within the range of detectability. Calculations for larger particle impact parameters where the particle is heated over a a longer period, do not produce such large temperature differences. Studies that are more systematic with respect to impact parameter and incident velocity are in progress. Carbonaceous particles will also be investigated. Here the results may be even more dramatic since the phase transformation energies are higher than in the hydrated silicates.

Computer Modeling of Particle Capture in Aerogel: Aerogels are sol-gel derived, supercritically dried materials with extraordinarily large porosity, i.e. low density. Typical densities are around 100 kg/m^3, (95% porosity) although aerogels with densities as low as 2 kg/m^3 have been manufactured. These exotic materials have been used for the capture of particles traveling at hypersonic speeds in excess of 6 km/s without inordinate effects to the particle.

Calculating the effects of the interaction between the hypersonic particle and the capture medium seems deceptively simple if viewed only in terms of the Rankine-Hugoniot relations themselves which describe the resulting shock wave's penetration through the medium. However, the subsequent effect on the medium must consider its equation of state as the shock velocity varies, the elastic and plastic deformation of the aerogel cells, and the transfer of the stresses and energy from the shocked material to the particle itself. These modeling studies at NASA-Ames use CTH, a software system that models multidimensional, multi-material, large deformation, strong shock wave physics. Current computations use a numerically derived "two-state" equation of state where the material changes instantaneously from the initial aerogel to that of fused quartz. The stresses and temperatures are similarly transmitted from those of the medium to those of the particle. These assumptions of "instantaneous" effects need further investigation, particularly since the carnelian particle now being modeled has been found to come to rest in only ≈ 40 μs. Additionally the particles in the current simulations must be given inordinately large fracture stresses. Else the particles fragment, in disagreement with observed results.

The calculations have been improved by incorporating more reliable data for the velocity of sound [6] (and the associated compressive moduli). It had been found, for example, that the velocity of sound being used was almost an order of magnitude too high. Velocity of sound data which will be used in the future are shown in the graphs below together with suitable power law fits. The two graphs are necessary for the two density regions, since the actual processes for manufacturing the aerogel are different.

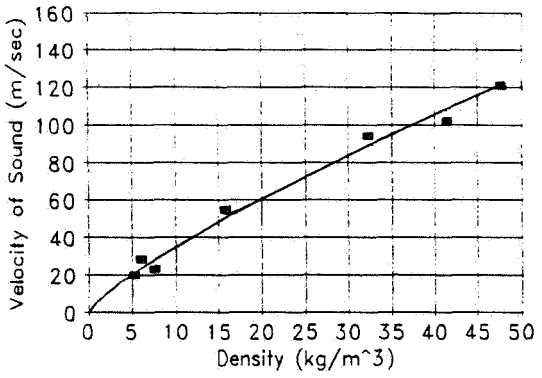

Figure 2. Velocity of sound in low density aerogel under vacuum

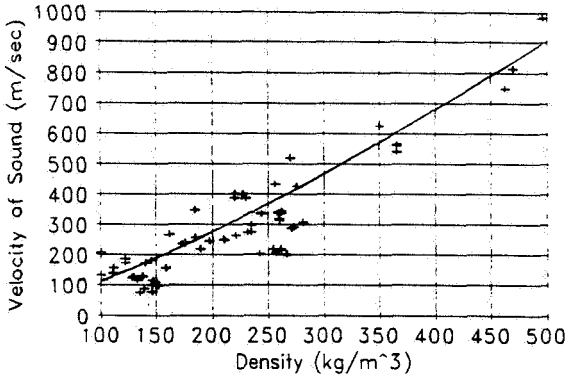

Figure 3. Velocity of sound in higher density silica aerogel at atmospheric pressure.

Improved data have also been provided for shear moduli and thermal conductivities, should these be needed in a more detailed model.

The modeling is in a crucial validation stage for velocity ranges and particle sizes which will be typical for the capture of cometary dust for the Stardust mission (although this is not the focus of the validation). Experimental studies using gun-launched particles indicate little difficulty for the capture in aerogel for cometary dust. A pioneering effort of Stardust is the capture of interstellar dust several orders of magnitude smaller (possibly tens of nanometers) than interplanetary dust and traveling at speeds which can exceed 25 km/s. To the best of my knowledge no data are available to determine what effects there will be on such particles captured in aerogel or polyfoams.

References:

[1] R.L. Bell, et al., "CTH User's Manual and Input Instructions", Version 1.026, Sandia National Laboratories, July, 1992.

[2] K.L. Thomas, et al., Geochemica et Cosmochemica Acta 59, 2797 (1995).

[3] P.P. Szydlik and G.J. Flynn, Meteoritics 27, 294 (1992).

[4] Ph. Bonny, et al., Lunar Planet Sci. XIX, 118 (1988).

[5] G.J. Flynn, Lunar Planet Sci. XIX, 683 (1988).

[6] J. Gross, J. Fricke and L.W. Hrubesh, J. Acoust. Soc. Am. 91, 2004 (1992).

NASA-ASEE-Stanford Summer Faculty Fellowship 1996 - Final Report

LINE COUPLING IN ATMOSPHERIC SPECTRA

R. H. Tipping, Department of Physics and Astronomy, University of Alabama, Tuscaloosa, AL 35487

Introduction. The theoretical modeling of atmospheric spectra is important for a number of different applications: for instance, in the determination of minor atmospheric constituents such as ozone, carbon dioxide, CFC's etc.; in monitoring the temperature profile for climate studies; and in measuring the incoming and outgoing radiation to input into global climate models. In order to accomplish the above mentioned goal, one needs to know the spectral parameters characterizing the individual spectral lines (frequency, width, strength, and shape) as well as the physical parameters of the atmosphere (temperature, abundances, and pressure). When all these parameters are known, it is usually assumed that the resultant spectra and concomitant absorption coefficient can then be calculated by a superposition of individual profiles of appropriate frequency, strength and shape. However, this is not true if the lines are "coupled." Line coupling is a subtle effect that takes place when lines of a particular molecule overlap in frequency. In this case when the initial states and the final states of two transitions are connected by collisions, there is a quantum interference resulting in perturbed shapes. In general, this results in the narrowing of Q-branches (those in which the rotational quantum number does not change), and vibration-rotational R- and P-branches (those in which the rotational quantum number changes by $\pm$ 1), and in the spectral region beyond band heads (regions where the spectral lines pile up due to centrifugal distortion). Because these features and spectral regions are often those of interest in the determination of the abundances and pressure-temperature profiles, one must take this effect into account in atmospheric models.

Theory. Because of collisions, a particular transition is spread out over a range of frequencies (the line profile or line shape), the details of which depend on the temperature and the collision partner. Each line can be characterized by a central region around the peak absorption and the line wings that extend out from the central frequency. The detailed theoretical calculation of the spectral profile over the entire range of frequencies is an intractable physical problem; however, line-shape theories valid near the line centers (impact theories based on the assumption of instantaneous collisions) and theories valid in the far wings (quasistatic theories based on collisions of infinite duration) have been developed. Line coupling for these distinct regions have also been derived. In the former case, one can write the theoretical expression for the absorption coefficient in the following form[1]

$$\alpha(\omega) = (n_a/\pi)\ \mathrm{Im}\ \{ \sum_{i,f} \mu_f \langle\langle f |\ [\ \omega - \omega_0 - iW]^{-1}\ | i\rangle\rangle\ \mu_i\ \rho_i \}\ , \quad (1)$$

where Im designates the imaginary part, n_a is the number density of absorbers, the indices f and i represent transitions in "line space", μ are the transition dipole moments, and ρ_i is the fractional population of the lower level of the i transition. The relaxation matrix W embodies the effects of the collisions; its real and imaginary diagonal elements are the line widths γ_i and shifts δ_i, respectively. The diagonal matrices ω and ω_0 correspond to the frequency of interest and the transition center frequencies. If one neglects the off-diagonal matrix elements of W (those responsible for line coupling), Eq. 1 can be written in the following form

$$\alpha(\omega) = \sum_i S_i\ (\gamma_i/\pi)\ /\ [(\omega - \omega_i - \delta_i)^2 + \gamma_i^2] \quad (2)$$

where S_i is the line strength. From Eq. 2, it is clear that in this case, the absorption coefficient can be written as a superposition of Lorentzian shaped lines, characterized by their frequency, shape and strength. As a first-approximation, including the effects of line coupling, one can write Eq. 1 in the form[2]

$$\alpha(\omega) = \sum_i S_i\ (\gamma_i/\pi)[1 + C_i(\omega - \omega_i)]\ /\ [(\omega - \omega_i - \delta_i)^2 + \gamma_i^2]\ ; \quad (3)$$

the strength of the coupling is proportional to C_i, and from the form of Eq. 3, one can see that this coupling does not affect the integrated intensity of the line but alters its shape.

In the far wings, the theoretical inclusion of line coupling is more difficult; over the past few years, we have developed a first-principle theory for the absorption coefficient that can be cast into the following form[3,4]

$$\alpha(\omega) = (n_a/\pi) \sum_{\omega_{ij}>0} S_{ij}\ \frac{\omega\ \mathrm{sh}(\hbar\omega/2kT)}{\omega_{ij}\ \mathrm{sh}(\hbar\omega_{ij}/2kT)}$$

$$\left[\frac{1}{(\omega - \omega_{ij})^2}\ \chi_+(\omega - \omega_{ij}) + \frac{1}{(\omega + \omega_{ij})^2}\ \chi_-(\omega + \omega_{ij})\right]\ , \quad (4)$$

where two line shapes have been introduced. These can be calculated within the quasistatic framework if an accurate anisotropic potential is known.

A spectral region of considerable interest in remote sounding of the Earth's atmosphere is the high-frequency side of the ν_3 fundamental band of CO_2.[5] In this window region, there is little absorption due to water vapor and only a weak transitions of N_2O. Because of its widespread use, it is of importance to characterize accurately the high-frequency wing of the N_2 broadened CO_2 lines. This implies a need for accurate calculation of the corresponding absorption coefficient, including its frequency and temperature dependences. This in turn implies that one must use a quasistatic approach including all the effects of line coupling. This is the subject of interest in the current theoretical study. We have modified the theory from our previous application to CO_2-Ar to CO_2-N_2; the latter case is more general due to the internal structure of N_2. After a literature search, we found that at present there is no accurate anisotropic potential. Because this is necessary, we have initiated talks with the quantum chemists at Ames who are the world leaders in this type of calculations. It appears to be possible although time consuming. If this proves unfeasible, we will use the current site-site potential (where a simple form of the interaction between each atom of CO_2 interacts with each atom of N_2 is assumed) and expand it in a series of products of spherical harmonics appropriate for introduction into our theory. Then we hope to carry out the necessary computations of the absorption coefficient. This will be compared to the existing laboratory data for validation and eventually used to improve the retrieval of the atmospheric parameters from satellite data.

References

1. M. Baranger, Phys. Rev. 111, 494 (1958).
2. P. W. Rosenkranz, IEEE Trans. Antennas Propagat. AP-23, 498 (1975).
3. Q. Ma and R. H. Tipping, J. Chem. Phys. 100, 8720 (1994).
4. Q. Ma and R. H. Tipping, J. Chem. Phys. 104, 9678 (1996).
5. A. Levy, N. Lacome, and C. Chackerian, Jr., in *Spectroscopy of the Earth's Atmosphere and Interstellar Medium*, Eds. K. Narahari Rao and A. Weber, Academic Press, Boston, 1992.

NASA-ASEE-Stanford Summer Fellowship 1996 - Final Report

THE YEH-STRATTON CRITERION FOR STRESS CONCENTRATIONS ON FIBER-REINFORCED COMPOSITE MATERIALS

Hsien-Yang Yeh, Ph.D. Professor, Mechanical Engineering, California State University, Long Beach, CA

Introduction. The Yeh-Stratton criterion developed from a yielding criterion is modified to a generalized failure criterion and applied to fiber-reinforced composites with a central crack or a circular cutout under tensile loadings. The purpose of a material failure criterion is to establish a theoretical margin of safety and to be validated by experiments. It is necessary to obtain the crack tip stress field before a failure criterion of composite materials is applied. However, the crack tip stress field is complicated since there are numerous factors that influence the crack tip stress distribution. The understanding of the factors that contribute to crack tip stress field is of critical importance in analyzing composite laminates.

Stress Concentration of Composites. First, the stress concentration in fiber-reinforced composites with tensile loadings is discussed. In fracture analysis, it is significant to consider the crack tip stress field. Lekhnitskii extended Muskhelishvili's work in the plane theory of isotropic elasticity to the anisotropic case [1]. Later, Sih et al [2] derived the stress field equations for the anisotropic elastic body with a crack. However, the crack tip stress field equations established by Lekhnitskii and Sih were in a complex form. Theocaris and Philippidis modified these stress field equations into a real number solution [3]. These crack tip stress field equations will be applied to the following discussion and substituted into the failure criteria to analyze the fracture situations of the composites with cracks.

Fracture Criteria of the Composite Materials. Once the stress distribution of a composite is calculated, the point of interest should be examined with a failure criterion to determine whether the composite will fail or not. In [4], the Yeh-Stratton criterion was generalized for fibrous composites. Although the generalized Yeh-Stratton criterion was developed for uncracked bodies, it should be able to apply to cracked bodies of anisotropic materials because the criterion is based on continuum mechanics. Some other relevant criteria to be compared are the Tsai-Wu theory, the Hoffman theory, the Fischer Criterion and the Cowin criterion [5].

Considerable efforts have been devoted to the formulation of composite failure criteria and to their correlation with experimental data, but no criterion has been fully adequate. The analyses of the Hoffman theory, the Fischer theory and the Cowin theory are valid rigorously only under special cases. This limits their direct application to general materials.

Results and Conclusion. In this study, experimental results obtained by Tan [6] for AS4/3502 $[\pm\theta_2]$s family of laminates with central holes and normal cracks were examined by the Yeh-Stratton criterion and several other failure theories. The fracture of AS4/3502 $[\pm\theta_2]_s$ is a mixed-mode type and dominated by the epoxy matrix. The experimental results and geometric dimensions of the samples for the graphite/epoxy AS4/3502 $[\pm\theta_2]_s$ from Tan [6] are borrowed. Each group of samples has five different circular hole diameters in various plate widths as well as five different normal crack lengths in various plate widths. Figures 1 and 2 display the predictions from the Yeh-Stratton criterion, the Tsai-Wu theory and experimental data. The prediction curves from both theories are very close. This indicates that the Yeh-Stratton criterion is reliable and accurate as compared to the most popular strength criterion. Table 1 shows an error analysis of this study. For the Yeh-Stratton criterion, the predictions of failure stresses are off by 10%. All of these criteria have good results with this AS4/3500 $[\pm\theta_2]_s$ material. However, the Yeh-Stratton criterion offers better predictions among the various other theories.

For a constant crack length or a constant circular hole diameter on the AS4/3502 [$\pm\theta_2$]s composite plate, the required externally applied failure stress increases when the distance from the crack tip to the initial failure point increases. This indicates that the influence from the existing cracks or holes to the material failure is a localized effect. However, for a constant distance from the crack tip to the initial failure point, the applied failure stress is in inverse proportion to the crack lengths or hole diameters. In other words, the failure stress reduces when the crack lengths or the hole diameters increases. This indicates that the existing cracks or holes will reduce the strength of materials.

One basic assumption in the theory of linear elastic fracture mechanics (LEFM) is that the distance from the crack tip to the initial failure point i.e. size of the plastic zone or the damage zone is much less than the crack length. However, the distances from the crack tip to the initial failure point of the composite material AS4/3502 [±60]s are about the same order of magnitude as their crack lengths, for example 9.6 mm to 15.14 mm, 5.76 mm to 10.14 mm and 4.16 mm to 7.62 mm etc. as shown in Table 2. The violation of the basic assumption in the theory of linear elastic fracture mechanics presents a challenge task in the fracture research of composite materials. The distance from a crack tip or a cutout to the initial failure point is increased as the direction of the fiber angle increased. This is due to the increase of the fiber direction angle, the material needs a larger damage zone in order to cover the larger region with lower fiber stress, making the distance from crack tip to the initial failure point increased up to about the same order of magnitude of their initial crack lengths.

Future Activities. The better understanding of the failure or damage about composite materials will provide a more reliable design methodology in the applications of advanced composite materials. To further understand this research subject, more experimental data as well as theoretical model development are definitely required.

Theory		Center Crack			Circular Hole	
	30°	45°	60°	30°	45°	60°
Yeh-Stratton	10.0%	10.0%	10.2%	10.0%	9.9%	10.0%
Tsai-Wu	11.0%	11.0%	10.7%	10.0%	10.0%	10.2%
Cowin	10.5%	10.6%	10.6%	10.3%	10.2%	11.0%
Hoffman	10.4%	10.6%	10.6%	10.3%	10.2%	11.0%
Fischer	11.0%	11.0%	10.8%	12.0%	11.0%	11.0%

Table 1. Error analysis of the data of AS4/3502 [$\pm\theta_2$]s from different theories.

30° (mm)	Crack length (mm)	45° (mm)	Crack length (mm)	60° (mm)	Crack length (mm)
0.018	1.35	0.096	1.47	0.744	1.29
0.03	2.67	0.136	2.74	1.32	2.59
0.068	7.47	0.324	7.54	4.16	7.62
0.084	10.03	0.4	10.06	5.76	10.14
0.136	15.16	0.64	15.16	9.6	15.14

Table 2. The distance from the crack tip to the initial failure point of AS4/3502 [$\pm\theta_2$]s with a central crack.

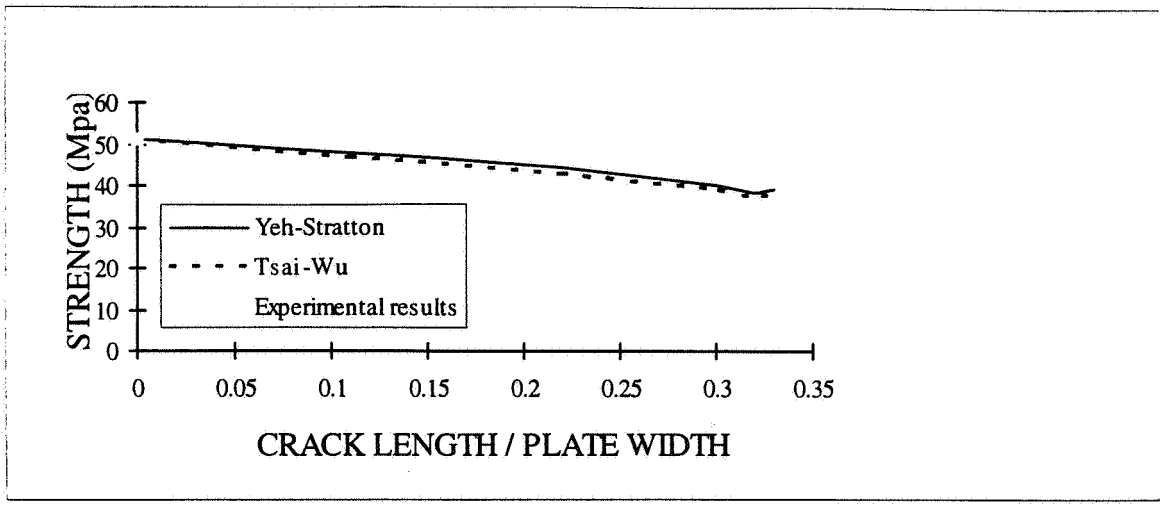

Figure 1. Comparison of the Yeh-Stratton, the Tsai-Wu theory, and experimental data for AS4/3502 $[\pm 30^{\circ}]_s$ with a center crack.

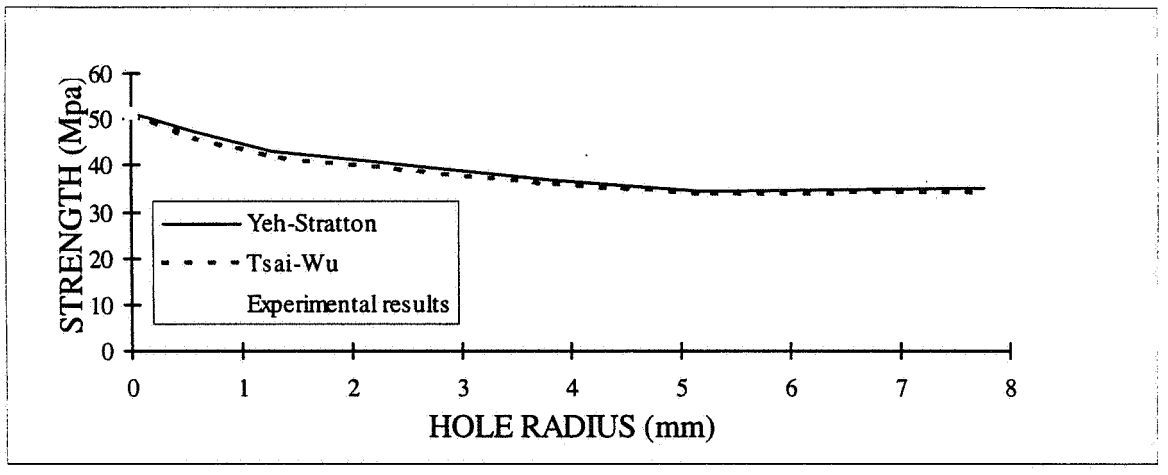

Figure 2. Comparison of the Yeh-Stratton, the Tsai-Wu theory, and experimental data for AS4/3502$[\pm 30^{\circ}]_s$ with a circular hole.

References

[1] S.G. Lekhnitskii, "Theory of Elasticity of an Anisotropic Elastic Body," trans. by P.E. Brandstatton, Holden-Day, Inc. 1963.

[2] Sih, G.C., P.C. Paris and G.R. Irwin. "On Cracks in Rectilinearly Anisotropic Bodies," Int. J. Fract. Mech., Vol.1, No. 3, Sept 1965, pp. 189-203.

[3] P. S. Theocaris, and T.P. Philippidis, "Mixed-Mode Fracture Mechanics of Anisotropic Plates by Means of the T-Criterion," Int. J. Fract. Mech., Vol. 52. No.3, Dec. 1991, pp. 223-237.

[4] H. -Y. Yeh, and C. H. Kim, "The Yeh-Stratton Criterion for Composite Materials," Journal of Composite Materials, Vol. 28, No. 10, Feb. 1994, pp. 926-939.

[5] R. E. Rowlands "Strength Theories and Their Experimental Correlation," Chapter II, Handbook of Composites, Vol. III, Failure Mechanics of Composites, Edited by G.C. Sih and A. M. Skudra, 1985 Elsevier Science Publishers.

[6] S. C. Tan, "Mixed-Mode Fracture of Notched Unidirectional and Off-Axis Laminates under Tensile Loading," Journal of Composite Materials, Vol. 23, Nov. 1989, pp. 1082-1105.

NASA-ASEE-Stanford Summer Fellowship 1996 Final Report

Joshua McBee, Western Washington University, Bellingham, WA 98225

Introduction: Carbonyl Sulfide(OCS) is considered to be one of the major sources of sulfur appearing in the stratosphere due to its relative inertness, about 1 to 10 years[1]. However, the roles of OCS as well as other reduced sulfur compounds such as carbon disulfide (CS_2), hydrogen sulfide (H_2S), and dimethyl disulfide($(CH_3)_2S_2$, are not completely understood in the atmospheric sulfur cycle. Consequently very little information is available about the effect of sulfur compounds in the stratosphere.

The ability of OCS to penetrate into the stratosphere makes it an excellent tracer for study of the role of the sulfur cycle in stratospheric chemistry. Previously techniques such as gas chromatography and whole air sampling have been used to measure OCS analytically. Each technique had its drawbacks however, with both being quite slow, and whole air sampling being somewhat unreliable. With molecular spectroscopy, however, it has been found in recent years that the tunable diode laser absorption spectrometer (TDL) provides a very rapid and accurate method of measuring OCS and other trace gases[2-4]. The TDL is extremely well suited for this type of measurement because of its extremely high resolution (10^{-5} cm^{-1}), low signal to noise ratio, and compactness. Today, TDLs can be produced to provide a light source falling in the range of the 5μm atmospheric "window". Within this window the rotational fine structure of the ν_3 band of OCS can be differentiated from isotopic species, hot bands, and fine structure from other species such as H_2O, N_2O, and CH_4(figure 1). The TDL when coupled to a cell with a long path length (up to 117m) as shown by Fried et. al.[5] can be used to theoretically detect OCS in concentrations as low as 10 pptv.

One limiting factor to the airborne measurement of OCS is the lack of data relating to the line broadening effect of foreign gases on the vibrational/rotational transitions at various temperatures. A linear relationship can be developed between the pressure of a foreign gas, and the lorentzian width of the affected rotational transition. When these two values are plotted, the slope of the line found by linear least squares fit is called the line broadening coefficient. The value of the line broadening coefficient is dependent on the particular vibrational/rotational transition, the foreign gas, and the ambient temperature of the measured gases. Without these line broadening coefficients, airborne measurements would be all but impossible to interpret successfully.

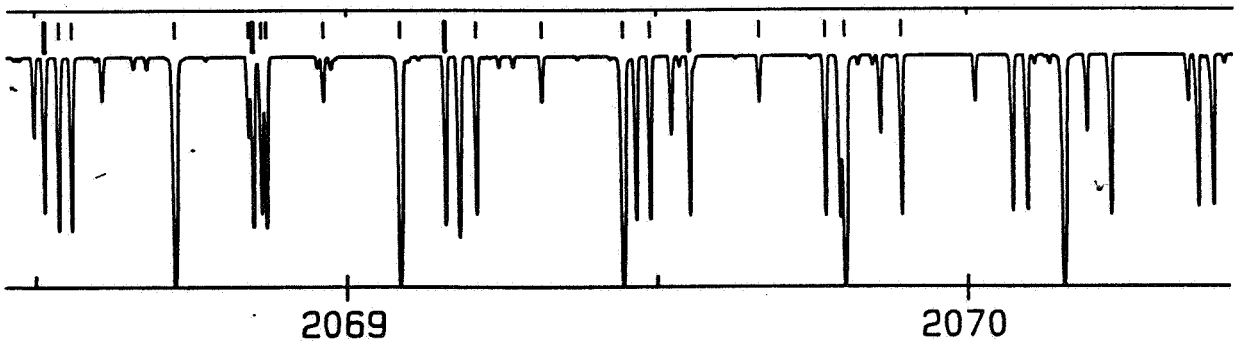

Figure 1. Sample of high resolution OCS spectrum showing distribution of fundamental, isotopic, and hot bands.

Summer Goals: Working with my research advisor, Dr. H William Wilson, and colleague Dr. Max Loewenstein, our goals for this summer involved several steps. The first step involved the incorporation of our TDL onto the optical bench where the instrument resided and to demonstrate successful operation. Second, write a computer program designed to acquire and store the data produced by the TDL using an analog to digital converter card located on a nearby PC. Finally, the examination of a number of rotational vibrational transitions of the ν_3 band of OCS. Pressure broadening coefficients would then be computed for selected transitions using nitrogen and oxygen as the foreign broadening gases at pressures ranging from 20 torr to 120 torr. These measurements would be taken at temperatures ranging from 180K to 295K to determine the affect of temperature on broadening. The lorentz widths would then be computed by fitting the pressure-affected rotational fine structure by using a hybrid voigt profile. The coefficients would subsequently be computed using a linear-least squares fit as described above.

Instrument Description: The instrument was assembled and operated using the sweep integration technique as described by Jennings[6]. The laser itself is constructed of a lead-sulfur selenium crystal with the formula: $PbS_{1-x}Se_x$
Where the molar ratios of sulfur and selenium are varied depending on the desired frequency range of the laser. The laser is stored in a special housing produced by Laser Photonics that allows the laser to be cooled to ~85K using liquid nitrogen. The frequency of the laser is fine tuned by adjusting both the temperature and the current that is placed across the lead-salt crystal. Because of the lasers extreme temperature sensitivity, the heater incorporated into the laser dewar housing is adjustable to temperatures as accurate as 1 milliKelvin.

For measurement taking, a cold cell with path length of 31.6 cm was utilized[7]. As shown in Figure 2, the cell is surrounded by a larger shroud with vacuum ports for both the inner and outer chambers. The outer shrowd permits the cooling of the cell using liquid nitrogen via the central vertical transfer line. The outer chamber can also be evacuated to less than 0.02 torr during operation thus facilitating better insulation. The temperature of the cell was equilibrated using a 20W heating element mounted on the cooling block. Temperature readings were determined by Fe-doped gold chromel thermocouples. The CaF_2 windows of the inner and outer cells were staggered 20° out of parallel in order to prevent interference fringes caused by reflections.

The detector used was an InSb photodetector cooled to 80K using liquid nitrogen manufactured by Infrared Associates. The analog signal produced by the photodetector is then processed by a matched pre-amplifier and is sent to a Keithley/Metrabyte DAS-1602 analog/digital data acquisition board. The A/D board is housed in a generic PC computer using an AMD 386DX-40 processor plus a 387 coprocessor combination.

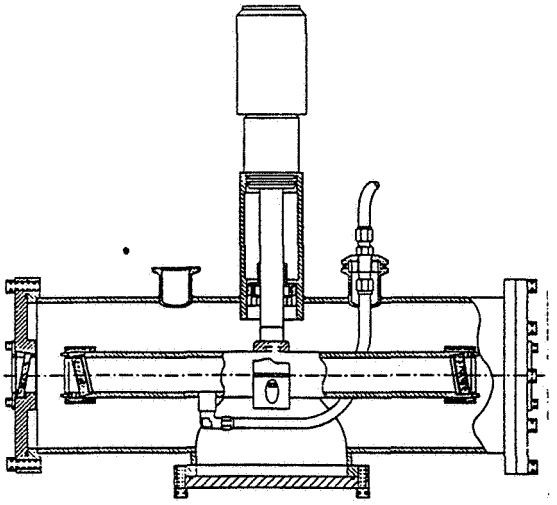

Figure 2. Cross section diagram of cold cell.

Summer Accomplishments: In all 14 rotational transitions were characterized and examined. In one mode the P(10) - P(14) lines were utilized, and in a second laser mode, the R(23), R(25), R(26), R(27), R(28), R(30), R(31), R(32), and R(33) lines. These rotational/vibrational bands were examined using both N_2 and O_2 as the broadening gases, and at four different temperatures, 185K, 225K, 275K, and 296K. Analysis of the data collected will provide information on the effect of temperature and broadening gas type on the broadening coefficients of each transition of OCS.

Future Work: Immediate work involves processing and analysis of the data collected this summer. Although work of this type was already been performed at room temperatures, many of the values that are published are dated. Our work this summer will provide revisions of these values using more up to date hardware and software resources. Much of the analysis will involve devising a method in which the fundamental rotational/vibrational transitions can be deconvolved from nearby isotopic lines.

In the future, we would like to expand our work to include measurement of atmospheric concentrations of OCS. This would include the construction of a multi-pass Herriott cell for long-path length measurements, as well as the construction of a more compact and portable version of the instrument that was utilized this summer. By doing this, the instrument could be transported to sites of interest outside of the laboratory to make on-site measurements.

References:

1. P.J. Crutzen, "The Possible Importance of CSO for the Sulfate Layer of the Stratosphere," *Geophys. Res Lett.* 1976, 3, 73.
2. M. Loewenstein, J.R. Podolske, K.R. Chan, and S.E. Strahan, "Nitrous Oxide as a Dynamical Tracer in the 1987 Airborne Antarctic Ozone Experiment," *J. Geophys. Res.* 1989, 94, 11589.
3. D.R. Hastie, G.I. Mackay, T. Iguchi, B.A. Ridley, and H.I. Schiff, "Tunable Diode Laser Systems for Measuring Trace Gases in the Troposphere," *Environ Sci. Technol.* 1983, 17, 352A.
4. C.R. Webster, R.D. May, C.A. Trimble, R.G. Chave, and J. Kendall, "Aircraft (ER-2) Laser Infrared Absorption Spectrometer (ALIAS) for In-situ Stratospheric Measurements of Hcl, N_2O, CH_4, NO_2, and HNO_3," *Appl. Opt.* 1994, 33(3), 454.
5. A. Fried, J.R. Drummond, B.Henry, and J. Fox, "Versatile Integrated Tunable Diode Laser System for High Precision; Application for Ambient Measurements of OCS," *Appl. Opt.* 1991, 30(15), 1917
6. D. E. Jennings, "Absolute Line Strengths in ν_4, $^{12}CH_4$: a Dual-Beam Diode Laser Spectrometer with Sweep Integration," *Appl. Opt.* **19**, 2695-2700 (1980).
7. Max Loewenstein and H.W. Wilson, "Line Width Temperature Dependence of Selected R-branch Transitions in the ν_3 Fundamental of $^{14}N_2{}^{16}O$ Between 135K and 295K," *Spectrochim. Acta.* 1992, 48A, 434.
8. J. Altmann, R. Baumgart, C. Weitkamp, "Two-mirror Multipass Absorption Cell," *Appl. Opt.* **20**, 995-999 (1981).

NASA-ASEE-Stanford Summer Fellowship 1996 - Final Report

LOSS OF SITUATION AWARENESS IN PILOTS: ANALYSIS OF INCIDENT REPORTS

Eric B. Villeda, The Ohio State University, Columbus, OH

Introduction

Approximately 75% of all aviation accidents and incidents are attributable to human failures in monitoring, managing, and operating systems [1]. Tactical decision errors were found to be a factor in 25 of 37 major US air transport accidents between 1978 and 1990 [2]. These two facts demonstrate the inability of some pilots to maintain situation awareness. Situation awareness (SA) is defined as "the perception of elements in the environment within a volume of time and space, the comprehension of their meaning, and the projection of their status in the near future" [3]. Thus, when a pilot loses SA, he or she is unable to either perceive, comprehend, or project the status of the aircraft. In pilot's terms, he or she has "fallen behind the airplane". Our study this summer involved an analysis of 190 NASA Aviation Safety Reporting System (ASRS) reports. By analyzing these reports, we hope to gain insight as to what causes pilots to lose SA, and what consequence(s) the loss brings about. Further study may enable us to improve pilot performance by altering the flight environment to facilitate SA, or by developing training programs that enhance individual SA and decision making.

Report Analysis

The Aviation Safety Reporting System is a program developed by NASA to form a database of incidents and accidents using voluntary reports of the people involved. The reporters are granted immunity from penalties resulting from unintentional violations. The identity of the reporter is kept confidential. This program allows NASA to collect detailed information about incidents from the parties involved. NASA ASRS reports were gathered using the following key words: aware, awareness, risk(y), safe, safety, unsafe, decision, decide(d), judgment, choice, workload, and CRM (crew resource management).

Two raters studied 190 ASRS reports. 159 of these were coded and analyzed. The following data was gathered from the ASRS reports: accession number, person filing the report, aircraft type, phase of flight when the loss of SA occurred, cause(s) of SA loss, consequences of SA loss, the person(s) who lost SA, and the person(s) taking action to correct the problem. The 31 uncoded reports did not involve a loss of SA.

Results and Discussion

Figure 1 shows the phase of flight where SA loss occurred. There were 10 phases of flight where SA loss occurred: Preflight, Taxi, Takeoff, Climb, Cruise, Descent, Approach, Landing, Multiple phases, and Other. It occurred most often during cruise flight and during taxi on the ground (35 times each). Higher incidences of SA loss during cruise flight is logical because the aircraft spends most of its time in this phase. Loss of SA during taxi occurred most often because of high workload or distractions and lack of communication or coordination (either between the flight crew members or between the flight crew and controllers).

Figure 2 shows what caused the loss of SA during each incident. For the 159 cases studied, there were 478 factors that contributed to the loss of SA. They were categorized into the following: High Workload or distractions, Lack of Communication/Coordination, Improper Procedure, Maintenance or aircraft equipment malfunction, Time pressure, Unfamiliarity (with the aircraft, crew, or airport), Weather, Fatigue, Night conditions, Emotional state, and Other. High Workload and distractions accounted for 21% (102), and Lack of Communication/Coordination accounted for 16.3% (78). Those causes falling under the category of Other may have been pressure by the pilot's employer, overshooting a runway, or being vectored by air traffic control (ATC) into an unfavorable position.

The consequence of SA loss is shown in Figure 3. There were four categories: Danger, Deviation, Violation, and Other. The aircraft was put in a position of imminent danger 61 times (38%). In these cases, the aircraft may have landed without clearance, experienced a conflict with other air traffic, transgressed onto the wrong runway or taxi way, or flown dangerously close to terrain. Deviations were changes in required airspeed, altitude or heading. Violations refer to non-adherence to a published procedure or

Federal Aviation Regulation, and Other refers to instances where the aircraft aborted takeoff, executed a missed approach, or when the loss of SA had no effect.

In the 159 incidents, there were 161 cases of SA loss (more than one party may have lost SA during the same incident). As shown in Figure 4, *both* crew members lost SA 97 times (60%). The captain lost SA 43 times (27%), the First Officer 11 times, the Second Officer twice and ATC three times. The Ground Crew lost SA twice and Others lost SA three times (gate agent, dispatcher and maintenance person -- once each).

The research conducted this summer has given us great insight as to what causes pilots to lose SA and when it occurs the most. This information will be useful in developing training methods, developing strategies for crew members, and developing equipment that is easier for pilots to use. Based on these results, one can make *preliminary* recommendations: pilot workload should somehow be reduced, pilots should receive more training so they can communicate better with each other and with ATC, and the use of proper procedures should be stressed during training sessions. Hopefully these developments will help reduce the number of mistakes made in the cockpit, thereby reducing the number of incidents and accidents that occur in the dynamic flight environment.

References

[1] Chappell, Sheryl L. (1994). "Using Voluntary Incident Reports for Human Factors Evaluations". In N. Johnston, N. McDonald & R. Fuller (Eds.), Aviation Psychology in Practice. (pp. 149-169). Aldershot, England: Ashgate.

[2] National Transportation Safety Board. (1994). A review of flightcrew-involved, major accidents of U.S. Air Carriers, 1978 through 1990. (PB94-917001, NTSB/SS-94-01). Washington, DC.

[3] Endsley, Mica R. & Bolstad, Cheryl A. (1994). "Individual Differences in Pilot Situation Awareness". The International Journal of Aviation Psychology, 4(3), (pp. 241-264). Lawrence Erlbaum Associates, Inc.

Figure 1: Phase of Flight (%)

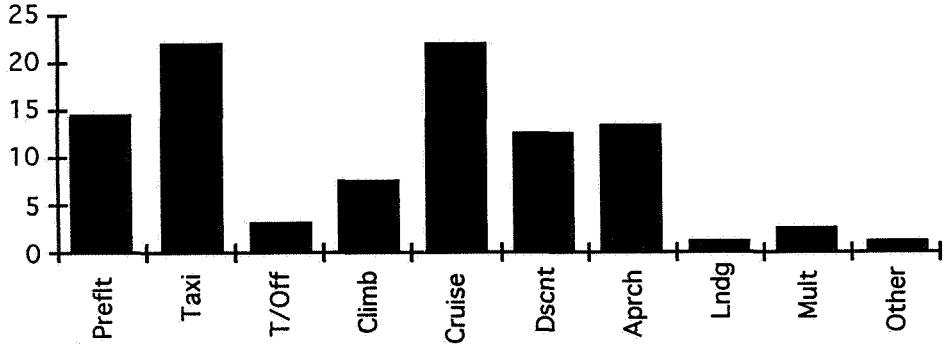

Figure 2: Cause of SA Loss (%)

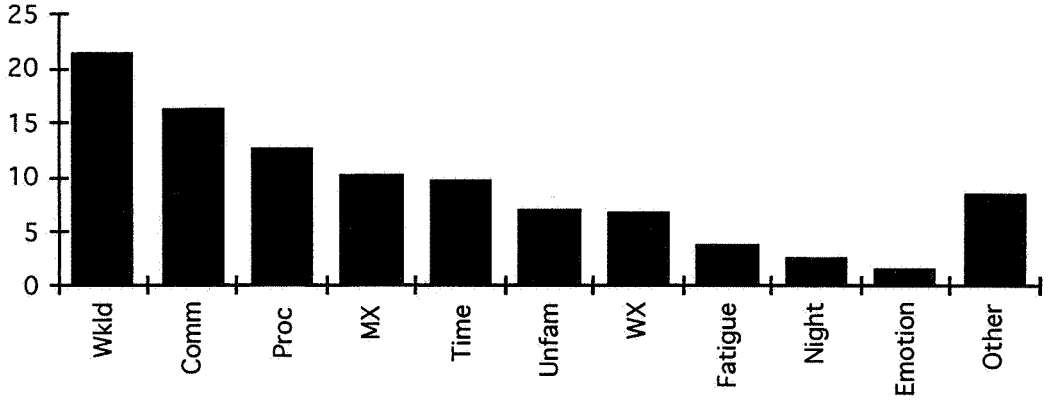

Figure 3: Consequence of SA Loss (%)

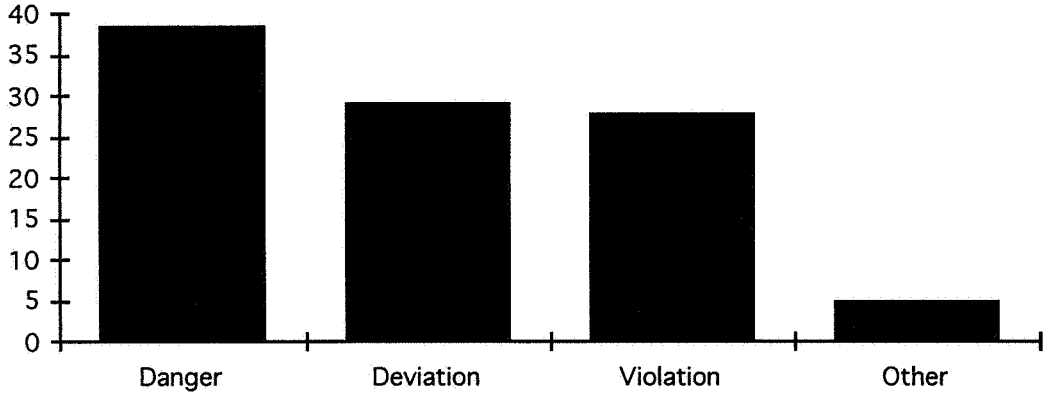

Figure 4: Who Lost SA? (%)